

# **Design of a Single Input Triple Output DC-DC converter for Solar Home System**

A Thesis Submitted  
in Partial Fulfillment of the Requirements for the Degree  
of

**MASTER OF SCIENCE IN  
ELECTRICAL AND ELECTRONIC ENGINEERING**

by

**Tanvir Ahmad**



**Department of Electrical and Electronic Engineering  
BANGLADESH UNIVERSITY OF ENGINEERING AND TECHNOLOGY**

**Dhaka, Bangladesh**

**March, 2018**

## Certificate of Approval

The thesis titled “Design of a Single Input Triple Output DC-DC converter for Solar Home System” submitted by Tanvir Ahmad, Roll No.: 0413062260 P, Session April 2013 has been accepted as satisfactory in partial fulfillment of the requirement for the degree of **Master of Science in Electrical and Electronic Engineering** on 31<sup>st</sup> March, 2018.

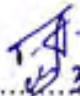
### BOARD OF EXAMINERS

1.   
\_\_\_\_\_  
**Dr. Md. Ziaur Rahman Khan**  
Professor  
Department of Electrical and Electronic Engineering,  
Bangladesh University of Engineering and Technology (BUET),  
Dhaka-1205, Bangladesh.  
Chairman  
(Supervisor)
2.   
\_\_\_\_\_  
**Dr. Quazi Deen Mohd Khosru**  
Head & Professor  
Department of Electrical and Electronic Engineering  
Bangladesh University of Engineering and Technology (BUET),  
Dhaka-1205, Bangladesh.  
Member  
(Ex-Officio)
3.   
\_\_\_\_\_  
**Dr. Mohammad Jahangir Alam**  
Professor  
Department of Electrical and Electronic Engineering  
Bangladesh University of Engineering and Technology (BUET),  
Dhaka-1205, Bangladesh.  
Member
4.   
\_\_\_\_\_  
**Dr. Md. Anwarul Abedin**  
Professor  
Department of Electrical and Electronic Engineering  
Dhaka University of Engineering and Technology (DUET),  
Gazipur, Bangladesh.  
Member  
(External)

## CANDIDATE'S DECLARATION

It is hereby declared that this thesis or any part of it has not been submitted elsewhere for the award of any degree or diploma.

Signature of the Candidate

  
..... 31/3/18

**Tanvir Ahmad**

**Dedicated**  
**To**  
**My Parents & Honorable Teachers...**

# Acknowledgement

I would like to express my heartiest gratitude to the Almighty Allah for providing me the strength to complete this thesis work. After the Almighty, it is my great pleasure to express gratitude to the people who made this thesis possible. Foremost, I would like to express my deepest gratitude to my honorable thesis supervisor Dr. Md. Ziaur Rahman Khan, Professor, Department of Electrical & Electronic Engineering, Bangladesh University of Engineering and Technology (BUET), for giving me the opportunity to work on this topic under his supervision. It was his enduring support, encouragement, motivation and guidance that has made this work possible. My supervisor's expertise, understanding and patience added significantly to my graduate experience.

I would like to acknowledge Prof. Dr. A.M.M. Safiullah, Vice-Chancellor, Ahsanullah University of Science & Technology (AUST), for permitting me to pursue my M.Sc. degree. My heartiest thank to Prof. Dr. Abdur Rahim Mollah, Dean, AUST and Prof. Dr. Satyen Biswas, Head, Department of Electrical & Electronic Engineering, AUST for allowing me with the facilities to complete the work.

I am also thankful to all the teachers and officials of the Dept. of EEE, BUET for their cooperation.

Finally, I am indebted to my family and friends for their relentless and invaluable support, love and encouragement.

# Abstract

A new improved model of isolated three port converter (ITPC) is designed along with single input triple output (SITO) attribute for solar home system (SHS). The input side of the converter is connected to a PV panel as a single input source and a battery is connected to provide the standalone system of the proposed converter. Spotlight of the system is focused on multilevel output from single input. A highly efficient topology “identically switched storage and load (ISSL) with shifted pulse” is proposed considering the drawbacks of existing topologies of earlier converters. The proposed model will incorporate with a single control scheme based on pulse width modulation plus phase angle shift (PPAS) to provide overvoltage and low voltage protection for triple output levels. Control scheme contains maximum power point tracking (MPPT) loop and output voltage control loop. MPPT can be implemented by controlling duty cycle of the converter switches by using “incremental conductance and integral regulator technique”. In the output voltage control loop the phase angle of the modulation carrier is the control variable and PI controller is used to regulate the output voltage. According to IDCOL (Infrastructure Development Company Limited), a typical SHS operates at a rated voltage of 12V DC and provides power to small electrical appliances. In IDCOL standard, it is also specified that the rated input and output voltage should be maintained within the range of 12V, 24V or 48V and 110V-240V, respectively. In SHS installed in Bangladesh 125 V DC is used for longer distance transmission within the same house. The proposed system is simulated in MATLAB/SIMULINK platform. The proposed system shows the better performance than the earlier systems. Three distinct voltage levels 80V, 60V, 40V show better and stable output. The simulated efficiency of the proposed system is 98%. A practical circuit is implemented in laboratory and various data is extracted from the circuit. The simulation output is compared with practical data. The efficiency of the practical data is also high. The circuit can be used to optimize the performance of the SHS in Bangladesh.

# TABLE OF CONTENTS

<b>Certificate of Approval</b>	<b>ii</b>
<b>Declaration</b>	<b>iii</b>
<b>Dedication</b>	<b>iv</b>
<b>Acknowledgement</b>	<b>v</b>
<b>Abstract</b>	<b>vi</b>
<b>Acronyms</b>	<b>x</b>
<b>List of Tables</b>	<b>xi</b>
<b>List of Figures</b>	<b>xii</b>

<b>Chapter 1</b>	<b>Introduction</b>	
1.1	Renewable Energy	1
1.2	Renewable Energy Prospect for Power Generation	3
1.3	Prospect of Solar Energy in Present World	6
1.4	Present Energy State and Prospect of Solar energy in Bangladesh	7
1.5	Literature Review	9
	1.5.1 Triple active bridge	10
	1.5.2 Multilevel power converter	10
1.6	Problem identification & Thesis motivation	12
1.7	Thesis objectives	13
1.8	Thesis organization	13
<b>Chapter 2</b>	<b>Isolated Switching Mode Power Supply (SMPS) DC-DC Converter</b>	
2.1	Advantages of SMPS over Linear Switching	14
2.2	Advantage of Isolated converter over non isolated converter	15
2.3	Isolated SMPS DC-DC converter Topologies	15
	2.3.1 Flyback Converter	15
	2.3.2 Forward Converter	18
	2.3.3 Push-Pull Converter	20
	2.3.4 Half-Bridge Converter	22
	2.3.5 Full-Bridge Converter	23
	2.3.6 Ringing Choke Converter	25

2.3.7	Combined Forward-Flyback Converter	26
2.3.8	Current Source DC-DC Converter	27
2.4	Photovoltaic power generation	28
2.5	Electrical Model of PV Cell	29
2.5.1	One Diode Model	30
2.5.2	Double Diode Model	30
2.5.3	Different Parameters	31
2.5.4	Efficiency	31
2.6	PV characteristics	32
2.6.1	Maximum Power Point Tracker (MPPT)	33
2.6.1.1	Fixed duty cycle	34
2.6.1.2	The Beta method	34
2.6.1.3	Perturb and observe	35
2.6.1.4	Incremental conductance	36
2.6.1.5	Constant voltage and current	36
2.6.1.6	Fractional open-circuit voltage	37
2.6.1.7	Modified open-circuit voltage method	37
2.6.1.8	Pilot cell	37
2.6.1.9	Some other MPPT technique	37
2.7	Emerging applications of solar PV technology	38
2.6.1	Solar home lighting systems	38
<b>Chapter 3</b>	<b>Single Input Triple Output (SITO) Isolated DC-DC converter</b>	
3.1	Overview	41
3.2	Proposed SITO Converter	42
3.2.1	Operating Modes of Proposed Converter	45
3.2.2	Operating Principle of Converter	45
3.2.3	Operating Principle of Battery Circuit and Load Circuit	50
3.3	Analysis of Converter Efficiency Regarding Duty Ratio	54
3.3.1	Analysis of Circuit Performance for $D \geq 0.5$	54
3.3.2	Analysis of Circuit Performance for $D < 0.5$	57
3.3.3	Simulated Result	60
3.4	Control Circuit	61

	3.4.1 Incremental Conductance and integral control technique	63
	3.4.2 Proportional integral controller	66
<b>Chapter 4</b>	<b>Comparison between Experimental and Simulated Work</b>	
4.1	Simulink Model of the circuit	69
4.2	Simulated Waveforms	71
	4.2.1 Electrical Properties	74
	4.2.2 Designed Parameters	75
	4.2.3 Observation	76
4.3	Experimental Setup	78
	4.3.1 Waveforms	78
	4.3.2 Comparison between Simulated data and practical data	81
<b>Chapter 5</b>	<b>Conclusion</b>	
5.1	Future Scope	83
<b>References</b>		

## Acronyms:

Bcf	Billion Cubic Feet
BIPV	Building Integrated Photovoltaics
CM	Common mode
CRT	Cathode ray tube
DCM	Discontinuous conduction mode
EMC	Electromagnetic compatibility
FC	Fuel cell
GHG	Green house gas
GW	Gigawatts
HVDC	High Voltage Direct Current
IDCOL	Infrastructure Development Company Limited
IncCond	Incremental Conductance
ISSL	Identically Switched Storage and Load
ITPC	Isolated three port converter
LVDC	Low Voltage Direct Current
MATLAB	Matrix Laboratory
MOSFET	Metal Oxide Field Effect Transistor
Mtoe	Million Tonnes of oil equivalent
PI	Proportional integral
PS	Phase shift
PV	Photovoltaic
PWM	Pulse width modulation
RE	Renewable energy
SEDA	Sustainable Energy Development Authority
SHS	Solar home system
SIMO	Single input multiple outputs
SITO	Single input triple output
SMPS	Switching Mode Power Supply
SPST	Single pole single throw
TAB	Triple active bridges
ZVS	Zero voltage switching

## List of Tables

<b>Table no.</b>	<b>Content</b>	<b>Page no.</b>
Table 1.1	World RE use by type	5
Table 1.2	Bangladesh's Power Sector at a Glance (2016)	8
Table 1.3	Country's Renewable Energy State at a Glance	9
Table 3.1	Effect of Duty cycle and phase shift angle of MOSFETs' on output voltage of DC-DC converter	60
Table 4.1	Electrical properties of input and output Flyback-Forward converter	74
Table 4.2	Electrical Properties of output levels	74
Table 4.3	Parameters of PV module	75
Table 4.4	Parameters of Isolated Flyback-Forward converter	75
Table 4.5	Parameters of Multiple output level circuit	76
Table 4.6	Parameters of Battery circuit	76
Table 4.7	Design control parameters	76
Table 4.8	Parameters of the prototype single input dual output converter	81
Table 4.9	Comparison between practical data and simulated data	82

# List of Figures

Figure no.	Content	Page no.
Figure 1.1	Estimated Renewable Energy Share of Global Final Energy Consumption, 2014	2
Figure 1.2	Average Annual Growth Rates of Renewable Energy Capacity and Biofuels Production, End-2010 to End-2015	3
Figure 1.3	Overview of RE sources	4
Figure 1.4	Energy resources of the world	4
Figure 1.5	Share of renewable by category	6
Figure 1.6	Electricity Generation Capacity of Bangladesh (by fuel)	8
Figure 2.1	Equivalent Circuit of Flyback converter	16
Figure 2.2	Mode-I Equivalent Circuit of Flyback converter	16
Figure 2.3	Mode-II Equivalent Circuit of Flyback converter	17
Figure 2.4	Waveshapes for Continuous conduction mode	17
Figure 2.5	Mode-III Equivalent Circuit of Flyback converter	17
Figure 2.6	Waveshapes of Discontinuous conduction Mode	18
Figure 2.7	Conventional Forward converter.	18
Figure 2.8	Mode-I Equivalent Circuit of Forward converter	19
Figure 2.9	Mode-II Equivalent Circuit Forward converter	19
Figure 2.10	Waveshapes for Forward converter	20
Figure 2.11	Push Pull converter (a) schematic diagram (b) waveshapes	21
Figure 2.12	Half Bridge Converter (a) schematic diagram (b) waveshapes	23
Figure 2.13	Full-Bridge converter (a) schematic diagram (b) waveshapes	24
Figure 2.14	Ringing Choke converter	25
Figure 2.15	Equivalent Circuit of Ringing Choke converter during (a) transistor on interval (b) transistor off interval	25
Figure 2.16	Waveforms of the reactor current $i_L$ and the output voltage $e_o$ Current Combined	26
Figure 2.17	Combined Forward-Flyback converter	27
Figure 2.18	Current source DC-DC converter	27
Figure 2.19	Schematic representation of photovoltaic power generation system	28
Figure 2.20	Electrical Model of One-Diode PV Cell	30
Figure 2.21	Electrical Model of Double-Diode PV Cell	30
Figure 2.22	PV current versus voltage characteristics	32
Figure 2.23	PV power characteristics for different irradiation levels	33
Figure 2.24	PV power characteristics for different temperature levels	33
Figure 2.25	Block diagram of the Beta method	35

<b>Figure no.</b>	<b>Content</b>	<b>Page no.</b>
Figure 2.26	Flow chart of perturb and observe method	35
Figure 2.27	Block diagram of Constant voltage MPPT technique	36
Figure 2.28	$V_{MPP}$ as a percentage of $V_{OC}$ as functions of temperature and irradiance	36
Figure 2.29	(a) OFF-grid AC solar power systems to provide power for normal AC appliances (b) OFF-grid DC solar power systems to provide power for only DC appliances	40
Figure 3.1	Overall system associated with SITO converter	41
Figure 3.2	Schematic of SITO converter	43
Figure 3.3	Schematic of “Battery circuit”	44
Figure 3.4	Schematic of “Triple output level circuit”	45
Figure 3.5	Three operation modes of the proposed system	45
Figure 3.6	Waveforms of the converter under Mode I	46
Figure 3.7	(a) Operating state 1 of the converter in mode 1 (b) Operating state 2 of the converter in mode 1 (c) Operating state 3 of the converter in mode 1 (d) Operating state 4 of the converter in mode 1	46 47 47 48
Figure 3.8	Schematic of the converter for “mode 2” operation	48
Figure 3.9	(a) Schematic of the converter for “mode 3” operation (b) Waveforms of the converter under “Mode 3”	49 49
Figure 3.10	Switching pulses of “Identically Switched Storage and Load (ISSL) with Shifted Pulse” topology	50
Figure 3.11	(a) “State 1” Operation of the “Battery Circuit” (b) “State 1” Operation of the “Triple Output Level Circuit”	51 52
Figure 3.12	(a) “State 2” Operation of the “Battery Circuit” (b) “State 2” Operation of the “Triple Output Level Circuit”	52 53
Figure 3.13	(a) “State 3” Operation of the “Battery Circuit” (b) “State 3” Operation of the “Triple Output Level Circuit”	53 54
Figure 3.14	Five operational cases for $D \geq 0.5$	55
Figure 3.15	Signal Waveform for Case 1	56
Figure 3.16	Five cases under $D < 0.5$	58
Figure 3.17	Waveshapes of Output voltage Vs. Phase angle of 4 converter switches for different combinations of duty ratio	61
Figure 3.18	Schematic of control circuit	62
Figure 3.19	Photovoltaic array power-voltage relationship	64
Figure 3.20	Incremental conductance algorithm flowchart	66

<b>Figure no.</b>	<b>Content</b>	<b>Page no.</b>
Figure 3.21	PI controller Structure	67
Figure 4.1	SIMULINK model of the entire circuit	69
Figure 4.2	SIMULINK blocks and parameters of converter, battery circuit and control circuit.	70
Figure 4.3	SIMULINK blocks of feedback control circuit	70
Figure 4.4	SIMULINK model of load circuit	71
Figure 4.5	Voltage of solar panel	71
Figure 4.6	Current of solar panel	72
Figure 4.7	Gate pulses of the ITPC	72
Figure 4.8	Multilevel voltage waveshapes	73
Figure 4.9	Multilevel current waveshapes	73
Figure 4.10	Gate pulses of dynamic ISSL scheme	74
Figure 4.11	Overall Experimental Setup	78
Figure 4.12	Top View of Individual Blocks	79
Figure 4.13	Two level Outputs from single input	79
Figure 4.14	Gate Pulses for Isolated Flyback-Forward Converter	80
Figure 4.15	Gate Pulses for Isolated Flyback-Forward Converter	80
Figure 4.16	Gate Pulses for Battery and Load circuit	81

# **Chapter 1**

## **Introduction**

Solar energy is the abundant source of electricity. A country like Bangladesh, which is located in a suitable global position, receives a large amount of annual sunlight. Bangladesh has topped a global list of countries that have installed the highest number of solar home systems (SHS) [1-3]. With four million of the systems set up so far, the country is also at the forefront of nations using clean stoves and biogas plants, and promoting the cause of renewable energy that constitutes a fifth of the world's final power consumption. This growth in renewable energy use also helped increase employment in Bangladesh. As of 2016, more than 6 million SHS and kits were in operation worldwide, with 25 million people benefiting from them. Bangladesh, the largest SHS market worldwide, now has more than 4 million units installed [1]. Currently, 2.86 percent of all power generated in the country comes from renewable energy, including solar power, according to power and energy ministry data. The cumbersome process of providing electricity access through grid extension alone is becoming obsolete, as new business models and technologies enables the development of off-grid markets. Approximately 60 million people or 38 percent of the population in Bangladesh have no access to electricity [1]. Standalone PV solar home system (SHS) is one of the best solutions to provide the user suitable means of energy for small electrical loads. Earlier single input multiple output (SIMO) DC-DC converters are designed. But using isolated converter with reduction of switching complexity and losses couldn't be achieved. Along with better control of input and output at a time is not concentrated yet. A system is proposed in this work for multilevel high efficient DC-DC converter with better control of input and output at a time, where power is being transmitted simultaneously to shorter and longer distances. Multilevel DC-DC converter is one of the best solution for SHS to provide electricity from a single source of PV to multiple loads. It reduces both cost and complexity.

### **1.1 Renewable Energy**

Renewable energy sources including biomass, geothermal, ocean, solar, and wind energy, as well as hydropower have a huge potential to provide a healthy energy services for the world. The renewable energy resource base is sufficient to meet several times the present world energy demand and potentially even 10 to 100 times than the demand [3].

Renewable energy is growing faster in recent days. In the year 2015 had seen a new era of developments that all have a bearing on renewable energy including a massive decline in global fossil fuel prices [1],[4]. Rapid growth of renewable energy throughout the world has taken the mainstream source of energy. The year 2015 was of high-profile agreements and announcements related to renewable energy [1]. Renewable energy (RE) provided an estimated 19.2% (Figure 1.1) of global final energy consumption in 2014, and growth in capacity and generation continued in 2015 [5]. An estimated 147 gigawatts (GW) of renewable power capacity was added in 2015 [2], the largest annual increase ever. The power sector is blessed by renewable energy significantly. RE like, wind and solar PV has now increased to 77% (Figure 1.2). By the end of 2015, renewable capacity in place was enough to supply an estimated 23.7% of global electricity, with hydropower providing about 16.6% [6]. In 2015 and early 2016, expectations of further cost improvements were made evident by record low winning bids in power auctions in places ranging from Latin America, to the Middle East and North Africa region, to India [1]. Developing countries like Bangladesh is now relying on renewable energy, and other developing countries (e.g., Kenya, Uganda and Tanzania in Africa; China, India and Nepal in Asia; Brazil and Guyana in Latin America) are seeing rapid expansion of small-scale renewable systems, including renewables-based mini-grids, to provide electricity for people living far from the grid. Developed countries and regions– including Australia, Europe, Japan and North America – have seen significant growth in numbers of residential and industrial electricity customers who produce their own power [1].



Figure 1.1: Estimated Renewable Energy Share of Global Final Energy Consumption, 2014[1]

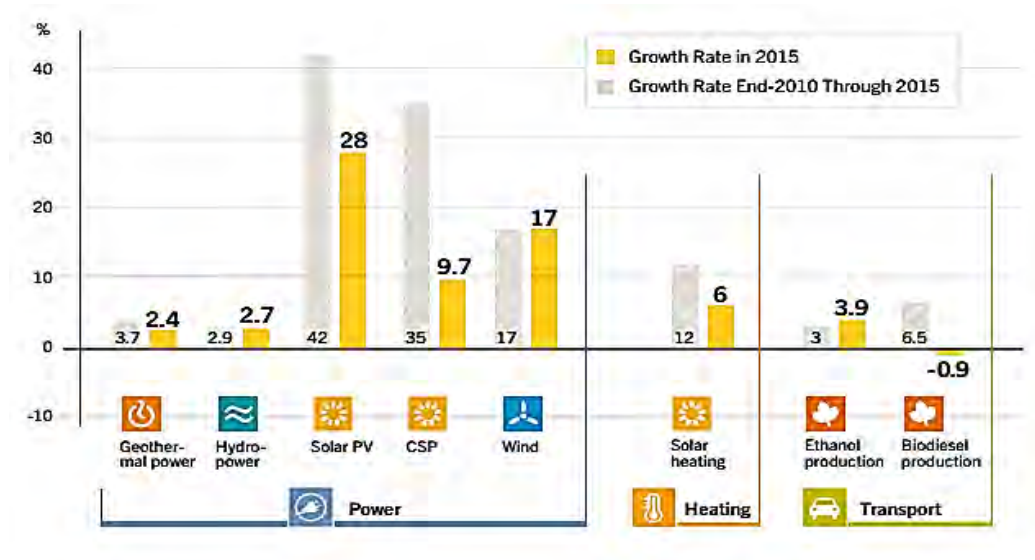


Figure 1.2: Average Annual Growth Rates of Renewable Energy Capacity and Biofuels Production, End-2010 to End-2015[1]

Demand for energy and associated services, to meet social and economic development and improve human welfare and health is increasing. All societies require energy services to meet basic human needs (e.g., lighting, cooking, space comfort, mobility and communication) and to serve productive processes. Worldwide usage of fossil fuels (coal, oil and gas) has increased to dominate energy supply, leading to a rapid growth in carbon dioxide (CO<sub>2</sub>) emissions. Recent data confirm that consumption of fossil fuels accounts for the majority of global anthropogenic greenhouse gas (GHG) emissions. Emissions continue to grow and CO<sub>2</sub> concentrations had increased to over 390 ppm, or 39% above preindustrial levels, by the end of 2010 [7].

So, having a large potential to mitigate climate change, RE can provide wider benefits. RE may, if implemented properly, contribute to social and economic development, energy access, a secure energy supply, and reducing negative impacts on the environment and health.

## 1.2 Renewable Energy Prospect for Power Generation

Renewable energies are energy sources that are continually refilled by nature and derived directly from the sun (such as thermal, photo-chemical, and photo-electric), indirectly from the sun (such as wind, hydropower, and photosynthetic energy stored in biomass), or from other natural movements and mechanisms of the environment (such as geothermal and tidal energy) [8]. Renewable energy does not include energy resources

extract from fossil fuels, waste products from fossil sources, or waste products from inorganic sources.

Figure 1.3 shows an overview of renewable energy sources. Renewable energy technologies turn these natural energy sources into usable forms of energy; such as electricity, heat and fuels.

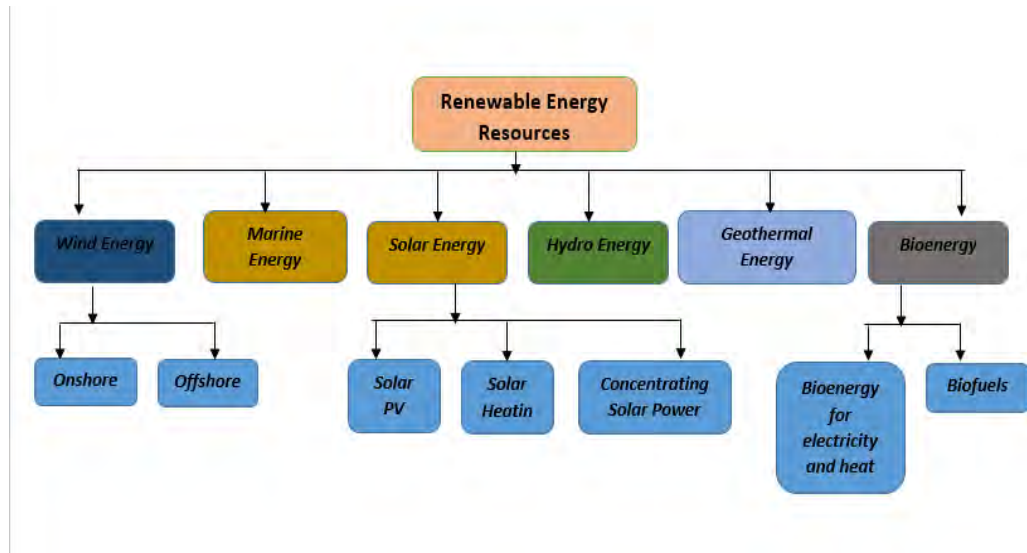


Figure 1.3: Overview of RE sources [3]

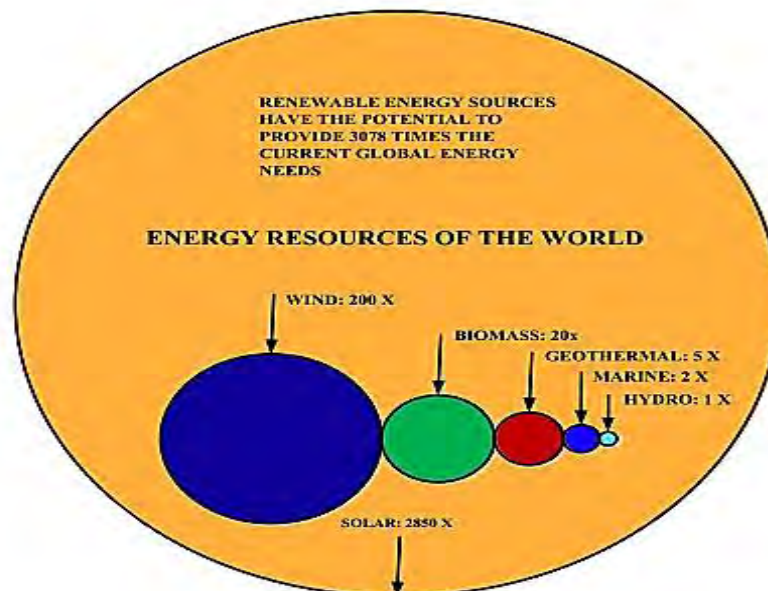


Figure 1.4: Energy resources of the world [3]

Figure 1.4 illustrates the ability of renewable energy sources to provide over 3000 times the current global energy needs [9]. Renewable energy markets of electricity, heating and transportation have been growing sharply over the last five years. The installation of

established technologies, such as hydro, as well as newer technologies such as wind and solar photovoltaic, has risen quickly, which has increased confidence in the technologies, reduced costs and opened up new opportunities.

Global electricity generation from renewable energy sources is expected to grow 2.7 times between 2010 and 2035 [10], as indicated by Table 1.1. Consumption of biofuels is projected to more than triple over the same period to reach 4.5 million barrels of oil equivalent per day (mboe/d), up from 1.3 mboe/d in 2010 [11]. Almost all biofuels are used in road transport, but the consumption of aviation biofuels will make an inroad towards 2035. The use of modern renewables to produce heat will almost double, from 337 Mtoe in 2010 to 604 Mtoe in 2035 [9]. The share of renewables in electricity generation is higher than in heat production or transportation road, as shown in Figure 1.5.

Table 1.1: World RE use by type [3]

Year	2010	Forecasted Result	
		2020	2035
<b>Electricity generation(TW h)</b>	<b>4206</b>	<b>69999</b>	<b>11342</b>
Bioenergy	331	696	1487
Hydro	3431	4513	5677
Wind	342	1272	2681
Geothermal	68	131	315
Solar PV	32	332	846
Concentrating Solar Power	2	50	278
Marine	1	5	57
Share of Total generation	20%	25%	31%
Heat Demand (Mtoe)	337	447	604
Industry	207	263	324
Building and agriculture	131	184	280
Share of total production	10%	12%	14%
Biofuels (mboe/d)	1.3	2.4	4.5

Road transport	1.3	2.4	4.4
Aviation	-	-	0.1
Share of total transport	2%	4%	6%

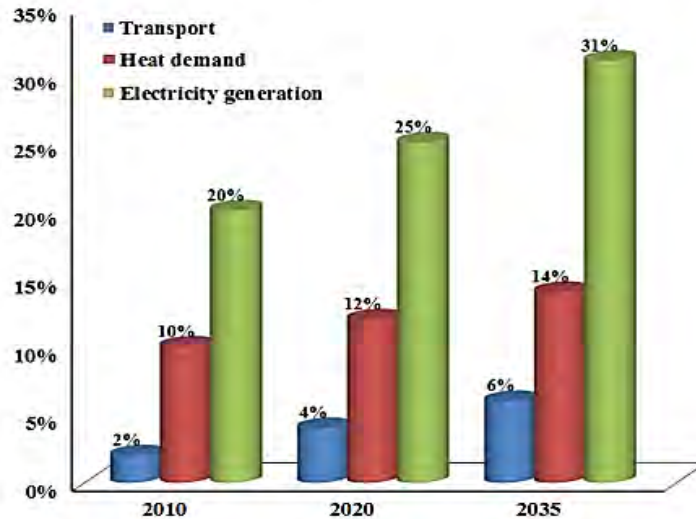


Figure 1.5: Share of renewable by category [3]

### 1.3 Prospect of Solar Energy in Present World

Solar energy is one of the renewable energy sources that has clear environmental advantages over other energy sources and will never diminish as a natural resource, and free from CO<sub>2</sub> emission, or liquid or solid waste products [12-14].

Photovoltaic (PV) is the direct transfiguration of sunlight into electricity, is advantageous in many ways [15]:

- Produce clean electricity without the help of machines or any moving devices.
- It is an inexhaustible energy source.
- PV systems offer longer service times with minimum maintenance costs.
- PV elements are scratchy and simple to design.

The efficiency of PV cell is affected by local environmental temperature, relative humidity, dust in air, and global solar radiation intensity and it varies between 40–60% for low to medium temperature [16-17]. PV technology is more suitable for off-grid applications of low to medium power in remote areas due to its reliability and ease scaling of input source. Along with the efficiency improvement, this technology is blessed with techno-economic feasibility. Solar energy is the primary source of energy and abandon in the earth. It has been estimated that the solar energy coming to the earth is almost 5000

times higher than the total supplied primary energy in the world. Considering the average daily solar irradiation  $200 \text{ W/m}^2$  and cross sectional area of earth  $127,400,000 \text{ m}^2$ , it is estimated that the earth receives about 222,504,000 Tera watt hours solar energy per year equivalent to 19,349,957 Mtoe [18].

Solar power generation demand increases worldwide as countries strive to reach goals for emission reduction and renewable power generations. Malaysia has a target of 40% less emissions by 2020. Malaysia's SEDA (Sustainable Energy Development Authority) has developed many strategies to increase the country's usage of solar energy as the primary source of energy by 2050.

European countries have taken different steps and utilized different policies to develop renewable energy systems that increase the share of renewable energy, to reduce  $\text{CO}_2$ , and reduce dependency on fossil fuels [18]. Japan targets to develop R&D, provide incentives for installation, and to install easily with lower investment costs. In Germany PV roof program soft loans introduced to increase the SHS program. In France, total PV production capacity was 1054 MW in 2010. By providing the FiT (Feed in Tariff), tax reductions, and subsidies, the total PV production increased to 2500 MW in 2011. China also rolled out two national solar subsidies programs: the Building Integrated Photovoltaics (BIPV) subsidy program and the Golden Sun program.

We can summarize this section as overcoming the negative impacts on the environment caused by fossil fuels, many countries have been forced to move on environmental friendly alternative energy sources. So, PV is a proper solution for betterment of our future generation and drag the world to a new era of green energy.

#### **1.4 Present Energy State and Prospect of Solar energy in Bangladesh**

Lack of access to electricity is one of the major impediments to the economic growth and development for any developing country. As well as limited reserve of conventional fuel and geo-location of Bangladesh arise the demand to find an effective alternative energy source, especially for rural electrification [19]. Figure 1.6 presents that natural gas is used as main fuel for electricity generation in Bangladesh [20]. Alarming issue is that, the country's gas reserves stand at 14.16 trillion cubic feet (tcf) as of June 2015 and 12.96 bcf (billion cubic feet) gases was extracted until May, 2015 [19],[22]. If the current rate of extraction remains unchanged, the reserve would last until 2031.

Bangladesh lies between  $20^\circ 34'$  and  $26^\circ 38'$  north latitude and  $88^\circ 01'$  and  $92^\circ 41'$  east longitude, which is an ideal location for harnessing solar energy effectually. The solar

intensity varies according to the seasonal and climatic conditions of the country with a daily average between 4 and 6.5kWh/m<sup>2</sup> [23]. Taking in account the daily average solar radiation, the total solar energy available in Bangladesh is estimated about (1018 X 10<sup>18</sup>) Joule.

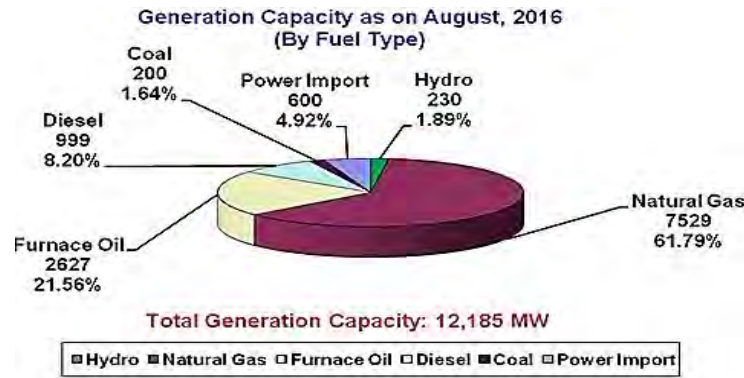


Figure 1.6: Electricity Generation Capacity of Bangladesh (by fuel) [20]

Table 1.2: Bangladesh's Power Sector at a Glance (2016) [24]

Generation Capacity : 12,365 MW* (July, 2016)
Highest Generation : 9,036 MW (30 June, 2016)
Total Consumers : 21.8 Million (June, 2016)
Transmission Line: 9,893 ckt. km (June,2016)
Distribution Line : 3,78,000 km (June,2016)
Distribution Loss : 10.69% (June,2016)
Per Capita Generation : 380 KWh (June,2016)
Access to Electricity : 76%

\*without captive and solar home system

According to Table 1.2, country provides electricity to only 76% of its population and maximum people in rural areas are living without electricity [20]. Under this circumstance solar based power generation could be found effective for country's development. Standalone off grid SHS is getting momentum and becoming the most effective option to rural electrification due to the high increase rate of kerosene price. Table 1.3, gives an outline of present renewable energy state in Bangladesh [21].

Bangladesh government has declared a vision to eliminate load shedding and electrify the entire country by 2020. Thus initiatives should take to expand solar mini-grid in off-grid areas to avoid the high distribution cost of grid connection.

Table 1.3: Country's Renewable Energy State at a Glance [24]

	<b>Mwatt</b>
Solar home system	175
Solar system for government and private offices	3
Solar system for commercial buildings and shopping malls	1
Solar PV installation for new electricity connection	11
Solar irrigation	2
Wind based power plant	2
Biomass based electricity	1
Biogas based electricity	5
Hydro	230
Total	430

### 1.5 Literature Review

Photovoltaic (PV) is direct transformation of sunlight energy into electricity. Different materials have been developed to make of PV modules. Relatively low light to electricity power conversion ratio, reaching 30%, is the main disadvantage of commercially available PV modules. Hence, low voltage photovoltaic systems require highly efficient converters to deliver as much as possible energy to the load with high gain DC voltage conversion [25].

Standalone systems are isolated from the electric distribution grid. The number of components in the system will depend on the type of the load that is being served. DC-DC converter is needed to be connected with PV module for DC load. Whereas, system requires inverter in case of AC load [26-28].

A chopper is a static power electronic device that converts fixed DC input voltage to a variable DC output voltage and known as DC-DC converter [29]. Function of DC-DC converter is to shift DC power to another DC power level [30-31]. Hence it can be considered as DC equivalent to an AC transformer with a continuously variable turns ratio. At present, DC-DC switching converters are at the base of both small electronic devices and of industrial equipment's. High efficiency, high power density, fast dynamic response, low cost and easy control make them advantageous in power electronic world. There are two types of DC-DC converters; non-isolated and isolated; our main focus is on isolated three port DC-DC converter. Isolated converter topologies include: Flyback

converter, Forward converter, Push-Pull converter, Half Bridge converter, Full Bridge converter, Ringing Choke converter, Combined Forward-Flyback converter, Current Source DC-DC converter.

Several articles are found to address different limitations of conventional DC-DC converters for PV applications.

### **1.5.1 Triple active bridge**

The isolated three-port converter (ITPC) utilizes the triple active bridges (TAB) with inherent features of power controllability and zero voltage switching (ZVS). Their soft-switching performance can be improved if two series-resonant tanks are implemented. An advanced modulation strategy is reported in [32] which incorporates a phase shift (PS) and a pulse width modulation (PWM) to extend the operating range of ZVS. Nonetheless, the TAB topology suffers from the circuit complexity using three active full bridges or half bridges and the power loss caused by reactive power circulation.

Therefore, a Buck-Boost converter [33] is proposed to integrate a three-port topology in the half bridge and to decompose the multivariable control problem into a series of independent single-loop subsystems. By doing so, the power flow in each loop can be independently controlled. The system is suitable for PV-battery applications since one converter interfaces the three components of the PV array, battery, and loads.

### **1.5.2 Multilevel power converter:**

Multilevel converters can be used to interface with renewable energy and/or distributed energy resources because several batteries, fuel cells, solar cells, wind turbines, and micro turbines can be connected through a multilevel converter to supply a load or the ac grid without voltage balancing problems. In [30] author presents detailed discussion regarding multilevel converters. A multilevel converter has several advantages over a conventional two-level converter that uses high switching frequency PWM.

The attractive features of a multilevel converter can be briefly summarized as follows-

a) Staircase waveform quality:

Multilevel converters not only can generate the output voltages with very low distortion, but also can reduce the  $dv/dt$  stresses; therefore, electromagnetic compatibility (EMC) problems can be reduced.

b) Common-mode (CM) voltage:

Multilevel converters produce smaller CM voltage; therefore, the stress in the bearings of a motor connected to a multilevel motor drive can be reduced. Furthermore, CM voltage can be eliminated by using advanced modulation strategies such as that proposed in [38].

c) Input current:

Multilevel converters can draw input current with low distortion.

d) Switching frequency:

Multilevel converters can operate at both fundamental switching frequency and high switching frequency PWM. It should be noted that lower switching frequency usually means lower switching loss and higher efficiency.

Major Multilevel converter topologies include: Cascaded H-Bridges, Diode-Clamped Multilevel Inverter and Flying Capacitor Multilevel Inverter [39].

The number of possible output voltage levels is more than twice the number of DC sources ( $m = 2s + 1$ ) for “Cascaded H-Bridges” topology [39]. The series of H-bridges makes for modularized layout and packaging. This will enable the manufacturing process to be done more quickly and cheaply. But it has the disadvantage that separate DC sources are required for each of the H-bridges. This will limit its application to products that already have multiple SDCSs readily available.

Merits of “Diode-Clamped Multilevel” [40] topology are that, all of the phases share a common DC bus, which minimizes the capacitance requirements of the converter; The capacitors can be pre-charged as a group; efficiency is high for fundamental frequency switching. Demerits are as real power flow is difficult for a single inverter because the intermediate DC levels will tend to overcharge or discharge without precise monitoring and control; and the number of clamping diodes required is quadratically related to the number of levels.

Complicated control strategy, poor efficiency for real power transmission and the presence of expensive and bulky capacitors are the disadvantages of “Flying Capacitor Multilevel” topology.

However, it has the advantages of large number of capacitors that enable the converter to ride through short duration outages and deep voltage sags [41]. Phase redundancies are available for balancing the voltage levels of the capacitors. Real and reactive power flow can also be controlled in this topology.

Patra et al. [42] presented a SIMO DC-DC converter capable of generating buck, boost, and inverted outputs simultaneously. However, over three switches for one output were required. This scheme is only suitable for the low output voltage and power application, and its power conversion is degenerated due to the operation of hard switching.

Nami et al. [43] proposed a new DC-DC multi-output boost converter, which can share its total output between different series of output voltages for low- and high-power applications. Unfortunately, over two switches for one output were required, and its control scheme was complicated. Besides, the corresponding output power cannot be supplied for individual loads independently.

Chen et al. [44] investigated a multiple-output DC-DC converter with shared zero-current switching (ZCS) lagging leg. Although this converter with the soft-switching property can reduce the switching losses, this combination scheme with three full-bridge converters is more complicated, so that the objective of high-efficiency power conversion is difficult to achieve, and its cost is inevitably increased.

Wai et al. addresses a highly efficient multilevel converter with coupled inductor. Which has several advantages as the voltage gain can be substantially increased by using a coupled inductor. The stray energy can be recycled by a clamped capacitor into the auxiliary battery module or high-voltage DC bus to ensure the property of voltage clamping and an auxiliary inductor is designed for providing the charging power to the auxiliary battery module and assisting the switch turned ON under the condition of ZCS. Unfortunately, this converter is applicable only for non-isolated converter with step up attribute as well as increasing output level may complicate the converter circuit. Use of single switch limits the control activity to either input control or output control.

## **1.6 Problem identification & Thesis motivation:**

For long-distance transmission, HVDC [45] systems may be less expensive and suffer lower electrical losses. But cost and loss, both are increased for short distance. Thus arise the need of a compact system effective for both long and concise distance according to destination demand. According to IDCOL (Infrastructure Development Company Limited) for Bangladesh, a typical SHS operates at a rated voltage of 12V DC and provides power to small electrical appliances. Standards mentioned by IDCOL for HV system, the rated input (like 12V, 24V or 48V etc.) and the rated output voltage should be maintained within the range of 110V-240V [46-48]. For longer distance, transmission should be accomplished using HV system. As HV system is suffered from arcing

problems, voltage should be transmitted according to distance [49-51]. In SHS installed in Bangladesh 125 V DC is used for longer distance transmission within the same house. In converters like this HV is used even for lower distance. Such problems can be rectified by using a single input multiple output converter. A converter like this can divide voltage levels according to user's need. Earlier single input multiple output (SIMO) DC-DC converters are designed [52]. But the designed SIMO converter has problems like isolation, circuit complexity, limited number of output levels and restricted control strategy. So the system was not suitable for SHS rather applicable to only DC-DC conversion for multiple loads. A multi-level DC-DC isolated system is yet to be investigated.

### **1.7 Thesis objectives:**

The objectives of this work are:

1. To propose a dynamic SITO (single input triple output) isolated DC-DC converter providing different voltage levels for numerous loading conditions and affiliate it with a three port standalone photovoltaic system.
2. To design a single control scheme by merging “Incremental conductance and integral control” MPPT algorithm and PI controller for controlling diversified output voltage levels. Both phase-shifted control and pulse width modulation (PWM) techniques are served for this purpose.
3. To verify the proposed model with SIMULINK simulation results.

Successful completion of this work presents a model of isolated three port SITO converter with specific voltage levels considering distance and loading conditions.

### **1.8 Thesis organization:**

The remaining part of this thesis is organized in the following sequence:

**Chapter 2:** Presents a literature review of different isolated converters. Solar Cell Technology: Overview of PV cell model, MPPT, SHS and their future use and emerging technology.

**Chapter 3:** Proposes a SITO (single input triple output) isolated DC-DC converter providing multiple voltage levels for numerous loading conditions and affiliate it with a three port standalone photovoltaic system.

**Chapter 4:** Summarizes the practical work and comparison between simulated and practical data.

**Chapter 5:** Summarizes the research work presented in this thesis and discusses the scope for future works also.

## **Chapter 2**

### **Isolated Switching Mode Power Supply (SMPS) DC-DC Converter**

A switched-mode power supply (SMPS) is an electronic power supply that incorporates a switching regulator to convert electrical power efficiently. Like other power supplies, an SMPS transfers power from a DC or AC source (often-main power) to DC loads, such as a personal computer, while converting voltage and current characteristics. Unlike a linear power supply, the pass transistor of a switching-mode supply continually switches between low-dissipation, full-on and full-off states, and spends very little time in the high dissipation transitions, which minimizes wasted energy.

#### **2.1 Advantages of SMPS Over Linear Switching**

SMPS have efficiency of 68% to 90% regardless of the input voltage. Thus drastically reducing heat sink size, cost. Normally linear regulators have 30% to 60% efficiency. It means every watt delivered to the load, more than one watt is lost within the supply. This loss is called headroom loss. It occurs in the pass-transistor. Heat sink is required over the transistor for the heat dissipation. It occupies space and increase in system cost.

The power transistors within the switching mode power supply (SMPS) operate at their most efficient points of operation, saturation and cutoff. It means that the power transistors can deliver many times their power rating to the load and less expensive, lower power packages can be used. Since the input voltage is chopped into an AC waveform and placed into a magnetic element, additional windings can be added to provide for more than one output voltage. But linear power supply operates only as step down regulator.

For transformer-isolated switching power supplies, the output voltages are independent of the input voltage. i.e., the input voltage can vary above and/or below the level of output voltages without affecting the operation of the supply. Linear switching power supply has only one output voltage. To get additional output voltage, an entire separate linear regulator must be added. It increases system cost.

SMPS can be used as step up or step down regulator with smooth output as user's choice. Whereas, linear switching power supply can be used only as a step down regulator. In case of AC-DC power supplies, a transformer with rectification and filtering must be placed before the linear power supply. This pre-power conditioning increases the cost.

Frequency of operation of magnetic components (Inductors, Capacitors) is very much greater than line frequency. It reduces the size and cost of components particularly at high power levels. Linear regulators cannot be used for high power applications.

## **2.2 Advantage of Isolated converter over non isolated converter**

Non-isolated DC-DC converters are common and of lower cost, they are used in most negative ground application in vehicles for various DC powered appliances and equipment. However, they have one big disadvantage in the electrical connection between the input and output which offers little or no protection to the load for any high electrical voltage and current etc. occurs on the input side. They also have less noise filtering blockage.

Isolated DC-DC converters have high isolation (barrier) voltage from several hundreds to thousand volts depending on the type of standard. They can be used as negative grounded or positive ground or floating ground for various equipment's from data com to telecom. They have strong noise and interference blocking capability thus provide the load with a cleaner DC source which is required by many sensitive load [53].

## **2.3 Isolated SMPS DC-DC converter Topologies**

Isolated SMPS DC-DC converters are classified as

- a) Flyback converter
- b) Forward converter
- c) Push-Pull converter
- d) Half Bridge converter
- e) Full Bridge converter
- f) Ringing Choke converter
- g) Combined Forward-Flyback converter
- h) Current Source DC-DC converter

### **2.3.1 Flyback Converter**

Fly-back converter is the most commonly used SMPS circuits.

- Low output power applications.
- The output voltage needs to be isolated from the input main supply.
- The output power may vary from few watts to less than 100 watts.
- The circuit can offer single or multiple isolated output voltages.
- Operate over wide range of input voltage variation.

In respect of energy-efficiency, fly-back power supplies are inferior to many other SMPS circuits but it's simple topology and low cost makes it popular in low output power range. Typical efficiency of a fly-back converter is around 65%-75% [30-31, 54]

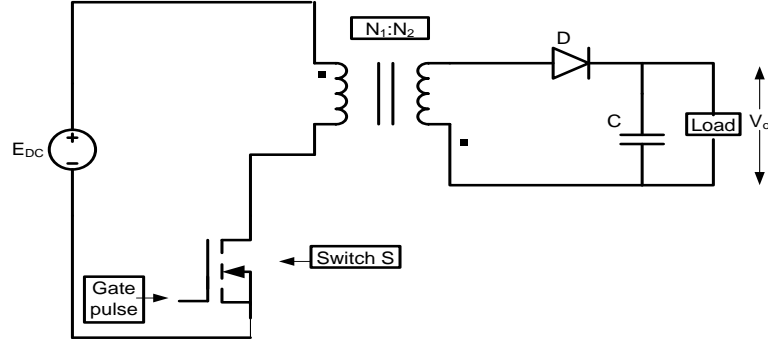


Figure 2.1: Equivalent Circuit of Flyback converter [31]

## Operation

### Mode-I:

Switch is ON; Diode is OFF;  $E_{DC} = L_{Pri} \cdot \frac{d}{dt} i_{Pri}$ .

At the end of Mode-1, energy stored in the primary winding is,  $\frac{L_{Pri} \cdot I_p^2}{2}$ .

When the switch is closed, the primary of the transformer is directly connected to the input voltage source. The primary current and magnetic flux in the transformer increases, storing energy in the transformer. The voltage induced in the secondary winding is negative, so the diode is reverse-biased (i.e., blocked). The output capacitor supplies energy to the output load.

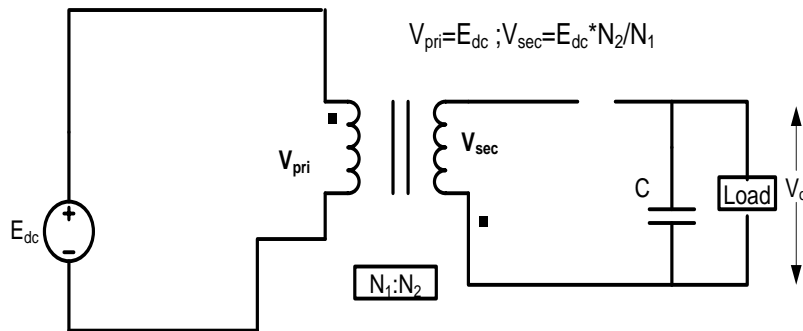


Figure 2.2: Mode-I Equivalent Circuit of Flyback converter [31]

### Mode-II:

When the switch is opened, the primary current and magnetic flux drops. The secondary voltage is positive, forward-biasing the diode, allowing current to flow from the

transformer. The energy from the transformer core recharges the capacitor and supplies the load.

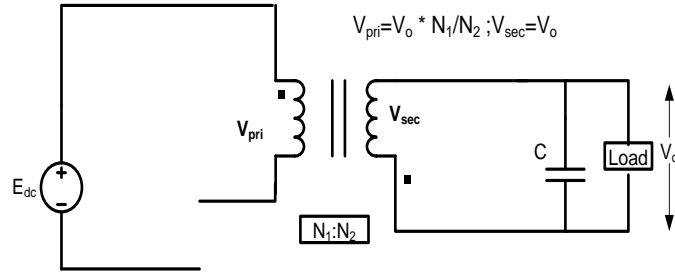


Figure 2.3: Mode-II equivalent circuit of Flyback converter [31]

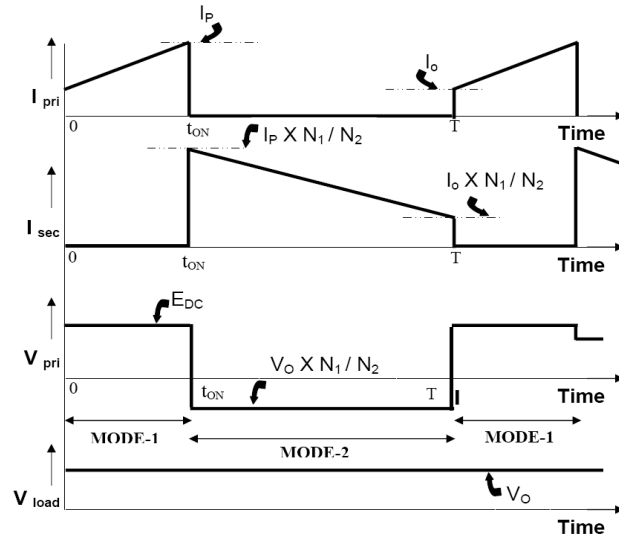


Figure 2.4: Waveshapes for continuous conduction mode [31]

### Mode-III:

During discontinuous mode, MOSFET is OFF; Diode is OFF. The output capacitor continues to supply uninterrupted voltage to the load.

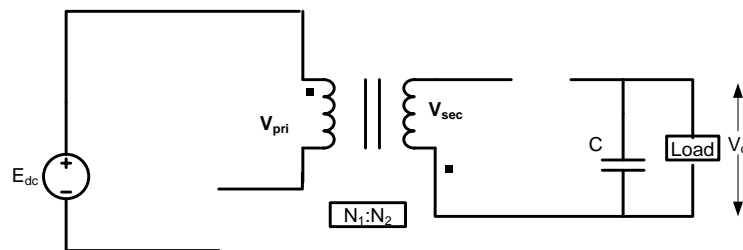


Figure 2.5: Mode-III equivalent circuit of Flyback converter [31]

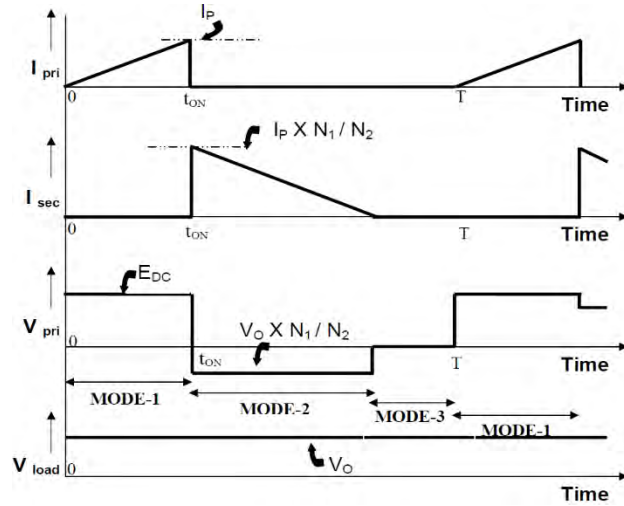


Figure 2.6: Waveshapes of discontinuous conduction Mode [31]

Output voltage of Flyback converter is mentioned below,

$$V_o = \frac{N_2}{N_1} \cdot \frac{D}{1 - D} \cdot E_{DC}$$

### 2.3.2 Forward Converter

Forward converter is another popular switched mode power supply (SMPS) circuit that is used for producing isolated and controlled DC voltage from the unregulated DC input supply. As in the case of fly-back converter the input DC supply is often derived after rectifying (and little filtering) of the utility ac voltage. The forward converter, when compared with the fly-back circuit, is generally more energy efficient and is used for applications requiring little higher power output (in the range of 100 watts to 200 watts). However, the circuit topology, especially the output filtering circuit is not as simple as in the fly-back converter [30-31, 55].

It consists of a fast switching device ‘S’ along with its control circuitry, a transformer with its primary winding connected in series with switch ‘S’ to the input supply and a rectification and filtering circuit for the transformer secondary winding. The load is connected across the rectified output of the transformer-secondary.

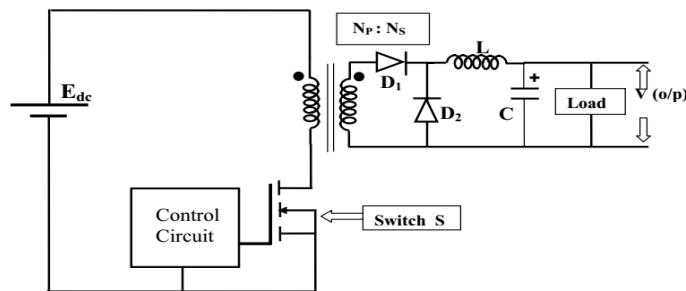


Figure 2.7: Conventional Forward converter [31]

## Operation:

### Mode-I:

Switch 'S' closed, diode D1 in the secondary circuit gets forward biased and the input voltage, scaled by the transformer turns ratio, gets applied to the secondary circuit. Diode D2 does not conduct during mode-1, as it remains reverse biased. The load gets a voltage equal to  $N_s/N_p \cdot E_{DC}$ .

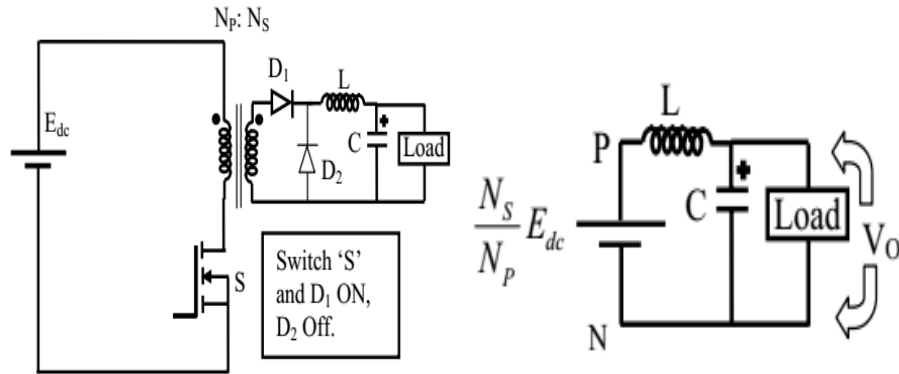


Figure 2.8: Mode-I equivalent circuit of Forward converter [31]

### Mode-II:

Points 'P' and 'N' of the equivalent circuit are effectively shorted due to conduction of diode 'D2'. The inductor current continues to flow through the parallel combination of the load and the output capacitor. During mode-2, there is no power flow from source to load but still the load voltage is maintained nearly constant by the large output capacitor 'C'. The charged capacitor and the inductor provide continuity in load voltage.

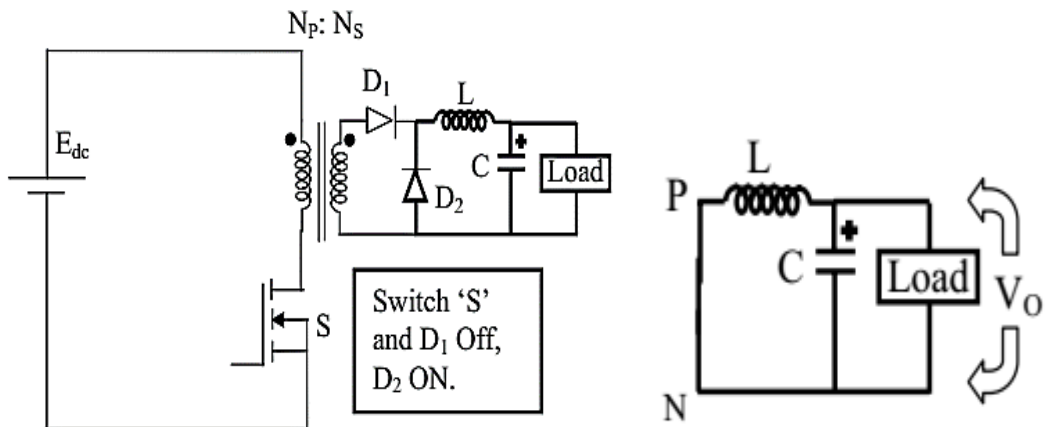


Figure 2.9: Mode-II equivalent circuit of Forward converter [31]

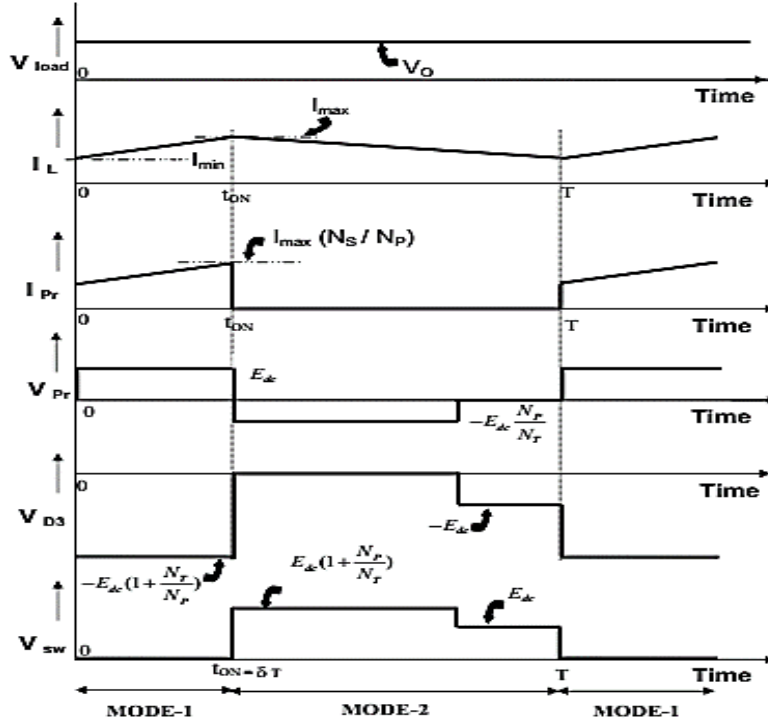


Figure 2.10: Waveshapes for Forward converter [31]

The instantaneous value of inductor voltage ( $e_L$ ) during mode-I can be written as:

$$e_L = \frac{N_S}{N_P} E_{DC} - V_o ; \text{ for } 0 \leq t \ll DT$$

Where  $t = 0$  is the time instant when mode-I of any steady state switching cycle starts,  $T$  is the switching time period that may be assumed to be constant and  $D$  is the duty ratio of the switch. It can be seen that  $DT$  is the time duration of mode-I and  $(1-D)T$  is the time duration of mode-II. The inductor voltage during mode-II may similarly be written as:

$$e_L = -V_o ; \text{ for } DT \leq t \ll T$$

Now,

$$\left[ \frac{N_S}{N_P} E_{DC} - V_o \right] \cdot D + [-V_o] \cdot (1 - D) = 0$$

$$V_o = D \cdot \frac{N_S}{N_P} E_{DC}$$

Under discontinuous inductor current, the relation between output voltage and switch duty ratio becomes non-linear and is load dependent.

### 2.3.3 Push-Pull Converter:

Push pull converter produces a square wave ac at the input of the high frequency transformer. A center tapped secondary is used, which results in only one diode voltage drop on the secondary side [31, 56].

**Mode -I:**

When  $T_1$  is on,  $D_1$  conducts and  $D_2$  gets reverse biased. This result in  $V_{oi} = \frac{N_2}{N_1} V_d - V_o$ .

Therefore, the voltage across the filter inductor is given as:

$$v_L = \frac{N_2}{N_1} V_d - V_o, 0 < t < t_{on}$$

And  $i_L$  through  $D_1$  increase linearly.

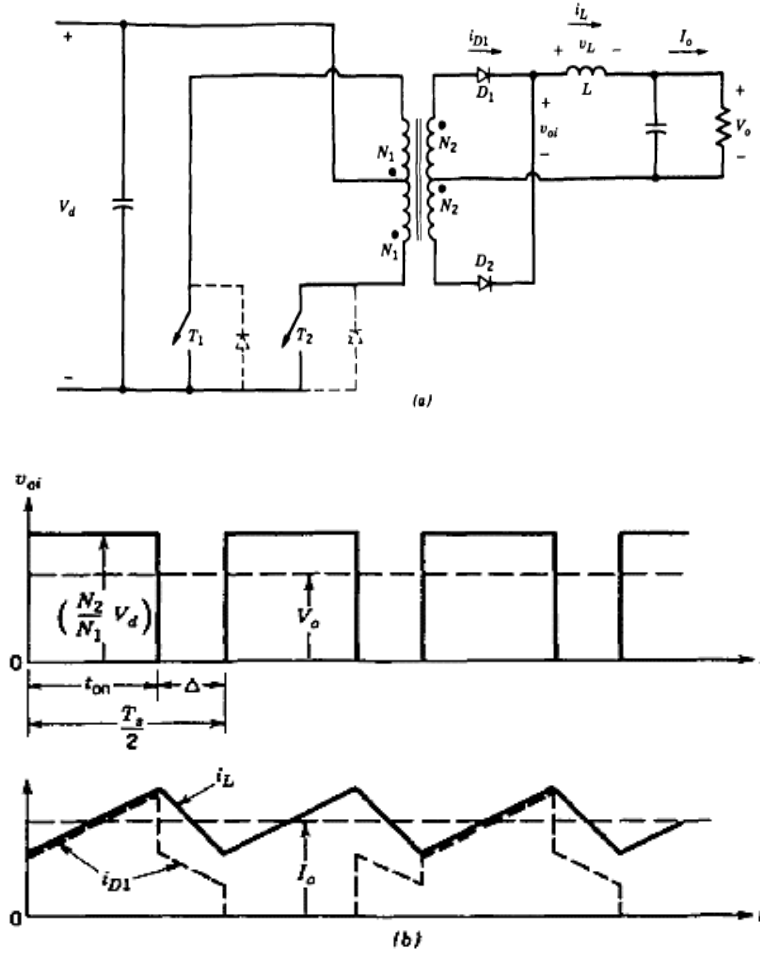


Figure 2.11: Push Pull converter (a) schematic diagram (b) waveshapes [56]

**Mode-II:**

During the interval  $\Delta$ , when both the switches are off, the inductor current splits equally between two secondary half windings and  $v_{oi} = 0$ . Therefore, during  $t_{on} < t < t_{on} + \Delta$ ,

$$v_L = -V_o$$

$$i_{D1} = i_{D2} = \frac{1}{2} i_L$$

The next half-cycle consists of  $t_{on}$  (during which T2 is on) and the interval is  $\Delta$ . The waveforms repeat with a period  $\frac{1}{2}T_s$ .

$$t_{on} + \Delta = \frac{1}{2}T_s$$

Now,

$$\frac{V_o}{V_d} = 2 \cdot \frac{N_2}{N_1} \cdot D, \quad 0 < D < 0.5$$

In Push-Pull converter, the feedback diodes connected in anti-parallel to the switches to provide a path for the current required due to the leakage flux of the transformer.

### 2.3.4 Half-Bridge Converter:

In Half Bridge, capacitors  $C_1$  and  $C_2$  establish a voltage midpoint between zero and the input DC voltage. The switches T1 and T2 are turned on alternatively, each an interval  $t_{on}$  [31, 57].

#### **Mode-I:**

T<sub>1</sub> is on and therefore,

$$v_{oi} = \frac{N_2}{N_1} \frac{V_d}{2} - V_o, \quad 0 < t < t_{on}$$

#### **Mode-II:**

During the interval  $\Delta$ , both switches are off, the inductor current splits equally between the two secondary halves. Assuming ideal diodes,  $v_{oi} = 0$ , and therefore,

$$v_L = -V_o, \quad t_{on} < t < t_{on} + \Delta$$

In steady state, the waveforms repeat with a period  $0.5 * T_s$  and

$$t_{on} + \Delta = \frac{1}{2}T_s$$

Equating above mentioned equations:

$$\frac{V_o}{V_d} = \frac{N_2}{N_1} D$$

Where,  $0 < \text{Duty cycle (D)} < 0.5$

The average value of  $v_{oi}$  equals  $V_o$ . The diodes in antiparallel with the switches  $T_1$  and  $T_2$  are used for switch protection.

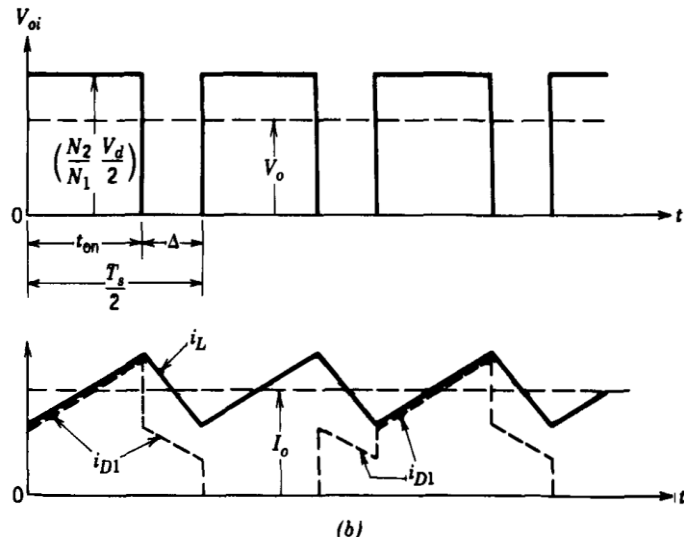
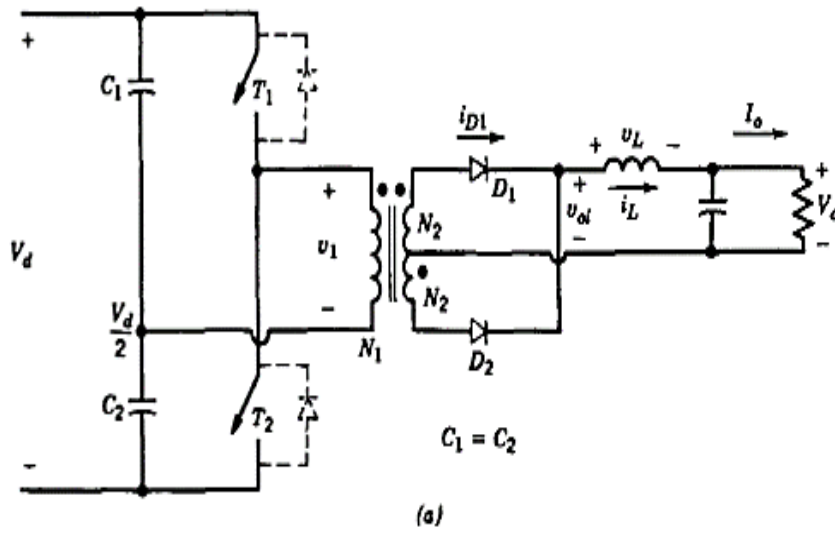


Figure 2.12: Half Bridge Converter (a) schematic diagram (b) waveshapes [56]

### 2.3.5 Full-Bridge Converter:

Full bridge converter consists of  $(T_1, T_2)$  and  $(T_3, T_4)$  switches as pairs alternatively at the selected switching frequency [31, 55].

#### Mode-I:

When  $(T_1, T_2)$  or  $(T_3, T_4)$  are on,

$$v_{oi} = \frac{N_2}{N_1} V_d - V_o, 0 < t < t_{on}$$

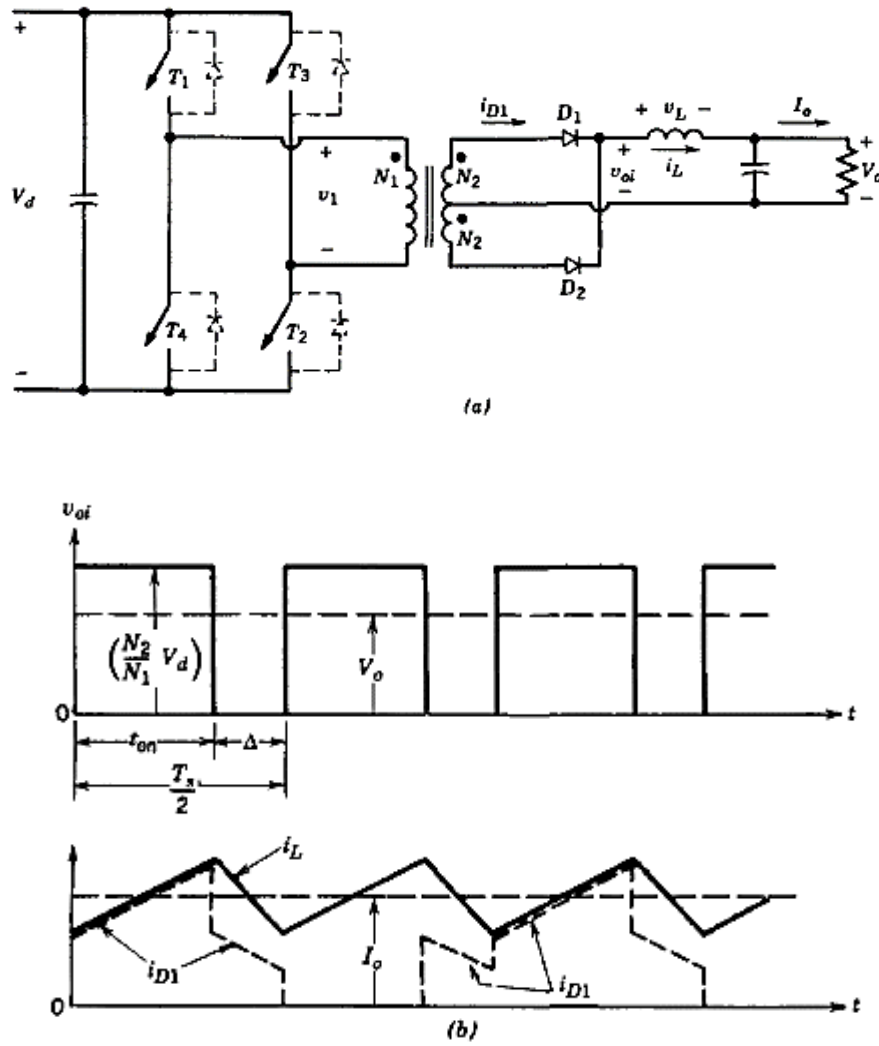


Figure 2.13: Full-Bridge converter (a) schematic diagram (b) waveshapes [56]

### Mode-II:

When both switch pairs are off, the inductor current splits equally between the two secondary halves. Assuming ideal diodes,  $v_{oi}=0$  and therefore,

$$v_L = -V_o, t_{on} < t < t_{on} + \Delta$$

Equating the time integral of the inductor voltages over one time period to zero in steady state and recognizing that  $t_{on} + \Delta = \frac{1}{2} T_s$  give

$$\frac{V_o}{V_d} = 2 \frac{N_2}{N_1} D, 0 < D < 0.5$$

The diodes connected in antiparallel to the switches provide a path to the current due to the energy associated with the primary winding leakage inductance.

### 2.3.6 Ringing Choke Converter:

Ringing choke converters (RCC) are widely used for electronic power supplies with a small capacity and power supplies for IC's because of simplicity in the circuit configuration, few components contained, low cost and high reliability.

RCC is essentially a self-oscillating converter and is always operated at the boundary between the continuous mode and the discontinuous mode of the reactor current. The switching frequency of the converter varies so that this operating condition is maintained for the variations of input and load.

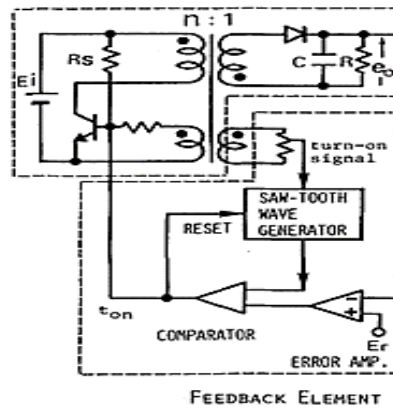


Figure 2.14: Ringing Choke converter [58]

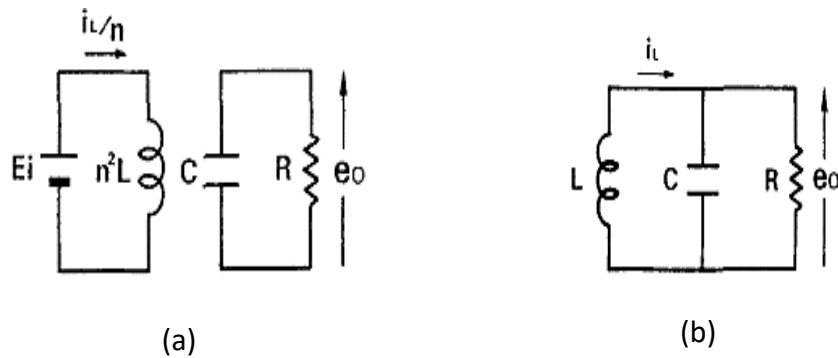


Figure 2.15: Equivalent Circuit of Ringing Choke converter during (a) transistor on interval (b) transistor off interval [58]

Figure 2.14 shows the circuit configuration of RCC. The upper portion is for the power conversion stage and the lower portion is the feedback circuit for voltage adjustment. For simplicity of analysis, the winding resistance, the resistances in the on-interval of transistors and diode and the equivalent series resistance (ESR) in the smoothing

capacitor is assumed to be sufficiently small and are neglected. Since the driving resistor  $R_s$  is sufficiently large and the current flow in it is sufficiently small, its effect is neglected. Hence, from the previous explanation of operation, the equivalent circuits during the transistor on-interval and off-interval are as shown in Figure 2.15(a) & 2.15(b) respectively. Here,  $E$  is the input voltage,  $L$  is the reactor inductance observed from the primary side,  $n$  is the winding ratio,  $C$  is the capacitance of the smoothing capacitor and  $R$  is the load resistance. From the equivalent circuits in Figure 2.15(a) and 2.15(b), the following circuit equations can be obtained for the reactor current  $i$ , (converted to the secondary side) and the voltage  $e_o$  across the smoothing capacitor (output voltage) [58].

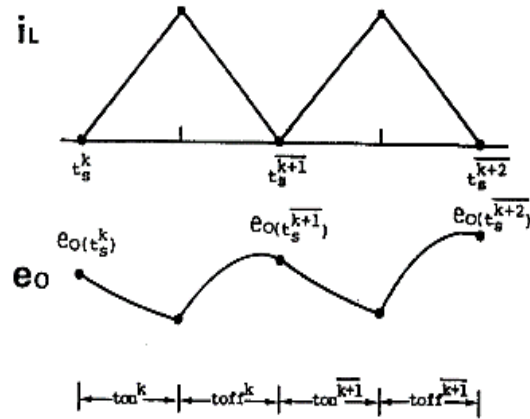


Figure 2.16: Waveforms of the reactor current  $i_L$  and the output voltage  $e_o$  [58]

**State I (transistor is on):**

$$\frac{di_L}{dt} = \frac{E_i}{nL}$$

$$\frac{de_o}{dt} = -\frac{e_o}{CR}$$

**State II (transistor is off):**

$$\frac{di_L}{dt} = -\frac{e_o}{L}$$

$$\frac{de_o}{dt} = \frac{i_L}{C} - \frac{e_o}{CR}$$

### 2.3.7 Combined Forward-Flyback converter

The new combined forward-flyback converter needs only two windings and one diode. The converter consists of a transformer with the windings  $N_1$  and  $N_2$ , a capacitor  $C$ , an

active switch S, and a passive switch D. To demagnetize the core a capacitor is used to transport the magnetizing energy to the output [59-61].

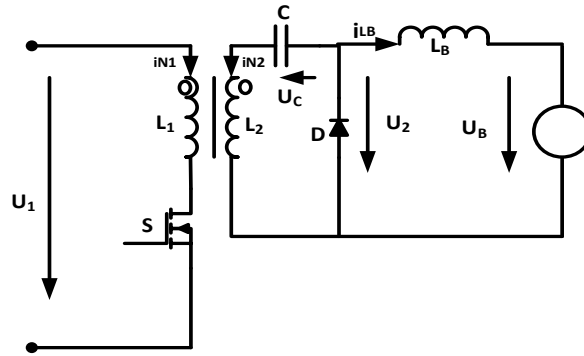


Figure 2.17: Combined Forward-Flyback converter [59]

The positive pole of the output voltage is the cathode of the diode. When used as a battery charger, an additional inductor  $L_B$  has to be switched in series to the battery. The battery is modeled by a voltage source  $U_B$ . The mean value of the output voltage  $U_2$  (across the diode), with the duty ratio of the active switch  $d$  (the on-time of the active switch referred to the switching period) and neglecting the losses is-

$$U_2 = \frac{N_2}{N_1} \frac{d}{(1-d)} \cdot U_1$$

### 2.3.8 Current source DC-DC converter:

Current source converters have the disadvantage of having a low power-to weight ratio compared to voltage source converters [31].

#### **Mode-I:**

When both switches are on, the voltage across each primary winding becomes zero. The input current builds up linearly and the energy is stored in the primary inductor.

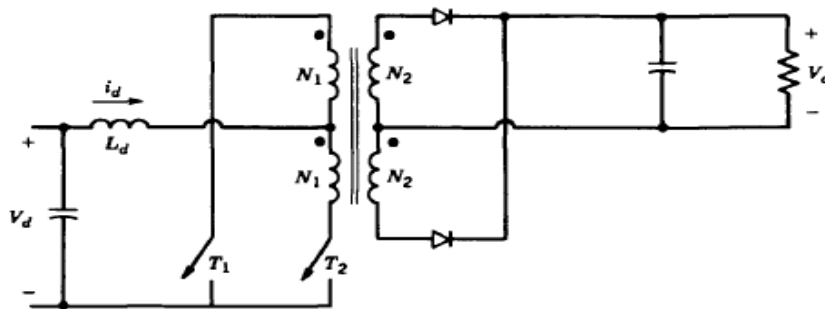


Figure 2.18: Current source DC-DC converter [31]

### **Mode -II:**

When only one of the two switches is conducting, the input voltage and the stored energy in the input inductor supply the output stage. Therefore, this circuit operates in a manner similar to the step-up converter.

Its voltage ratio can be derived as:

$$\frac{V_o}{V_d} = \frac{N_2}{N_1} \frac{1}{2(1-D)} , D > 0.5$$

## **2.4 Photovoltaic Power Generation**

PV system is a combination of many elements such as cells, mechanical, and electrical mountings, among others, where electric power is generated from sunlight irradiation. PV power generation systems are built around a number of solar cells, batteries, inverters, chargers, discharge controllers, solar tracking control systems, and other equipment's. Figure 2.19 shows a schematic representation of solar PV power generation systems.

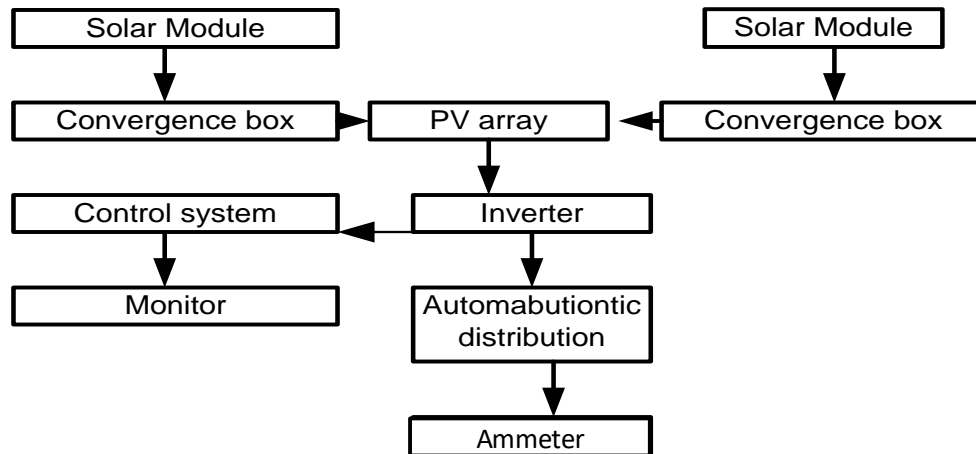


Figure 2.19: Schematic representation of photovoltaic power generation system [93]

Some important equipment's and their functions are as follows:

### **• Solar cell matrix:**

In the daytime, when solar radiation occurs, photons of the sunlight hit the surface of cells, and photons are absorbed by the cell material to create pairs of electrons and holes. If the pairs are mostly near the p–n junction, then the electrons and holes run towards the n-type side and p-type side, respectively. As the two sides of the PV cell are attached

through its load, an electric current produces and flows as long as sunlight is available to hit the cell.

- **Batteries:**

For a continuous supply of solar energy, batteries are an important element that is used to load electricity that is produced by the PV power generation system. The following features are essential for batteries [94]:

- i) they do not auto-discharge;
- ii) must have a long lifetime;
- iii) must have a high-discharge capacity;
- iv) have a high storage for charging;
- v) require minimum maintenance;
- vi) must have a high operating range for varying ranges of temperatures; and
- vii) must be low cost.

- **Charge and discharge controller:**

This device is the most important and is used to control overcharges or over discharges of the battery. Other major factors for battery lifetime are the number of times the battery is charged and discharged and the discharge level of the battery.

- **Inverter:**

The inverter is the most important element of PV power generation systems to convert from DC to AC. There are two types of inverters: square wave and sine wave. Square wave inverters are used for small projects and have a capacity less than 100W. This inverter is not in high demand because it is a harmonic system with a harmonic value, but they are low cost and simple. On the other hand, sine wave inverter prices are high but can be used for different types of loads [94].

PV systems are made from basic elements as follows: PV panels, cables, and mounting or fixing hardware. An inverter, charger, discharge controller, batteries, and other components for off-grid situations for special electricity meters or in the case of grid-connected systems.

## **2.5 Electrical Model of PV Cell**

For various commercial operations, distinct types of photovoltaic (PV) cell technologies have been used. These cell technologies can be classified as multicrystalline, mono-crystalline and thin film. Single and double diode PV models have been widely used for modelling the output characteristic of a PV module.

Single diode model is the simplest as it has a current source in parallel to a diode. This model is upgraded by the inclusion of one series resistance,  $R_s$ . In spite of its simplicity, it exhibits acute deficiencies when suffered from temperature deviations. An accretion of the model introduces a supplementary shunt resistance,  $R_p$ . Although momentous development is attained, this approach claims significant computing exertion. Moreover, its precision declines at low irradiance, particularly in the vicinity of open circuit voltage ( $V_{oc}$ ). Two-diode model (consisting  $R_p$  and  $R_s$ ) is recommended for improved accuracy.

### 2.5.1 One diode model

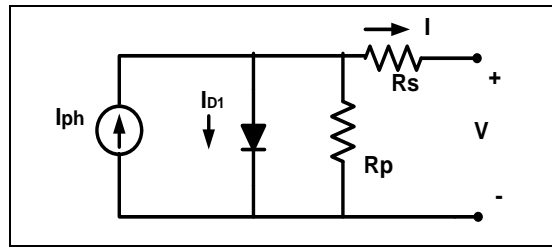


Figure 2.20: Electrical Model of One-Diode PV Cell [95-97]

$$I = I_{ph} - I_o \left[ \exp \left( \frac{V + IR_s}{aV_T} \right) - 1 \right] - \frac{V + IR_s}{R_p} \quad (2.1)$$

$$V_T = \frac{N_s k T}{q} \quad (2.2)$$

$$I_{ph} = \frac{G}{G_n} [I_{pvn} + K_1 (T - T_n)] \quad (2.3)$$

$$I_o = I_{on} \left( \frac{T_n}{T} \right)^3 \exp \left[ \frac{qE_g}{ak} \left( \frac{1}{T_n} - \frac{1}{T} \right) \right] \quad (2.4)$$

$$I_{on} = \frac{I_{scn}}{\exp(V_{ocn}/aV_{Tn}) - 1} \quad (2.5)$$

### 2.5.2 Double diode model

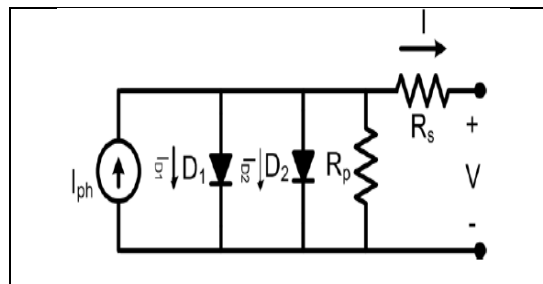


Figure 2.21: Electrical Model of Double-Diode PV Cell [97-99]

$$I = I_{ph} - I_{D1} - I_{D2} \quad (2.6)$$

$$I_{D1} = I_{o1} \left[ \exp \left( \frac{V + IR_s}{a1 * V_T} \right) - 1 \right] \quad (2.7)$$

$$I_{D2} = I_{o2} \left[ \exp \left( \frac{V + IR_s}{a2 * V_T} \right) - 1 \right] \quad (2.8)$$

$$I = I_{ph} - I_{o1} \left[ \exp \left( \frac{V + IR_s}{a1 * V_T} \right) - 1 \right] - I_{o2} \left[ \exp \left( \frac{V + IR_s}{a2 * V_T} \right) - 1 \right] - \frac{V + IR_s}{R_p} \quad (2.9)$$

$$I_{ph} = \frac{G}{G_n} [I_{ph,n} + K_I \Delta T] \quad (2.10)$$

$$I_{o1} = I_{o2} = \frac{I_{sc,n} + K_I \Delta T}{\exp \left( \frac{V_{oc,n} + K_V \Delta T}{((a1 + a2)/p) * V_T} \right) - 1} \quad (2.11)$$

### 2.5.3 Different parameters

$I_{ph}$  is the current generated by the incident light.

$I_{D1}$  is the Shockley diode equation due to diffusion.

$I_{D2}$  is the Shockley diode equation due to charge recombination mechanisms

$I$  is the output Current of PV cell.

$I_{o1}, I_{o2}$  [A] are the reverse saturation current of the diodes  $D_1$  and  $D_2$  respectively.

$q$  is the electron charge [ $1.60217646 * 10^{-19}$  C].

$k$  is the Boltzmann constant [ $1.3806503 * 10^{-23}$  J/K].

$T$  [K] is the temperature of the p-n junction.

$a1$  and  $a2$  are ideality factor of the diodes  $D_1$  and  $D_2$  respectively for two diode model.

$a$  is ideality factor of diode for one diode model.

$V_T$  is the thermal voltage of the module.

### 2.5.4 Efficiency

Proportion of output energy of the solar cell to input energy from the sun is described as efficiency. Simultaneously reflecting the capability of the solar cell itself, the efficiency relies upon the spectrum and intensity of the incident sunlight and the temperature of the solar cell. Therefore, conditions, which are used to measure efficiency, must be regulated cautiously in order to correlate the performance of one apparatus to another. Form factor (FF) is delineated as the ratio of the maximum power output from the solar cell to the product of open circuit voltage ( $V_{oc}$ ) and short circuit current ( $I_{sc}$ ).

$$FF = \frac{V_m I_m}{V_{oc} I_{sc}} \quad (2.12)$$

$$\eta = \frac{V_{oc} I_{sc} FF}{P_{in}} \quad (2.13)$$

$$\Delta T = T - T_n \quad (2.14)$$

Here,  $V_{oc}$  is open circuit voltage &  $I_{sc}$  is the short circuit current and  $G_n$  is the irradiance,  $T_n$  is the temperature, all at standard test conditions.

$K_v$  is the temperature coefficient of open circuit voltage &  $K_i$  is the temperature coefficient of short circuit current,  $\eta$  is efficiency.

The dominant phenomena that confine cell efficiency are:

- a) Reflection from the cell's exterior
- b) Light that is not enough dynamic to isolate electrons from their atomic bonds
- c) Light that has excess energy beyond that required to isolate electrons from bonds
- d) Light-produced electrons and holes (empty bonds) that casually collide with each other and recombine before they can promote to cell performance
- e) Light-produced electrons and holes that are brought together by exterior and material blemishes in the cell
- f) Resistance to current movement
- g) Self-shading ensuing from upper-surface electric contacts
- h) Performance degradation at non optimal (high or low) conducting temperatures

## 2.6 PV Characteristics

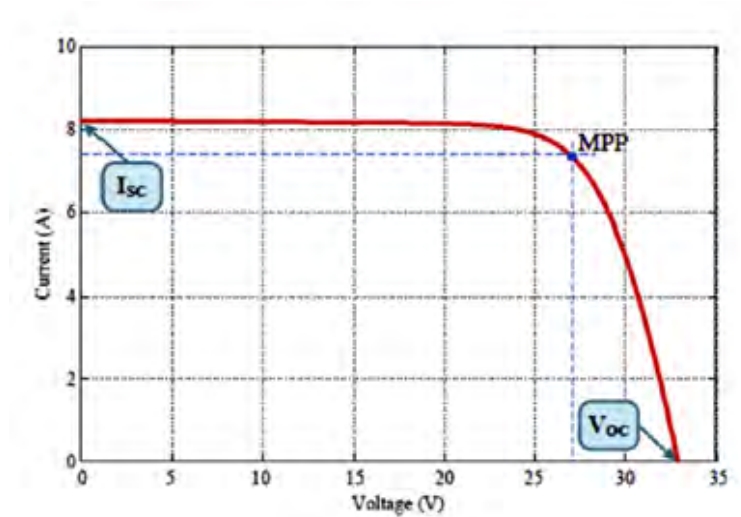


Figure 2.22: PV current versus voltage characteristics [100]

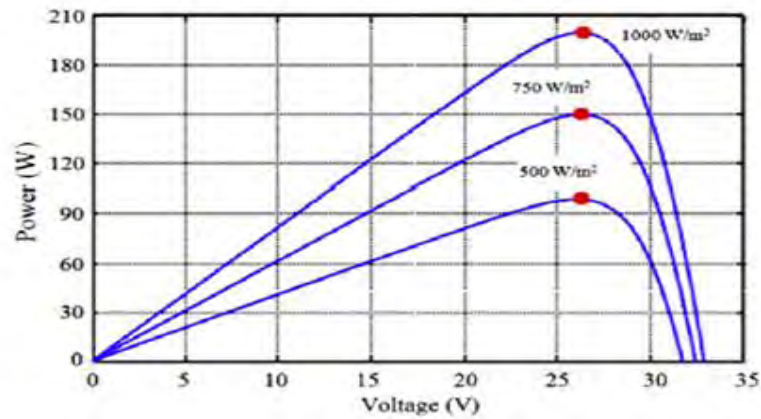


Figure 2.23: PV power characteristics for different irradiation levels [100]

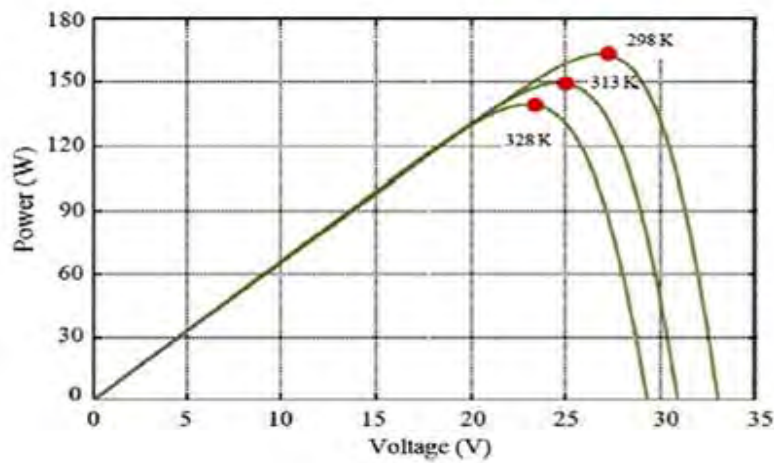


Figure 2.24: PV power characteristics for different temperature levels [100]

### 2.6.1 Maximum power point tracker (MPPT):

The MPPT is described as circuitry associated with utility- interactive inverters (and some larger stand-alone) that continuously adjust the DC operating point to obtain the maximum power available from a PV array at any given time. Despite all the advantages presented by the generation of energy with PVs, the efficiency of energy conversion is currently low and the initial cost for its implementation is still considered high, and thus it becomes necessary to use techniques to extract the maximum power from these panels, in order to achieve maximum efficiency in operation. It should be noted that there is only one maximum power point (MPP), and this varies according to climatic and irradiation conditions. The photovoltaic power characteristics is nonlinear, as shown in Figure 2.23 and 2.24, which vary with the level of solar irradiation and temperature, which make the extraction of maximum power a complex task, considering load variations. To overcome this problem, several methods for extracting the maximum power have been invented. A PV array under constant uniform irradiance has a current– voltage (I–V) characteristic

like that shown in Figure 2.22. There is a unique point on the curve, called the maximum power point (MPP), at which the array operates with maximum efficiency and produces maximum output power. When a PV array is directly connected to a load (also-called 'direct-coupled' system), the system's operating point will be at the intersection of the I–V curve of the PV array and load line. In general, this operating point is not at the PV array's MPP. Thus, in a direct-coupled system, the PV array must usually be over sized to ensure that the load's power requirements can be supplied. This leads to an overly expensive system. A maximum power point tracker is a device employing a micro process or to achieve both function of maximum power output and tracking by sampling the power output of the array at frequent intervals (usually 30ms). It compares each new value of the array power output with the previous value. If the power output has increased, then the array voltage is stepped up in the same direction otherwise it remains at the original position. Owing to changes in the solar radiation energy and the cell operating temperature, the output power of a solar array is not constant at all times. To overcome this problem, a switch-mode power converter, called a maximum power point tracker (MPPT), can be used to maintain the PV array's operating point at the MPP [100]. Therefore, works to solve the problems on maximum power point tracking (MPPT) have always been a hot topic for PV array utilization systems. The MPPT does this by controlling the PV array's voltage or current independently of those of the load. If properly controlled by an MPPT algorithm, the MPPT can locate and track the MPP of the PV array. However, the location of the MPP in the I–V plane is not known a priori. It must be located, either through model calculations or by a search algorithm. The situation is further complicated by the fact that the MPP depends in a nonlinear way on irradiance and temperature. The change in the array voltage at which the Figure 2.23 and 2.24 show the power characteristics of the analysed PV, considering the same temperature and solar irradiation, respectively. The curves show clearly nonlinear characteristics and they are strongly influenced by climate changes.

Furthermore, different techniques of MPPT are described briefly.

#### **2.6.1.1 Fixed duty cycle:**

The fixed duty cycle represents the simplest of the methods and it does not require any feedback, where the load impedance is adjusted only once for the maximum power point and it is not adjusted again.

### 2.6.1.2 The Beta method:

The Beta method is the approximation of the point of maximum power through the equation of an intermediate variable  $\beta$ .

$\beta$  can be continuously calculated using the voltage and current of the panel and inserted on a conventional closed loop with constant reference.

$$\beta = \ln \left( \frac{I_{pv}}{V_{pv}} \right) - c V_{pv} \quad (2.15)$$

$$\text{Where, } c = \frac{q}{\sigma \cdot K \cdot T \cdot N_s}$$

is a constant that depends on the electron charge, the quality factor of the junction panel, the Boltzmann constant, temperature and amount of photovoltaic cells in series [101].

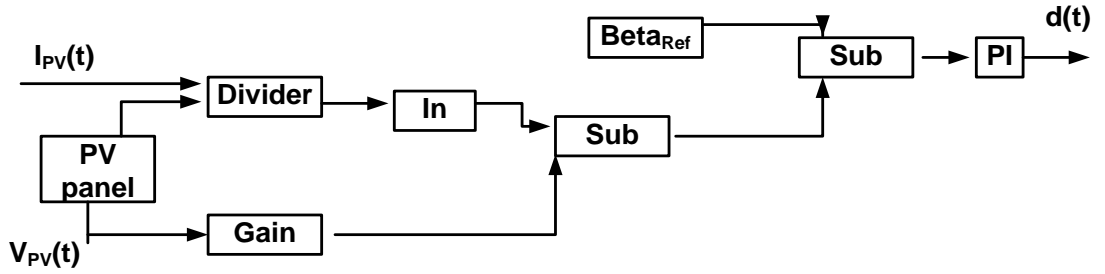


Figure 2.25: Block diagram of the Beta method

### 2.6.1.3 Perturb and observe:

In the P&O algorithm, the operating voltage of the PV array is perturbed by a small increment, and the resulting change in power,  $\Delta P$ , is measured. If  $\Delta P$  is positive, then the perturbation of the operating voltage moved the PV array's operating point closer to the MPP [102]. Thus, further voltage perturbations in the same direction (that is, with the same algebraic sign) should move the operating point toward the MPP.

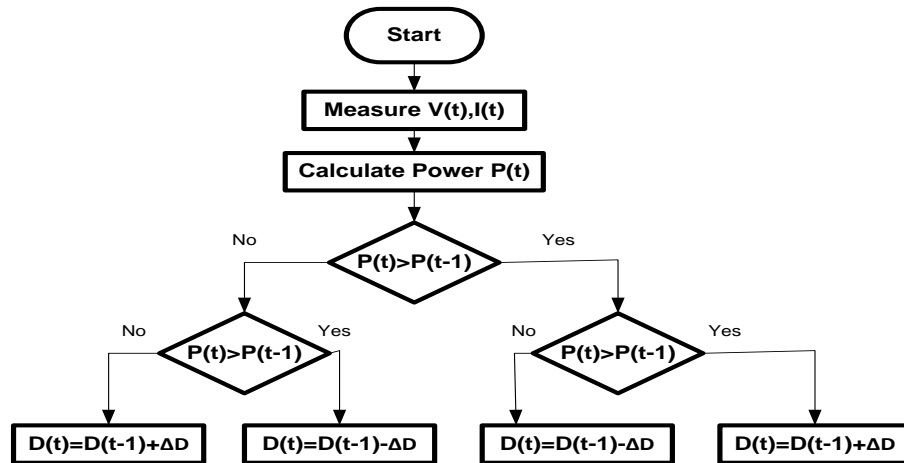


Figure 2.26: Flow chart of perturb and observe method [103]

If  $\Delta P$  is negative, the system operating point has moved away from the MPP, and the algebraic sign of the perturbation should be reversed to move back toward the MPP.

#### 2.6.1.4 Incremental conductance

The incremental conductance (IncCond) algorithm is derived by differentiating the PV array power with respect to voltage and setting the result equal to zero.

#### 2.6.1.5 Constant voltage and current:

The basis for the constant voltage (CV) algorithm is based on the observation of the ratio of the array's maximum power voltage,  $V_{MPP}$ , to its open-circuit voltage,  $V_{OC}$  [104].

The solar array is temporarily isolated from the MPPT, and a VOC measurement is taken. Next, the MPPT calculates the correct operating point using the equation mention below:

$$\frac{V_{MPP}}{V_{oc}} \cong K < 1$$

And the preset value of K, and adjusts the array's voltage until the calculated  $V_{MPP}$  is reached. This operation is repeated periodically to track the position of the MPP. Although this method is extremely simple, it is difficult to choose the optimal value of the constant K. Value of ranging from 73% to 80%.

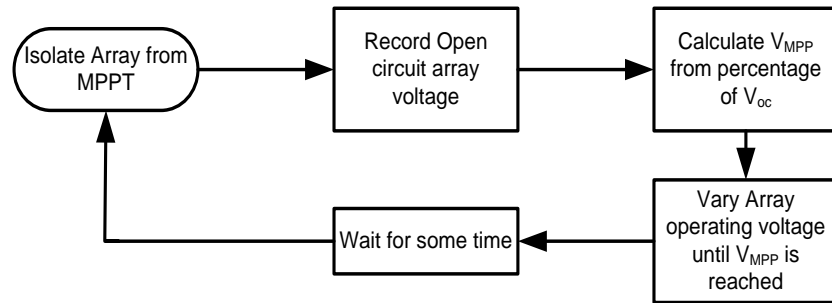


Figure 2.27: Block diagram of Constant voltage MPPT technique [105]

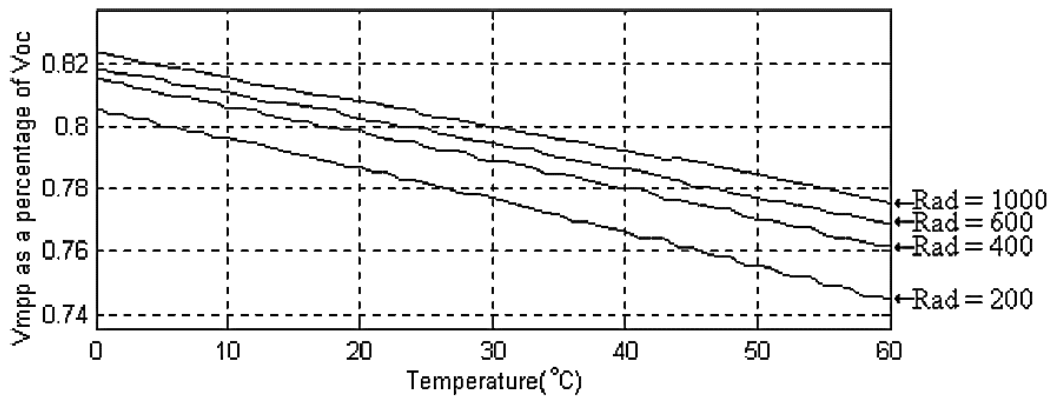


Figure 2.28:  $V_{MPP}$  as a percentage of  $V_{OC}$  as functions of temperature and irradiance [105]

Figure 2.28 shows the actual K values required for a given PV array over a temperature range of 0–60 °C and irradiance levels from 200 to 1000W/m<sup>2</sup>. These curves were calculated using the I–V relationship for a PV cell.

#### 2.6.1.6 Fractional open-circuit voltage:

The near linear relationship between  $V_{MPP}$  and  $V_{OC}$  of the PV array, under varying irradiance and temperature levels, has given rise to the fractional  $V_{OC}$  method.

$$V_{MPP} \approx k_1 V_{OC}$$

Where,  $k_1$  is a constant of proportionality. Since  $k_1$  is dependent on the characteristics of the PV array being used, it usually has to be computed beforehand by empirically determining  $V_{MPP}$  and  $V_{OC}$  for the specific PV array at different irradiance and temperature levels. The factor  $k_1$  has been reported to be between 0.71 and 0.78.

#### 2.6.1.7 Modified open-circuit voltage method:

In this method [100], the PV array is not temporarily isolated from MPPT, the open circuit voltage ( $V_{OC}$ ) is calculated for different values of insolation and temperature by making use of the following equations:

$$C_{TV} = \frac{V_{OCT}}{V_{OC}} = 1 + \left( \frac{k_v}{V_{OC}} \right) (T_x - T_c) \quad (2.16)$$

Where,  $k_v$  is the temperature coefficient of  $V_{OC}$ . The value of  $k_v$  taken is  $-0.16V/^{\circ}C$

$$C_{SV} = 1 + \beta_T \alpha_S (S_x - S_c) \quad (2.17)$$

Where,  $\alpha_S = (dT_c/S_x - S_c)$ ,  $dT_c$  is temperature change due to change in irradiance. The values of  $\beta_T$  and  $\alpha_S$  are taken .0042 and .0061 respectively.

So, the open circuit voltage is:

$$V_{OC(TG)} = C_{TV} C_{SV} V_{OC} \quad (2.18)$$

#### 2.6.1.8 Pilot cell

In the pilot cell MPPT algorithm, the constant voltage or current method is used, but the open-circuit voltage or short-circuit current measurements are made on a small solar cell, called a pilot cell, that has the same characteristics as the cells in the larger solar array. The pilot cell measurements can be used by the MPPT to operate the main solar array at its MPP, eliminating the loss of PV power during the  $V_{OC}$  or  $I_{SC}$  measurement [106].

#### 2.6.1.9 Some other MPPT technique:

- a) Fractional short-circuit current
- b) Modified short-circuit current method
- c) Parasitic capacitance/DC-link capacitor drop control

- d)  $dP/dV$  or  $dP/dI$  feedback control
- e) Fuzzy logic controller (FLC)
- f) Current sweep
- g) One-cycle control MPPT
- h) The best fixed voltage algorithm
- i) Linear reoriented coordinates method
- j) Slide control method
- k) The System Oscillation method
- l) The Ripple Correlation control (RCC)
- m) Array reconfiguration
- n) Linear current control
- o) State-based MPPT
- p) Look-up table method:
- q) Variable inductor MPPT method
- r) Variable step-size incremental resistance (INR) method

## **2.7 Emerging Applications of Solar PV Technology**

There has been an enormous effort from the scientific community to look for alternative and clean energy resources to fulfill the present and future needs. Also, due to limitation of conventional energy resources, there is an urgent need to explore renewable energy resources for healthy, competitive and sustainable economic growth worldwide, while keeping the environment neat and clean for the coming generation. The recent advances of PV technologies have filled up certain gaps between demand and supply of energy in a wide range of new and emerging applications in general and in some areas of technical thrust in particular, globally. Nowadays, there are different technologies available in PV sector to meet the increasing demand of energy with certain limitations. Among the available PV technologies, there is certain advancement in some specific areas, such as, solar PV based water pumping, solar PV home lighting systems, solar PV powered desalination plant, solar PV thermal, space technology, building integrated solar PV systems and concentrated solar PV systems and few of which are performing well in the field of real life applications [107].

### **2.7.1 Solar home lighting systems**

The home lighting is one the key factors for the development process and in most of the developing especially in the rural and remote areas, people still use traditional and

conventional sources such as, kerosene for home lighting. The kerosene based home lighting is not only inefficient source of lighting but also having lack of visibility and causing health related problems among the users. According to the world energy outlook report for the 2013 [108], it was revealed that approximately 1.3 billion people are in the scarce of electricity around the globe and kerosene is the only source being used for home lighting especially, in Asia and Africa. It is found that the lamp powered by conventional sources like kerosene not only produces very poor quality of light but also emits toxic gases and the children using kerosene based lighting cannot read properly and inhale toxic gases. Also, use of kerosene for home lighting provides only 0.03 lumens/ Watt in comparison of the compact fluorescent with 30–70 lumens/ Watt and white light emitting diode with 50–100 lumens/Watt of light. According to the World Bank estimation, more than 780 million women and children are breathing harmful particulate matter due to the use of kerosene lamps from home lighting only. The kerosene based lighting is dangerous, unhealthy and insufficient and causes serious health hazards such as, respiratory and eye problems, especially, in the developing countries. This affects overall development in the country as the children using the kerosene lamps are exposed to the toxic gases and hence, are living in unhealthy environment which ultimately creates barrier in the education. Therefore, the clean energy sources like solar PV are desperately needed for the lighting purposes which can not only produce the sufficient and good quality light but also environmental friendly energy source. In this context, solar photovoltaic based CFLs and WLEDs provide an option for clean, safe and good quality home lighting systems. The home lighting systems based on SPV(solar photovoltaic) for individual households is hard to reach in areas where there grid connectivity is more popular and easy to reach. The use of SPV systems for lighting purposes by replacing the kerosene and paraffin can reduce not only the running costs on a daily basis, but also the reduces the health risks among the end users, besides, it may contribute in terms of utility as the children will get the more time to study.

The detailed study on the home lighting pattern in the rural areas of mostly Asia and Africa was carried out by Pode [109] where he suggested the use of LED based solar home lighting systems to enhance the popularity and utility of these systems with better visibility (lumens/Watt) for home lighting solutions. He also discussed different aspects and case studies of conventional home lighting systems being used by the poor people around the globe including health issues, fire danger and greenhouse gas emissions by using kerosene oil besides, the economics of solar powered CFL and LED in detail. The

schematic view of off grid AC and DC powered solar home lighting system are shown in Figure 2.29. The quality of light was found to be improved by replacing the kerosene with the LED lights with number of co-benefits such as, the increased in study time with lower air pollution, while reducing the monthly electricity bill significantly, i.e. almost 70% by the use of later lighting systems. Sastry et al. [110] developed high performance white light emitting diode (WLED) based solar home lighting systems under the joint project between Solar Energy Centre (Gurgaon) and Agency for Non-Conventional Energy and Rural Technology (ANERT), India. In this project, a 1001 m/W WLED, 6W at 16.4 V PV module with 20 V of open circuit voltage and 0.4A current and 12 V and 7AH capacity of sealed maintenance free (SMF) valve regulated lead acid (VRLA) battery was selected for the performance analysis.

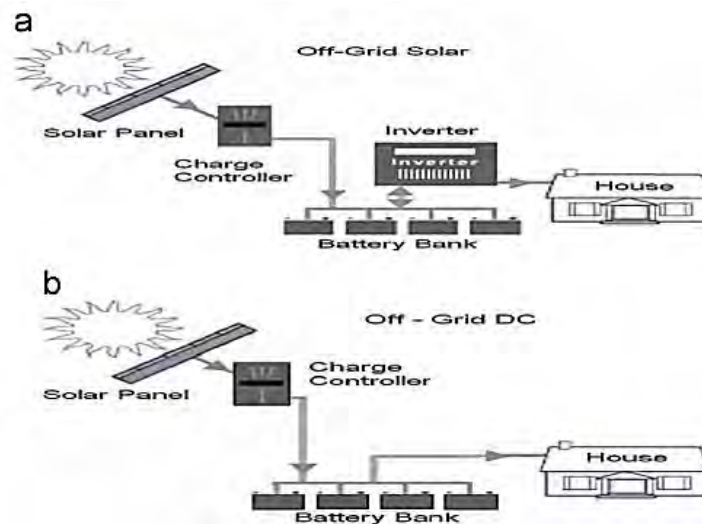


Figure 2.29: (a) OFF-grid AC solar power systems to provide power for normal AC appliances, (b) OFF-grid DC solar power systems to provide power for only DC appliances [109]

Komatsu et al. [111] determined the characteristics of households installing solar home systems (SHS) in Bangladesh and the factors affecting SHS user satisfaction were determined for making this technology popular in rural areas. It was found that the users using the SHS system as a replacement of kerosene were more satisfied and the users whose children got the extra time for study were highly satisfied. While from the econometrics analysis, it was found that SHS battery replacement has the negative impact on user satisfaction. Therefore, the reduction in frequency of battery replacement can improve the user satisfaction.

## Chapter 3

### Single Input Triple Output (SITO) Isolated DC-DC converter

Isolated DC/DC converters are required in a broad range of applications including power metering, industrial programmable logic controllers (PLCs), insulated-gate bipolar transistor (IGBT) driver power supplies, industrial fieldbus, and industrial automation [55]. These converters often are used to provide galvanic isolation, improve safety, and enhance noise immunity. Moreover, they can be used to generate multiple output voltage rails including dual-polarity rails [55-56].

Single input triple output DC-DC converter is an idea of multiple purpose from single source. A handy technique of integrated system which can transform the limited use of source into many users. The proposed technique which can bring multiple user in same platform with ease.

#### 3.1 Overview:

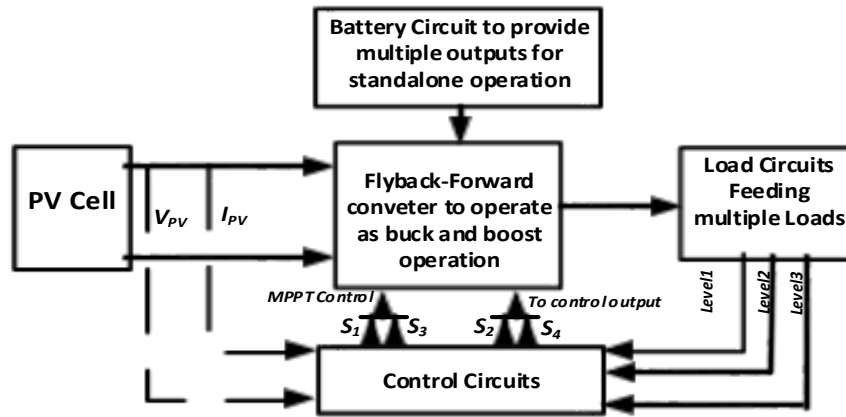


Figure 3.1: Overall system associated with SITO converter

A Photovoltaic module with standalone property is connected with an isolated three port DC-DC converter. Converter is incorporate with the ability to work for various applications owing to single energy source connection, single storage device, compact structure and low cost. The ability of conversion of multiple voltage level from a single input rectifies the problem of multi-level voltage users.

Multiple-output DC-DC converter is a potential solution for applications requiring multiple supplies. The proposed system will be capable of delivering different output voltage levels from single DC-DC converter at the load side at a time.

A high-frequency transformer is used to provide galvanic isolation and flexible voltage conversion ratio.

In particular, the system is ornamented with the isolated three-port converter (ITPC) topology. Proposed system integrates a three-port topology in the half bridge and decomposes the multivariable control problem into a series of independent single-loop subsystems.

Control scheme associated with an advanced modulation strategy which incorporates a phase shift (PS) and a PWM to extend the operating range of ZVS. It provides a compact single-unit solution with a combined feature of optimized MPPT and output voltage regulation.

**The main benefits of this topology are:**

- High efficiency which is of significant importance for high-power applications,
- Uninterrupted supply to the loads of multiple output levels,
- The voltage gain can be substantially increased by using a coupled inductor,
- Ascendible to meet any voltage levels considering distance of the user,
- Ability to endure with both HVDC and LVDC levels,
- A high conversion ratio, allow high switching frequency,
- More levels can be added without changing the main power converter,
- “Battery circuit” and “Triple output level circuit” are ornamented with synchronized gate pulses for each level,
- Single control scheme reduces circuit complexity by controlling multilevel voltage fluctuations.

### **3.2 Proposed SITO Converter:**

The proposed single input triple output (SITO) converter is an isolated three port Flyback-Forward converter shown in Figure 3.2. The converter is fed by a PV cell with capacitor in parallel for the purpose of attenuating input current ripples. Flyback-Forward converter is a kind of buck boost converter with galvanic isolation. This ITPC topology achieves decoupled port control, provides flexible power flow and high power capability while still making the system simple and cheap.

Unique approach of the system is the “Battery Circuit”, from where single voltage level is divided into three distinct levels. It’s the main part of the SITO converter for multiple feeding. A highly efficient topology “Identically Switched Storage and Load (ISSL) with Shifted Pulse” is proposed to serve the purpose of multiple users.

Comprehensive system is divided into three sub systems; flyback-forward converter with ITPC attribute, battery circuit and triple output level circuit.

Three-port DC-DC converter is illustrated in Figure 3.2 The main switches  $S_1$  and  $S_2$  work in interleaved or synchronous mode to transfer the energy from PV array to the battery or load, and the switches  $S_3$  and  $S_4$  work in the interleaved mode to transfer battery energy to the load. There are two coupled inductors in the proposed high step up converter, named  $L_1$  and  $L_2$ . The primary windings of the two coupled inductors  $L_{1a}$  and  $L_{2a}$  with  $n_1$  turns are employed as filter inductors, and the secondary windings  $L_{1s}$  and  $L_{2s}$  with  $n_2$  turns are connected in series to conform voltage-doubler configuration achieving high voltage gain. The coupling references are remarked as “\*” and “.” as shown in Figure 3.2  $L_{lk}$  is the summation of leakage inductance of the two coupled inductors. The turns ratio  $N$  is defined as  $n_2/n_1$ .  $C_{s1}$ ,  $C_{s2}$ ,  $C_{s3}$  and  $C_{s4}$  are parasitic capacitors of the main switches  $S_1$ ,  $S_2$ ,  $S_3$  and  $S_4$  respectively.  $D_{o1}$  and  $D_{o2}$  are rectifier diodes, and  $C_{o1}$  and  $C_{o2}$  are output capacitors.

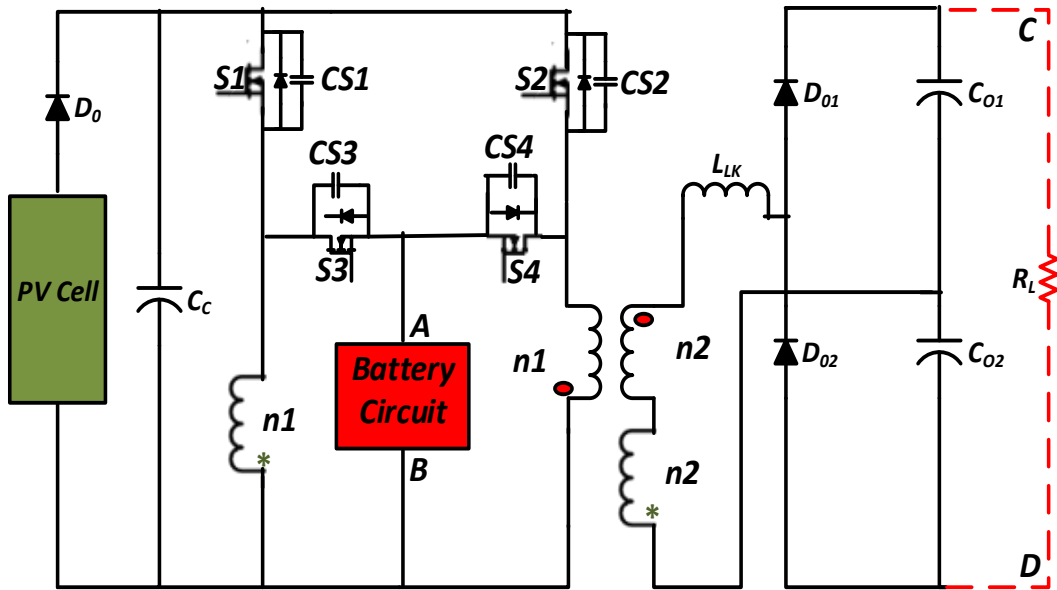


Figure 3.2: Schematic of SITO converter

“Battery circuit” (Figure 3.3) is connected to primary side of the transformer. This circuit includes three MOSFETs, a single diode and a storage device. Output voltage levels are controlled by the delayed gate pulses of MOSFETs. Capacitors are used as the voltage-dividing components.

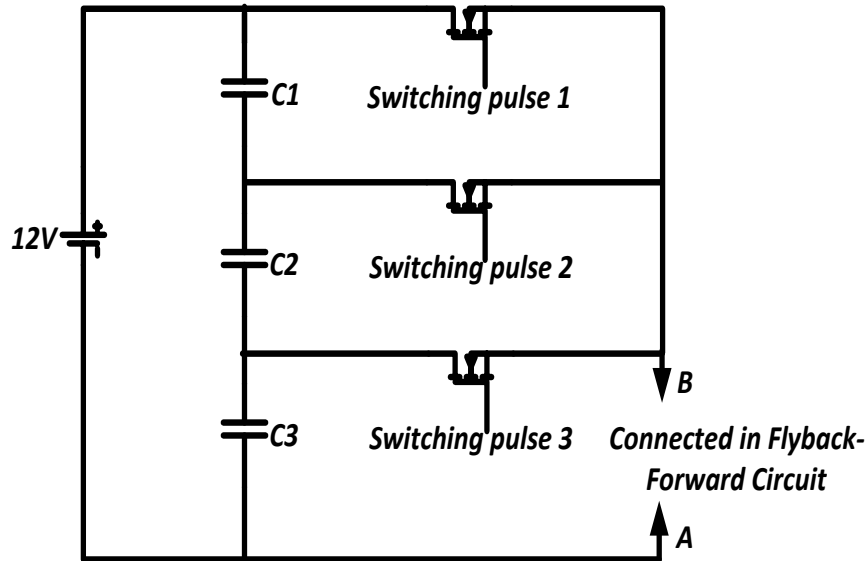


Figure 3.3: Schematic of “Battery circuit”

Capacitive networks, however, are a little more complex than plain resistive networks, because capacitors are reactive devices and it depends on the frequency on the input signal into the circuit. Voltage is divided up in a capacitive DC voltage divider according to the formula,  $V=Q/C$ . Therefore, voltage is inversely proportional to the capacitance value of the capacitor. So, the capacitor with the smaller capacitance will have the greater voltage, and conversely, the capacitor with the greater capacitance will have the smaller voltage. “Triple output level circuit” is shown in Figure 3.4, which provides a path to feed the loads by the converter circuit.

The circuit consolidates with three switching devices, three diodes, three capacitors and corresponding load resistances. Gate pulses of the switching devices are synced with switching devices of the battery circuit. Capacitors are used as storage device as well as output smoothing purpose. A capacitor can store electric energy when it is connected to its charging circuit. And when it is disconnected from its charging circuit, it can dissipate that stored energy, so it can be used like a temporary battery. Furthermore, output ripples are reduced due to the presence of capacitors.

Each level can be integrated with SPST (single pole single throw) switches to turn off unused levels from the overall system.

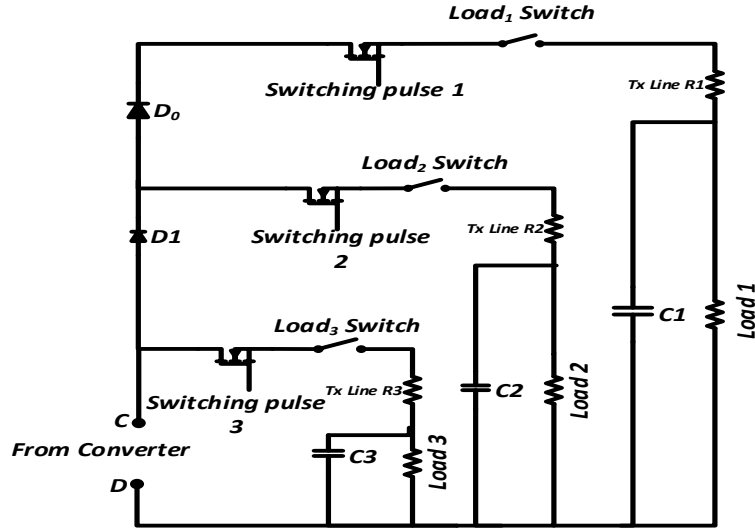


Figure 3.4: Schematic of “Triple output level circuit”

### 3.2.1 Operating modes of proposed converter:

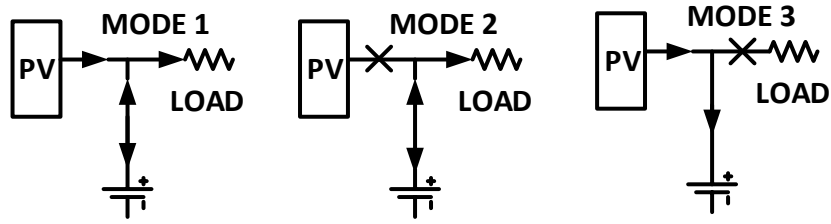


Figure 3.5: Three operation modes of the proposed system

There are three operational modes for the converter, as illustrated in Figure 3.5.

Mode 1, the PV array supplies power to load and possibly also to the battery, corresponding to the day time operation of the PV system.

Mode 2, the battery supplies power to the load, indicating the nighttime operation of the stand-alone system.

Mode 3, load is disconnected and the PV array charges battery without energy transferred to the load.

### 3.2.2 Operating Principle of Converter

The three operational modes briefly described with corresponding circuit diagram.

**Mode-1** (Energy flows from PV array to battery and load):

The PV supplies power to both load and battery at a time. Two  $180^\circ$  out-of-phase gate signals with the same duty ratio ( $D$ ) are applied to  $S_1$  and  $S_2$  while  $S_3$  and  $S_4$  remain in a synchronous rectification state. When in the steady-state operation, there are four states in one switching period, of which the equivalent circuits are shown in Figure 3.7.

The steady-state waveforms of the four states are depicted in Figure 3.6, where  $V_{GS1}$ ,  $V_{GS2}$ ,  $V_{GS3}$  and  $V_{GS4}$  are the gate drive signals,  $V_{ds1}$  and  $V_{ds2}$  are the voltage stresses of  $S_1$  and  $S_2$ ,  $i_{L1a}$  and  $i_{L2a}$  are the currents through  $L_{1a}$  and  $L_{2a}$ , respectively.  $i_B$  is the current through the battery,  $i_{S1}$  is the current through  $S_1$ ,  $v_{Do1}$  is the voltage stress of the output diode  $D_{o1}$ , and  $i_{Do1}$  is the current through  $D_{o1}$ [113].

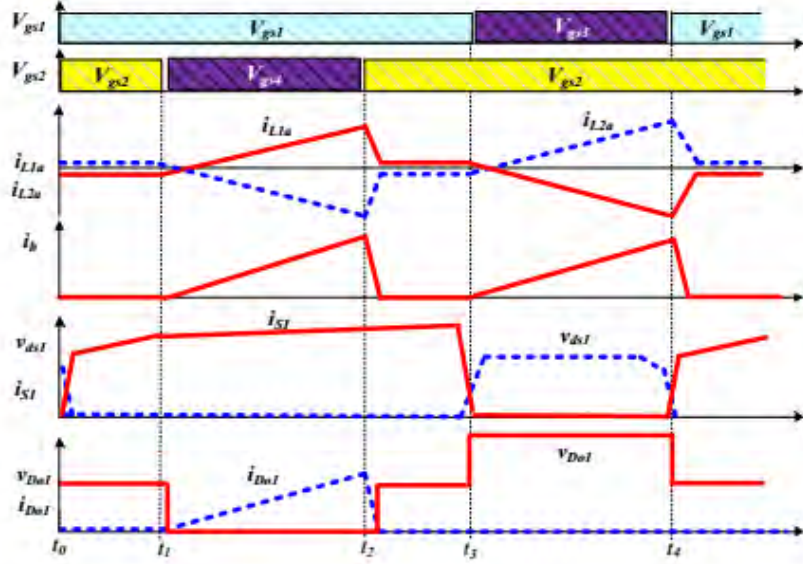


Figure 3.6: Waveforms of the converter under mode-1

At  $[t_0-t_1]$

The main switches  $S_1$  and  $S_2$  are both in turn-on state before  $t_0$ . The two coupled inductors work in the flyback state to store energy from the PV array. The output rectifier diodes  $D_{o1}$  and  $D_{o2}$  are both reverse-biased. The energy stored in the secondary output capacitors  $C_{o1}$  and  $C_{o2}$  transfers to the load.

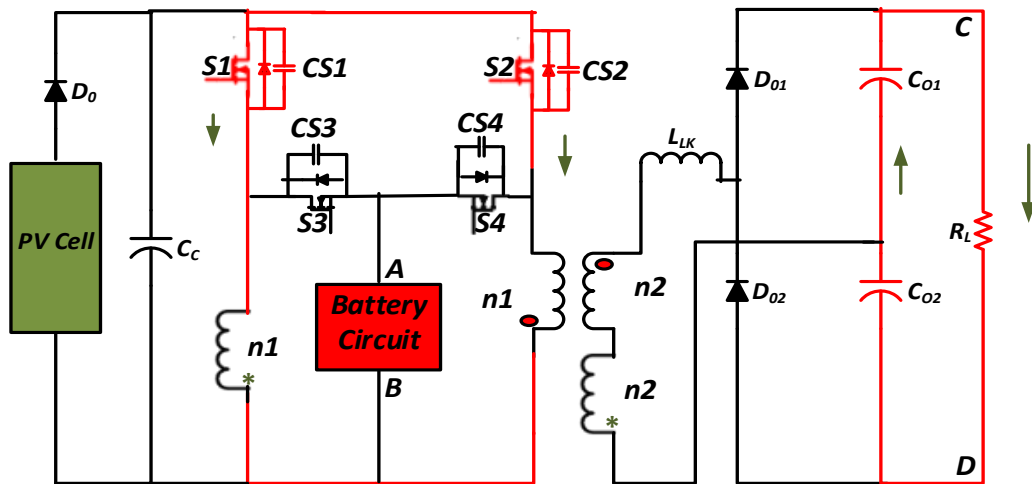


Figure 3.7(a): Operating state 1 of the converter in mode-1

At  $[t_1-t_2]$

At  $t_1$ ,  $S_2$  turns OFF,  $S_4$  turns ON, while the diodes  $D_{o1}$  is ON. The primary side of the coupled inductor  $L_2$  charges the battery through  $S_4$ . During this state,  $L_1$  operates in the forward mode and  $L_2$  operates in the flyback mode to transfer energy to the load. When  $S_1$  turns on and  $S_2$  turns off, the primary voltage of the coupled inductor  $L_1$  is  $V_{pv}$  and the voltage on  $L_2$  is  $-V_B$ .

According to the voltage balance law,

$$DV_{PV} = (1-D) V_B \quad (3.1)$$

$$V_{ab} = N \frac{1-D}{D} V_B - N(-V_B) = \frac{NV_B}{D} \quad (3.2)$$

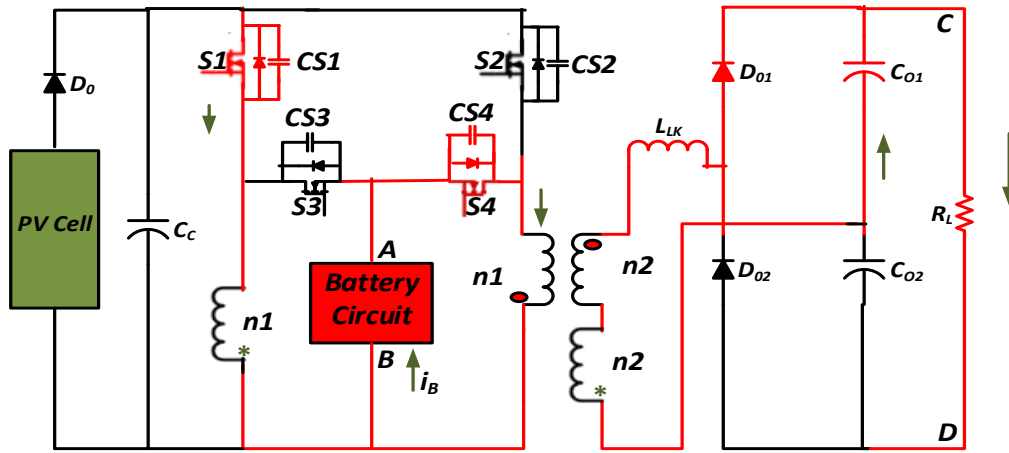


Figure 3.7(b): Operating state 2 of the converter in mode-1

At  $[t_2-t_3]$

At  $t_2$ ,  $S_2$  turns ON, which forces the two coupled inductors work in the flyback state to store energy and  $D_{o2}$  is reverse-biased. The energy stored in  $C_{o1}$  and  $C_{o2}$  transfers to the load. At  $t_3$ , the leakage inductor current decreases to zero and the diode  $D_{o1}$  turns OFF.

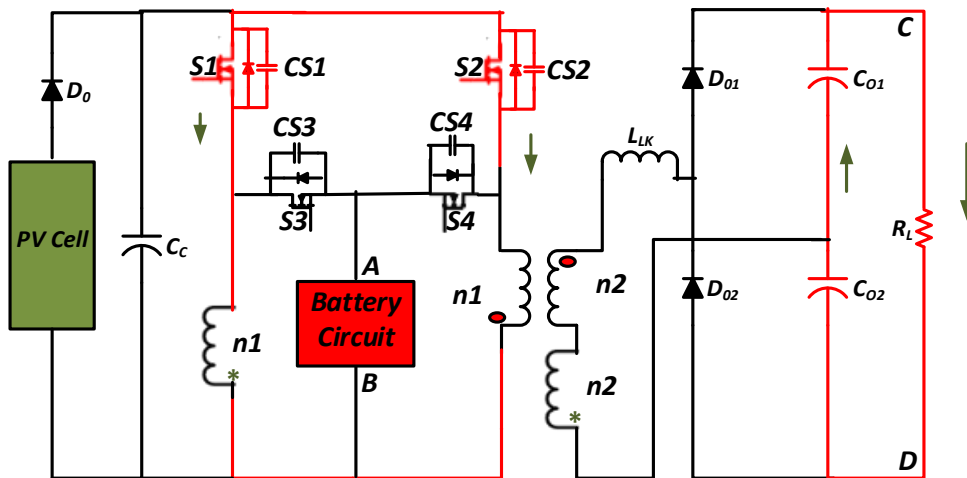


Figure 3.7(c): Operating state 3 of the converter in mode-1

At  $[t_3-t_4]$

At  $t_3$ ,  $S_1$  turns OFF and  $S_3$  turns ON, which turns  $D_{o2}$  ON. The primary side of coupled inductor  $L_1$  charges the battery through  $S_3$ . During this state,  $L_2$  operates in the forward mode and  $L_1$  operates in the flyback mode to transfer energy to the load. When  $S_1$  turns ON and  $D_{o2}$  turns OFF, followed by a new switching period.

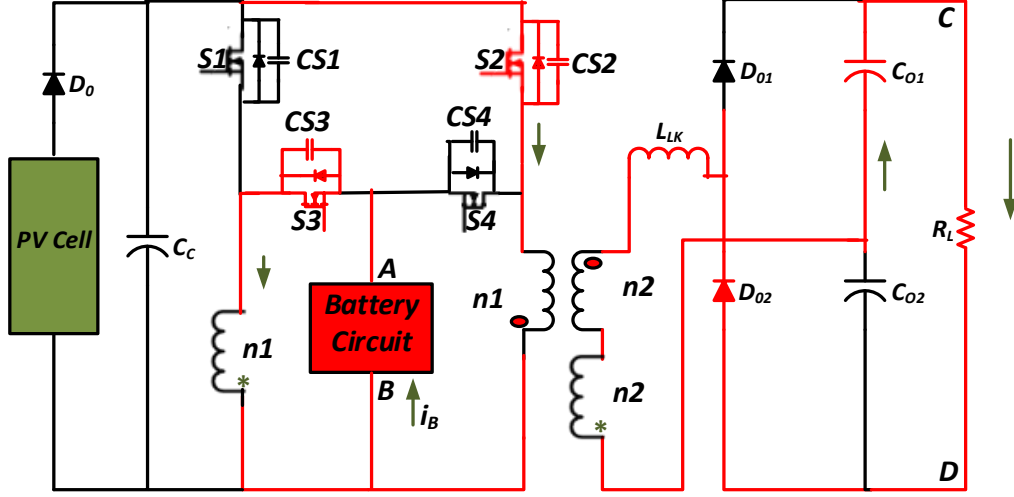


Figure 3.7(d): Operating state 4 of the converter in mode-1

**Mode-2** (Energy flows from battery to the load):

The battery supplies power to the load, as shown in Figure 3.8 indicating the nighttime operation of the stand-alone system. The circuit works as the Flyback-Forward converter, where  $S_3$  and  $S_4$  are the main switches,  $C_c$ ,  $S_1$  and  $S_2$  form an active clamp circuit.

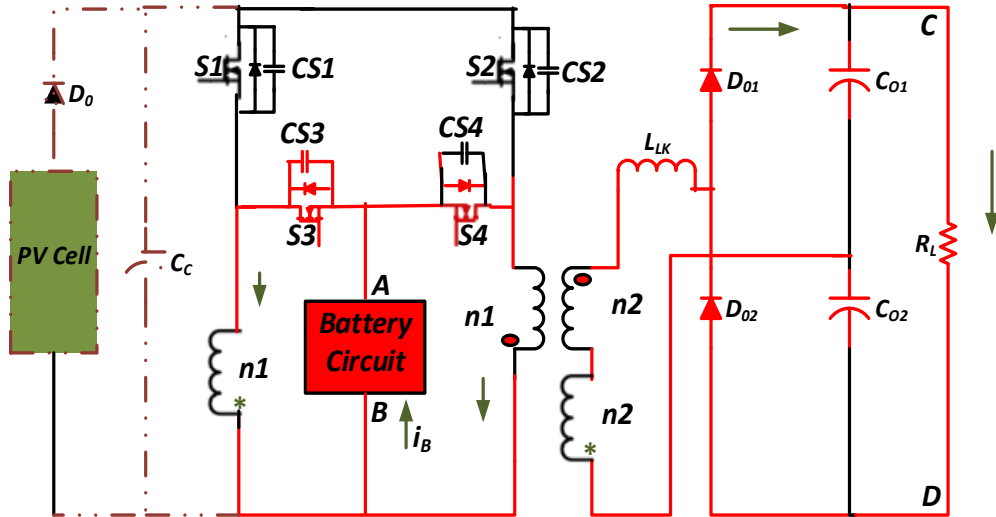


Figure 3.8: Schematic of the converter for “mode-2” operation

During this mode,  $S_1$  and  $S_2$  are turned off and  $S_3$  and  $S_4$  are turned on, but not at a time. The active clamp circuit, composed by another switch and capacitor are used to absorb leakage energy of coupled inductors and suppress the turnoff voltage spike on the main switches during its off state.

**Mode -3** (Energy flows from PV array to battery):

When the load is disconnected, the stand-alone system enters into mode 3. The PV array charges battery without energy transferred to the load due to the opposite series connected structure of the coupled inductor Figure 3.9.  $S_1$  and  $S_2$  work simultaneously and the topology is equivalent to two paralleled Buck-Boost converters.

At  $[t_0-t_1]$

$S_1$  and  $S_2$  are both in turn-ON state, and the two coupled inductors store energy. Due to the series structure of secondary side of two coupled inductors, the load voltage remains zero.

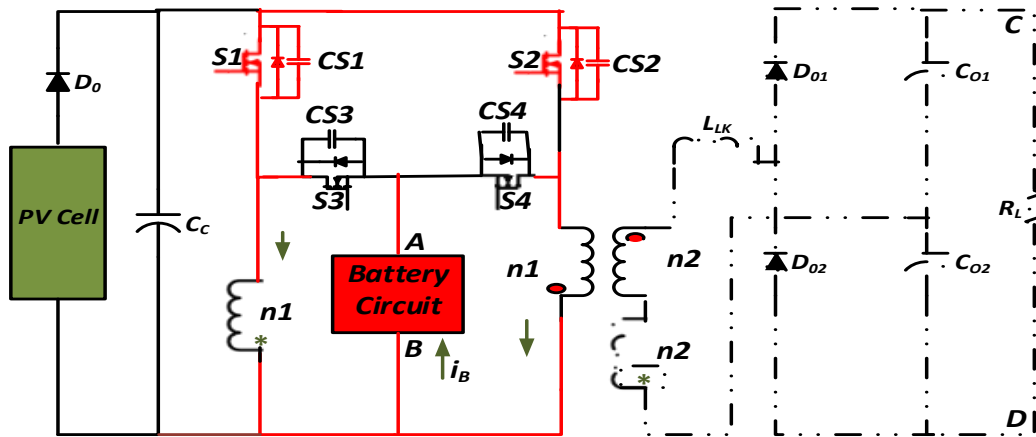


Figure 3.9(a): Schematic of the converter for “mode-3” operation

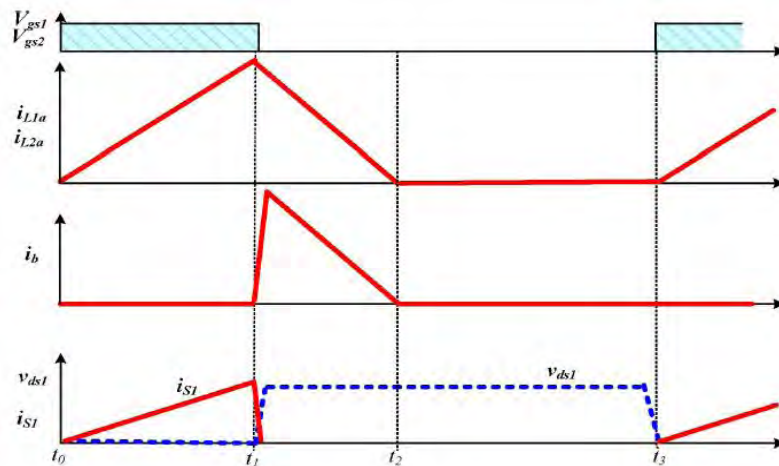


Figure 3.9 (b): Waveforms of the converter under “Mode 3”

*At  $[t_1-t_2]$*

$S_1$  and  $S_2$  both turn OFF, and the energy stored in coupled inductors discharges to the battery.

*At  $[t_2-t_3]$*

$S_1$  and  $S_2$  remain OFF, and the equivalent Buck-Boost converter works in discontinuous mode. When  $S_1$  and  $S_2$  turn ON again, a new switching period begins.

### 3.2.3 Operating principle of battery circuit and load circuit

Figure 3.10 exhibits the switching patterns of “Identically Switched Storage and Load (ISSL) with Shifted Pulse” scheme to provide multiple outputs. These pulses are synchronously operated with identical duty cycle. But each pulse conceives a delay from the previous pulse.

Medium and high voltage power MOSFETs are used in a variety of isolated converter topologies. Zero voltage switching (ZVS) is needed to eliminate turn-on switching losses. Insufficient dead time during turn off can result in the loss of ZVS, poor efficiency, and in the worst case, failure of the device due to shoot-through. The power train remains the same, only the sequence in which devices are turned on and off needs to be modified.

It is well known that a typical semiconducting device (switch) used in converter has an inbuilt delay time when it receives a signal from the gate drive to start up its switching action. Normally, the turning on action is quicker than the turning off. If a switch is turned on without turning off the previous level’s switch, interference may hamper the circuit’s operation. Delay time between turning off and turning on between two consecutive switches is generally defined as dead-time in PWM based converters.

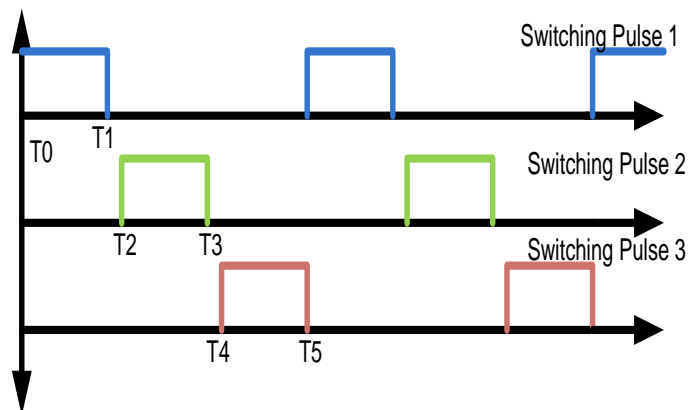


Figure 3.10: Switching pulses of “Identically Switched Storage and Load (ISSL) with Shifted Pulse” topology

In proposed system, the switching frequency is always fixed at 4 KHz (i.e., switching period = 25 ms) with 30% duty cycle whereas switching pulse 1 continues to high from 0 to  $0.75 \times 10^{-4}$  s and the switching pulse 2 starts from  $0.8 \times 10^{-4}$  s and the switching pulse 3 starts from  $1.6 \times 10^{-4}$  s. So the pulses do not overlap with each other.

Three capacitors are connected in series to store electrical energy and the capacitor bank is connected in parallel with the PV panel. Diode  $D_b$  ensures the single way current path from the battery circuit.

Battery Circuit as well as load circuit has three operating states; which are described as follows.

**At ( $T_0$ -  $T_1$ )**

“Switching pulse 1” obtains high value and  $M_{b1}$  is in ON state. Other two switches are in OFF state. Full battery voltage is fed directly to the converter circuit.

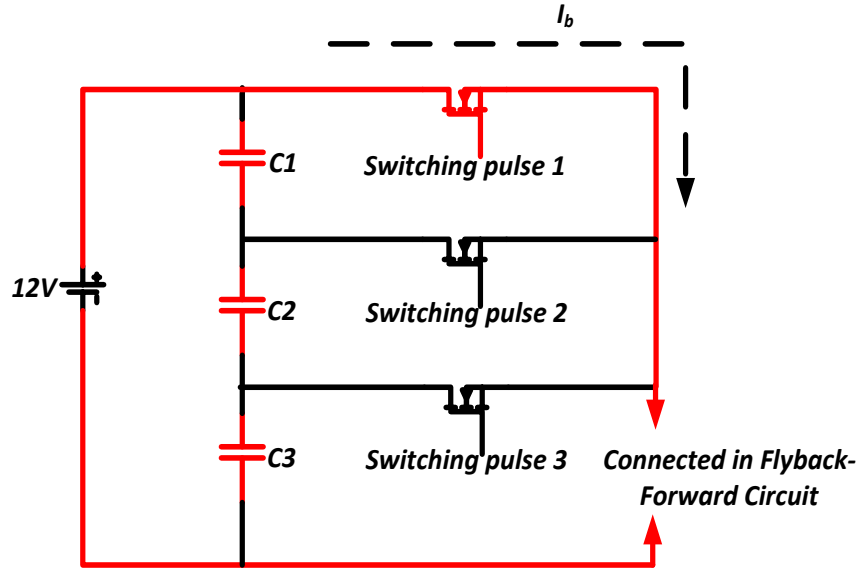


Figure 3.11(a): “State 1” Operation of the “Battery Circuit”

As the switching pulses are identically operated,  $M_{t1}$  is in ON state and “Level1” is directly connected to the converter through two forward biased diodes  $D_{t1}$  and  $D_{t2}$ , switch  $M_{t1}$  and transmission line resistance  $R_1$ . Other two levels are being isolated from the main power converter through respective switches and supplied energy from their own storage elements.

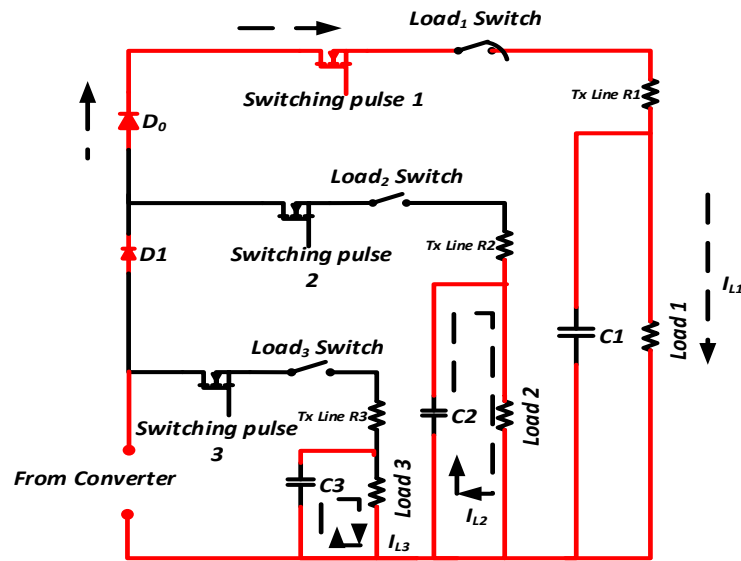


Figure 3.11(b): “State 1” Operation of the “Triple Output Level Circuit”

At ( $T_2$ -  $T_3$ )

“Switching pulse 2” obtains high value and  $M_{b2}$  is in ON state. Other two switches are in OFF state. A proportion of full battery voltage is fed to the converter circuit through capacitive voltage division. Converter terminals are connected with the capacitor bank consisting  $C_{b2}$  and  $C_{b3}$  capacitors.

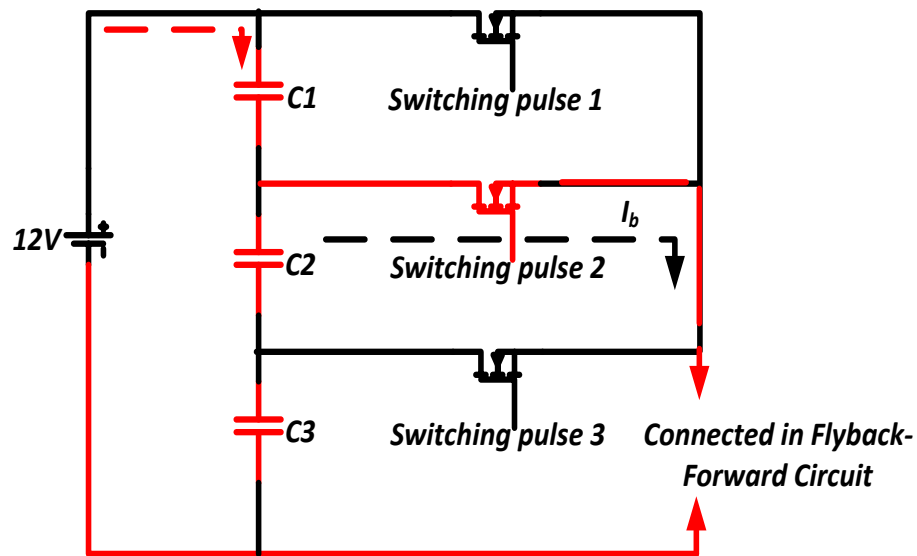


Figure 3.12(a): “State 2” Operation of the “Battery Circuit”

In case of the load circuit, switch  $M_{t2}$  is turned on with the synchronized switch of the battery circuit. Along with this “load 2” is connected directly with the isolated three port converter though diode  $D_{t2}$ , which is in forward bias condition. However, diode  $D_{t1}$  is in

reverse bias condition. During this time, though  $M_{t1}$  and  $M_{t3}$  are turned off, “level 1” and “level 3” are fed by their own capacitances.

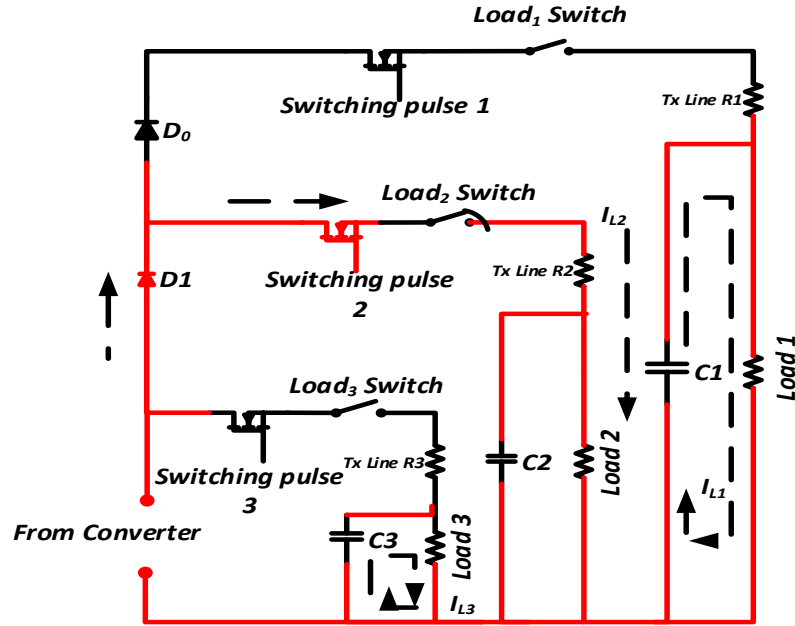


Figure 3.12(b): “State 2” Operation of the “Triple Output Level Circuit”

At ( $T_4$ -  $T_5$ )

“Switching pulse 2” obtains high value and  $M_{b3}$  is in ON state. Other two switches are in OFF state. Capacitor  $C_{b3}$  is connected in parallel with the converter terminals. Input side of the battery circuit complete its circuitry through diode  $D_b$ , and capacitors  $C_{b1}$ ,  $C_{b2}$  and  $C_{b3}$ . However, the output side of the battery circuit consists of only MOSFET  $M_{b3}$  and capacitor  $C_{b3}$ .

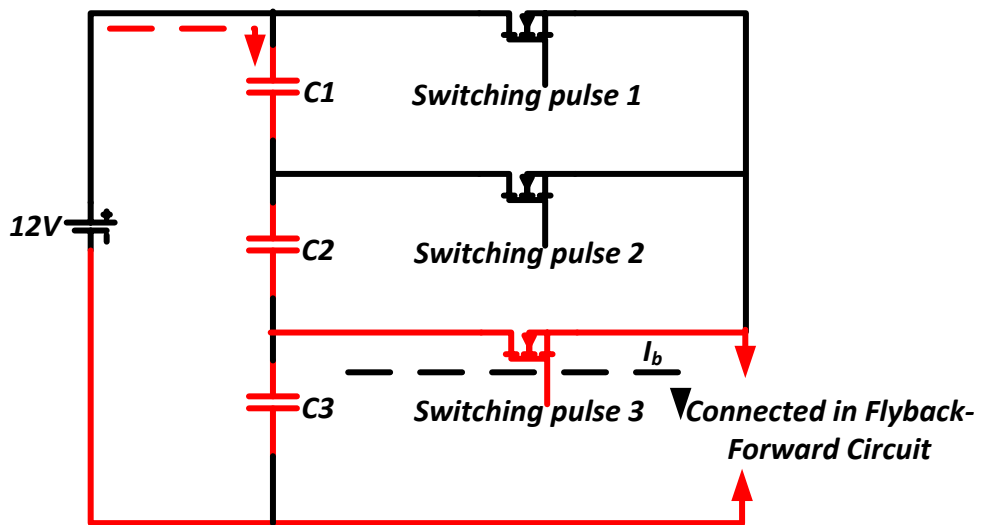


Figure 3.13(a): “State 3” Operation of the “Battery Circuit”

Figure 3.13(b) shows that MOSFET  $M_3$  turns on by switching pulse 3, which is also synced with the corresponding MOSFET of the battery circuit. So, the output is converted for lower voltage level. Both diodes are in reverse bias condition and third level completes its current path with the converter through only switch  $M_3$ .

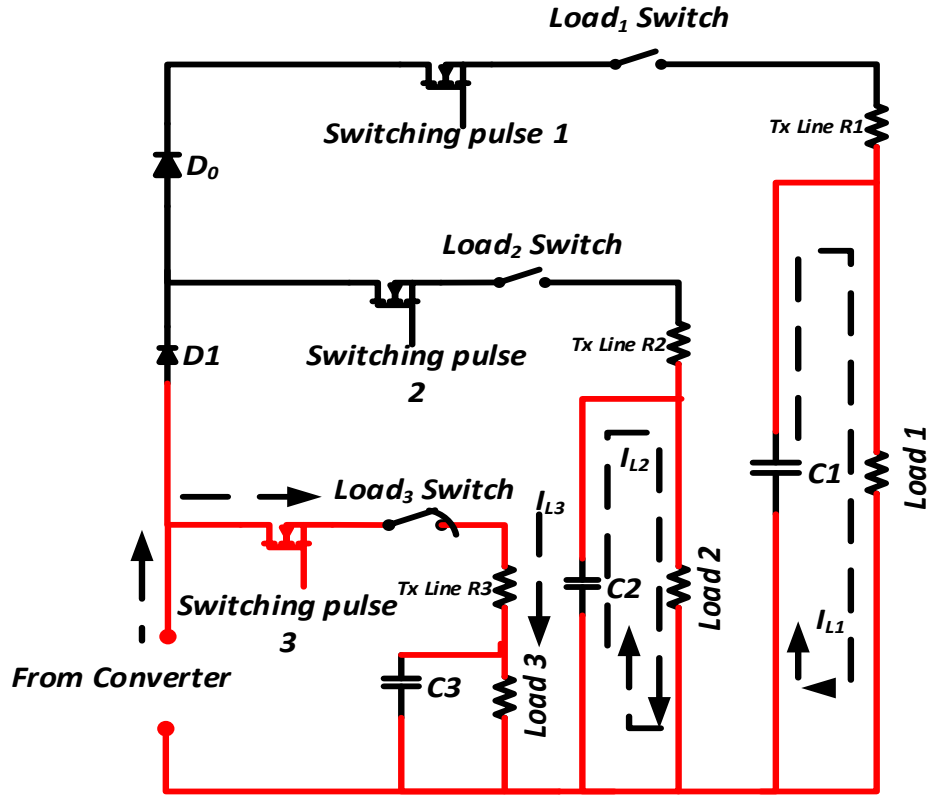


Figure 3.13(b): “State 3” Operation of the “Triple Output Level Circuit”

Proposed scheme has three more states of operation: during time  $T_1$  to  $T_2$ ,  $T_3$  to  $T_4$  and again from  $T_5$  to  $T_0$ . During these periods, all the three switches are theoretically turned off and the loads are supplied energy by their own capacitive elements. These periods are needed practically to rescue the system from interference problems.

### 3.3 Analysis of Converter Efficiency Regarding Duty Ratio:

The effect of change of duty ratio of the DC-DC converter is discussed below.

#### 3.3.1 Analysis of circuit performance for $D \geq 0.5$

When the duty cycle  $D \geq 0.5$ , there are five operating cases which need to be analyzed, as shown in Figure 3.14.

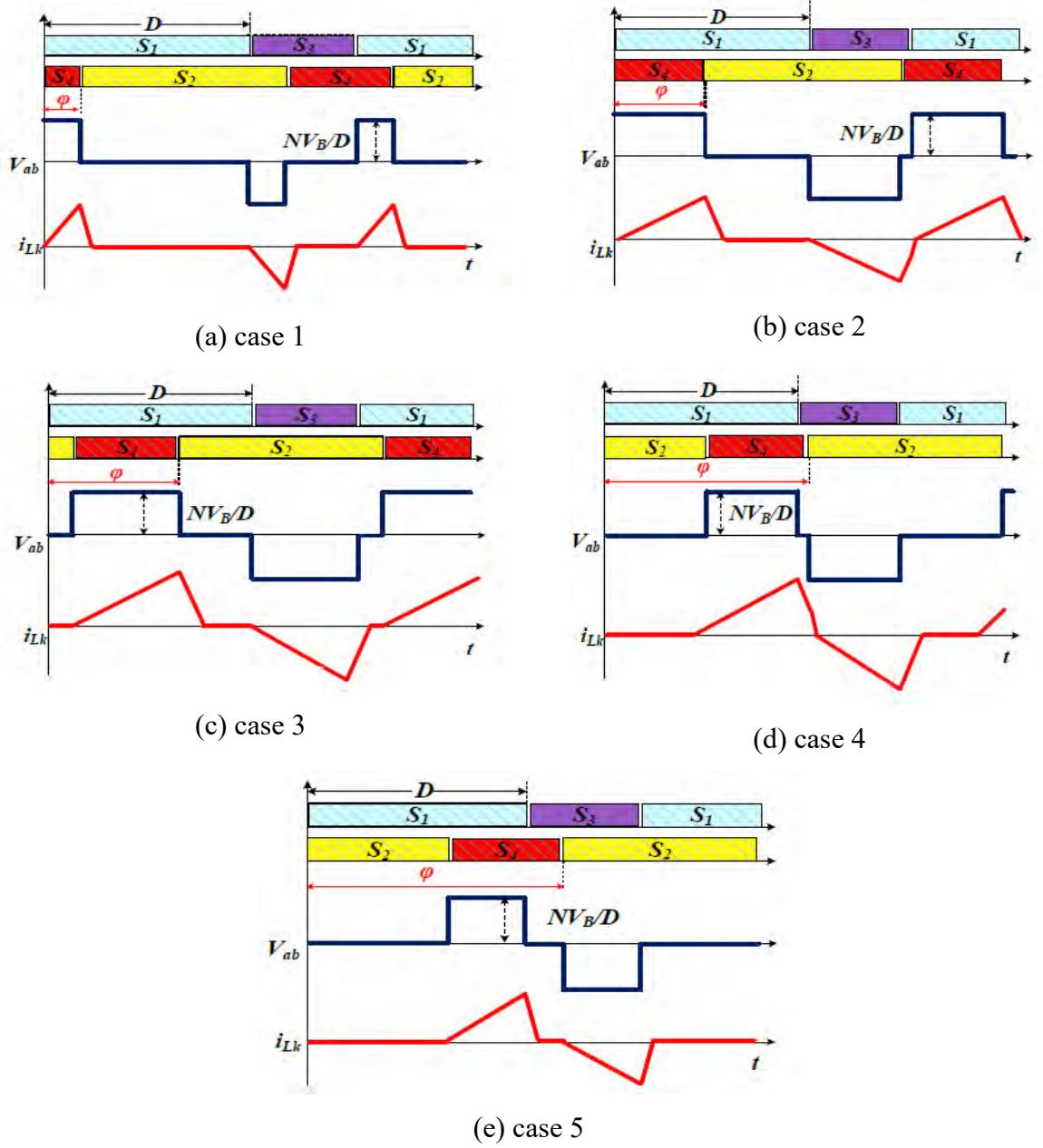


Figure 3.14. Five operational cases for  $D \geq 0.5$ .

**In case 1**, the phase shift angle is between  $0$  and  $\phi_{crit1}$ . From the waveform of the leakage inductor current, the secondary side of the coupled inductor is equivalent to a discontinuous conduction mode (DCM) of a Buck converter. When  $\phi = \phi_{crit1}$ , the current pulses  $A$  and  $B$  is in a boundary conduction mode, as shown in Figure 4.15. For pulse  $A$ , the current decreases to the negative peak value and increases to zero at the time of  $(1-D)T_s$ .

The decrement time is equal to  $T_s \phi_{crit1} / 2\pi$  and the increment time is  $(1 - D - \phi_{crit1} / 2\pi) T_s$ . Following the voltage-second balance (Eq. 3.3), the critical phase angle can be determined by Eq. 3.4.

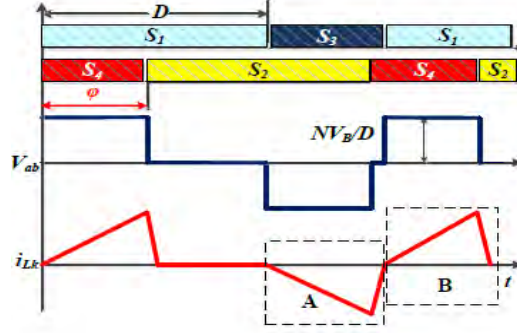


Figure 3.15. Signal waveforms for Case 1

$$\frac{NV_B}{D} \cdot \frac{\phi_{crit1}}{2\pi} \cdot T_s = \frac{V_o}{2} \left( 1 - D - \frac{\phi_{crit1}}{2\pi} \right) T_s \quad (3.3)$$

$$\phi_{crit1} = \pi \cdot D \cdot \left( 1 - D \right) \cdot \frac{V_o}{N \cdot V_B} \quad (3.4)$$

The secondary side of the coupled inductor is equivalent to two Buck converters connected in parallel at the DCM operational condition. The corresponding equivalent duty ratio of the Buck converter is  $\phi/2\pi$ . Provided the voltage gain of the Buck converter in DCM, the output voltage is given by:

$$V_o = 2 \cdot \frac{2}{1 + \sqrt{1 + \frac{4 \cdot 2 \cdot L_k}{R_o \cdot T_s \cdot (\phi/2\pi)^2 / 2}}} \cdot \frac{NV_B}{D} \quad (3.5)$$

**In case 2**, the phase shift angle is between  $\phi_{crit1}$  and  $\phi_{crit2}$ .  $\phi_{crit2}$  is the transition point from a continuous conduction mode (CCM) to a DCM, which can be determined by Eq. 3.6. The voltage equations at  $\phi_{crit1}$  and  $\phi_{crit2}$  are derived by Eqs. 3.7 and 3.8.

$$\phi_{crit2} = \frac{4\pi \cdot (1 - D)}{D} \cdot \frac{N \cdot V_B}{V_{out}} \quad (3.6)$$

$$\frac{NV_B}{DL_k} \cdot (1 - D) = \frac{V_o}{2 \cdot L_k} \cdot \frac{\phi_{crit2}}{2 \cdot \pi} \quad (3.7)$$

$$\frac{N \cdot V_B}{D \cdot L_k} \cdot \frac{\phi_{crit2}}{2 \cdot \pi} = \frac{V_o}{2 \cdot L_k} \cdot (1 - D) \quad (3.8)$$

**In case 3**, the angle shifts from  $\phi_{crit2}$  to  $\phi_{crit3}$ . The duty ratio of the secondary side of the Buck converter stays constant, and the voltage gain reaches the highest. Therefore, the

critical point,  $\phi_{crit3}$ , and the corresponding voltage can be calculated by Eqs. 3.9 and 3.10.  $\phi_{crit3}$  is the boundary point between DCM and CCM. With the increase in the PS angle, the voltage declines. In this case, the output voltage cannot be controlled by PS, as suggested by Eq. 3.11.

$$\phi_{crit3} = 2\pi - \phi_{crit2} \quad (3.9)$$

$$\frac{NV_B/D}{L_k} (1 - D) = \frac{V_o}{2L_k} \left(1 - \frac{\phi_{crit3}}{2\pi}\right) \quad (3.10)$$

$$V_o = 2 \cdot \frac{2}{1 + \sqrt{1 + \frac{4 \cdot 2 \cdot L_k}{R_o \cdot T_s \cdot (1 - D)^2 / 2}}} \cdot \frac{NV_B}{D} \quad (3.11)$$

**In case 4**, the PS angle ranges from  $\phi_{crit3}$  to  $\phi_{crit4}$ . The leakage inductor current is still higher than zero before next voltage pulse.  $\phi_{crit4}$  is the boundary point between DCM and CCM. The critical point,  $\phi_{crit4}$  and the corresponding voltage can be expressed as Eqs. 3.12 and 3.13.

$$\phi_{crit4} = 2\pi - \phi_{crit1} \quad (3.12)$$

$$\frac{N \cdot V}{D \cdot L_k} \cdot \left(1 - \frac{\phi_{crit4}}{2 \cdot \pi}\right) = \frac{V_o}{2 \cdot L_k} \cdot (1 - D) \quad (3.13)$$

**In case 5**, the phase shift angle increases from  $\phi_{crit4}$  to  $2\pi$ . The duty ratio of the secondary side Buck converter is  $1 - \phi/2\pi$ . The output voltage can be given by:

$$V_o = 2 \cdot \frac{2}{1 + \sqrt{1 + \frac{4 \cdot 2 \cdot L_k}{R_o \cdot T_s \cdot (1 - \phi/2\pi)^2 / 2}}} \cdot \frac{NV_B}{D} \quad (3.14)$$

### 3.3.2 Analysis of Circuit Performance for $D < 0.5$

Similarly, there are five operating cases for  $D < 0.5$ . The respective waveforms are shown in Figure 3.16

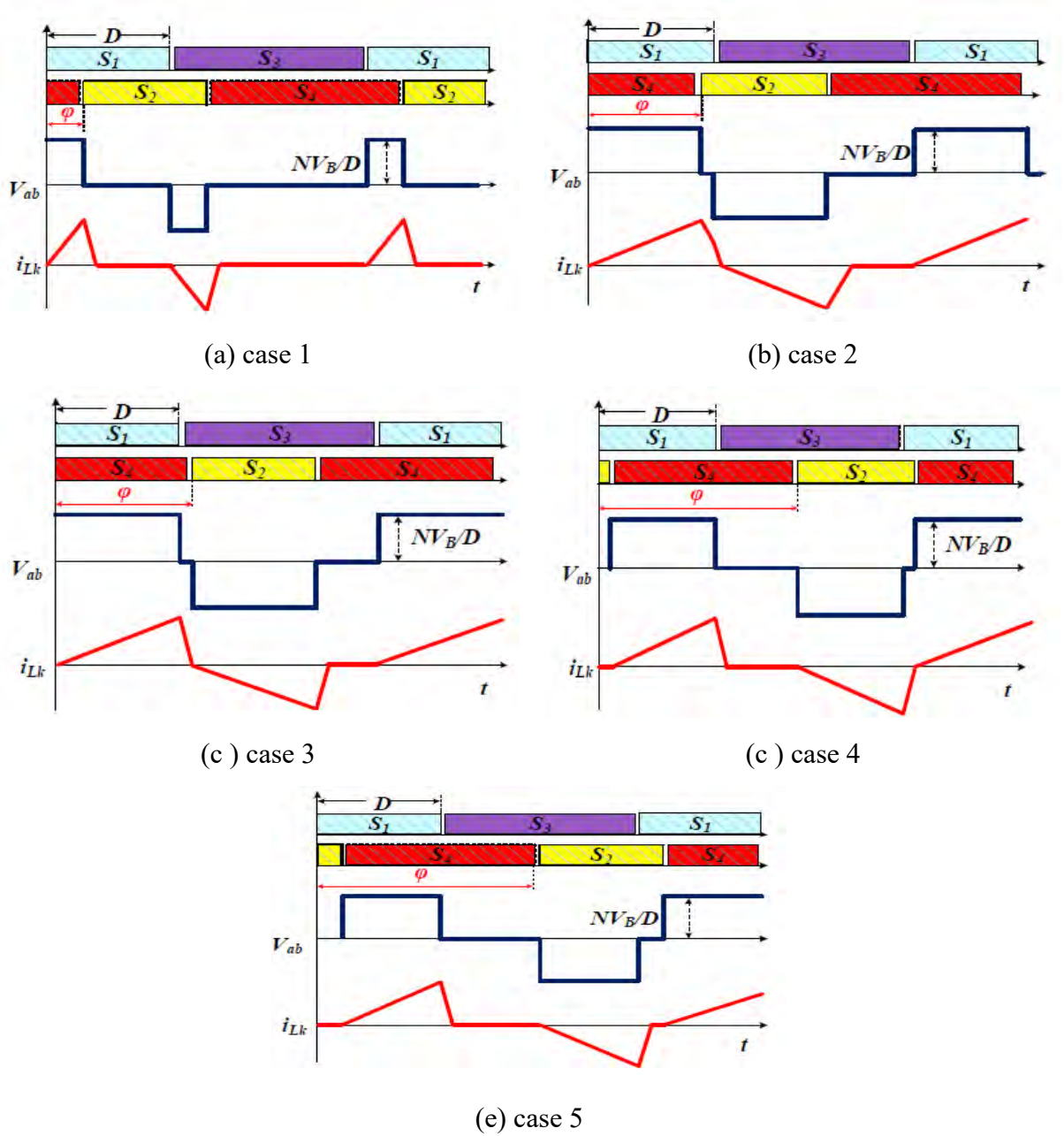


Figure 3.16: Five cases under  $D < 0.5$

**In Case 1** ( $0 < \phi < \phi_{crit1}$ ), considering the waveform of the leakage inductor current, the secondary side of the coupled inductor is equivalent to a DCM Buck converter, the corresponding duty ratio is  $D = \phi/2\pi$ . Thus the critical angle and the output voltage are:

$$\phi_{crit1} = \pi \cdot D^2 \cdot \frac{V_o}{N \cdot V_B} \quad (3.15)$$

$$V_o = 2 \cdot \frac{2}{1 + \sqrt{1 + \frac{4 \cdot 2 \cdot L_k}{R_o \cdot T_s \cdot (\phi/2\pi)^2/2}}} \cdot \frac{NV_B}{D} \quad (3.16)$$

**In case 2** ( $\phi_{crit1} < \phi < \phi_{crit2}$ ), the leakage inductor current is still above zero. The system equations can be expressed as:

$$\phi_{crit2} = 4\pi \cdot \frac{N \cdot V_B}{V_o} \quad (3.17)$$

$$\frac{N \cdot V_B}{D \cdot L_k} \cdot \frac{\phi_{crit1}}{2 \cdot \pi} = \frac{V_o}{2 \cdot L_k} \cdot D \quad (3.18)$$

$$\frac{NV_B}{DL_k} \cdot D = \frac{V_o}{2 \cdot L_k} \cdot \frac{\phi_{crit2}}{2 \cdot \pi} \quad (3.19)$$

**In case 3** ( $\phi_{crit2} < \phi < \phi_{crit3}$ ), the duty ratio of the secondary winding is equal to  $D$ . The system equations are

$$\phi_{crit3} = 2\pi - \phi_{crit4} \quad (3.20)$$

$$\frac{NV_B}{DL_k} \cdot D = \frac{V_o}{2 \cdot L_k} \cdot \left(1 - \frac{\phi_{crit3}}{2 \cdot \pi}\right) \quad (3.21)$$

$$V_o = 2 \cdot \frac{2}{1 + \sqrt{1 + \frac{4 \cdot 2 \cdot L_k}{R_o \cdot T_s \cdot (D)^2 / 2}}} \cdot \frac{NV_B}{D} \quad (3.22)$$

**In case 4** ( $\phi_{crit3} < \phi < \phi_{crit4}$ ), the leakage inductor current is still above zero. The system equations can be expressed as

$$\phi_{crit4} = 2\pi - \phi_{crit1} \quad (3.23)$$

$$\frac{N \cdot V_B}{D \cdot L_k} \cdot \left(1 - \frac{\phi_{crit4}}{2 \cdot \pi}\right) = \frac{V_o}{2 \cdot L_k} \cdot D \quad (3.24)$$

**In case 5** ( $\phi_{crit4} < \phi < 2\pi$ ), the duty ratio of the secondary winding is  $1 - \phi/2\pi$ . The output voltage is derived by

$$V_o = 2 \cdot \frac{2}{1 + \sqrt{1 + \frac{4 \cdot 2 \cdot L_k}{R_o \cdot T_s \cdot (1 - \phi/2\pi)^2 / 2}}} \cdot \frac{NV_B}{D} \quad (3.25)$$

### 3.3.3 Simulated result

For this standalone PV system, Duty ratio (D) is the control variable to balance the PV voltage and battery voltage and phase angle ( $\phi$ ) is employed to control the secondary output voltage. The two-freedom control makes it flexible to control the PV, battery and load. One condition should be applied to achieve decoupled control performance, which can be expressed as  $0 < \phi < \phi_{crit2}$  and  $\phi_{crit3} < \phi < 2\pi$ . If this is not satisfied, the secondary output voltage is dictated by the switching duty cycle instead of the phase shift angle as presented in Eqs. 3.22 and 3.25.

Table 3.1: Effect of Duty cycle and phase shift angle of MOSFETs' on output voltage of DC-DC converter

Duty cycle (D)	S1	S2	S3	S4	Duty cycle (D)	S1	S2	S3	S4	Duty cycle (D)	S1	S2	S3	S4
	.66	.66	.33	.33		.33	.33	.66	.66		.5	.5	.5	.5
Phase angle	Output voltage (Volt)				Phase angle	Output voltage (Volt)				Phase angle	Output voltage (Volt)			
50	53				50	80				50	80			
100	58.8				100	93.5				100	84.5			
125	58.8				125	91.7				125	86.4			
230	59				230	91.7				230	86.4			
260	58.5				260	88.7				260	84.1			

In mode 1, the primary side is equivalent to an interleaved Buck-Boost converter operating in the continuous conduction mode due to the asymmetrical complementary operation of the switching devices ( $S_1$ ,  $S_3$ ) and ( $S_2$ ,  $S_4$ ). The operation of the secondary side follows a Buck converter whose duty ratio can be controlled by phase shift angle except for case 3.

Simulation work is carried out in the MATLAB/SIMULINK platform to analyze the effect of duty cycle and phase shift on the output voltage of the ITPC. Table 3.1 exhibits the output voltage for different combination of the control variables. It is observed that, output voltage is increased with the increasing values of phase angle between the gate pulses of  $S_1$  and  $S_2$ . After a certain value, output voltage is reduced with increasing phase angle. When duty ration of  $S_1$  and  $S_2$  is above 50%, output voltage is being varied between 53 V to 59 V, whereas this value is varied from 80V to 93.5V for below 50% duty ratio of above mentioned switches. Figure 3.17 clearly illustrates that, for a specific

phase angle, converter provides better output for the duty ratio of less than 50% for switch  $S_1$  and  $S_2$ .

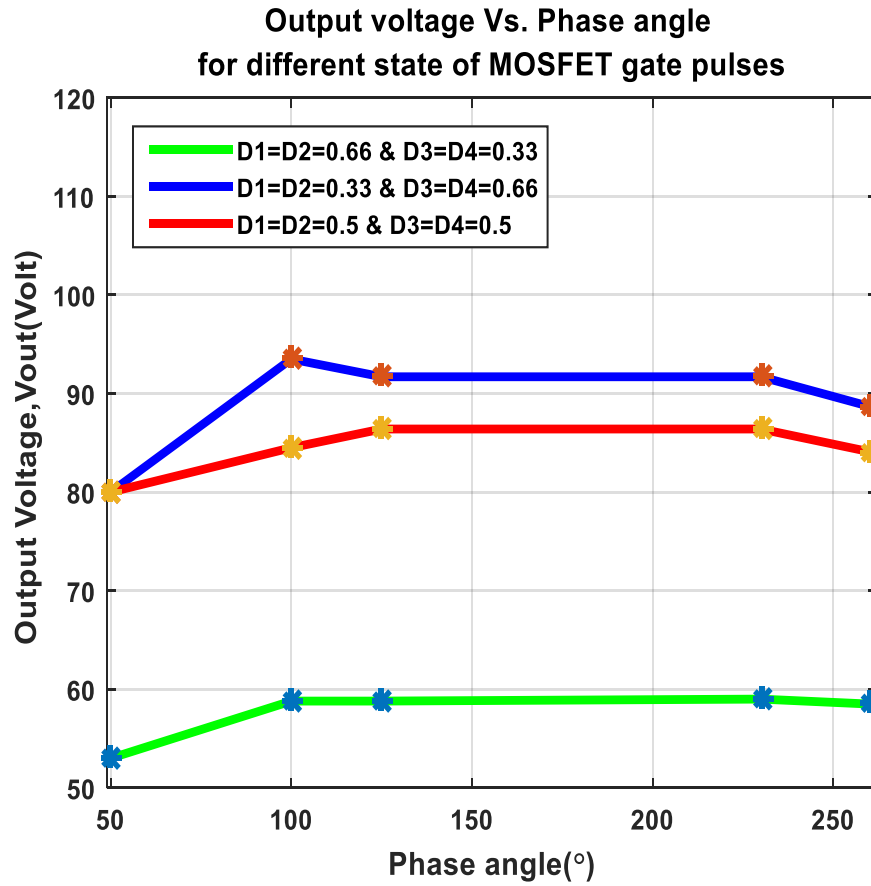


Figure 3.17: Waveshapes of Output voltage vs. Phase angle of 4 converter switches for different combinations of duty ratio

### 3.4 Control Circuit

In order to improve the device sharing ratio among different ports, realize soft-switching operation, and achieve decoupled control within a certain operating range, PWM plus phase angle shift (PPAS) control scheme is a novel solution. The switch duty cycle is adopted to achieve the maximum power point tracking (MPPT) performance and balance the voltages between the battery and the PV cells. Furthermore, the phase is employed as another control freedom to regulate the secondary output voltage. As a result, great control flexibility is provided.

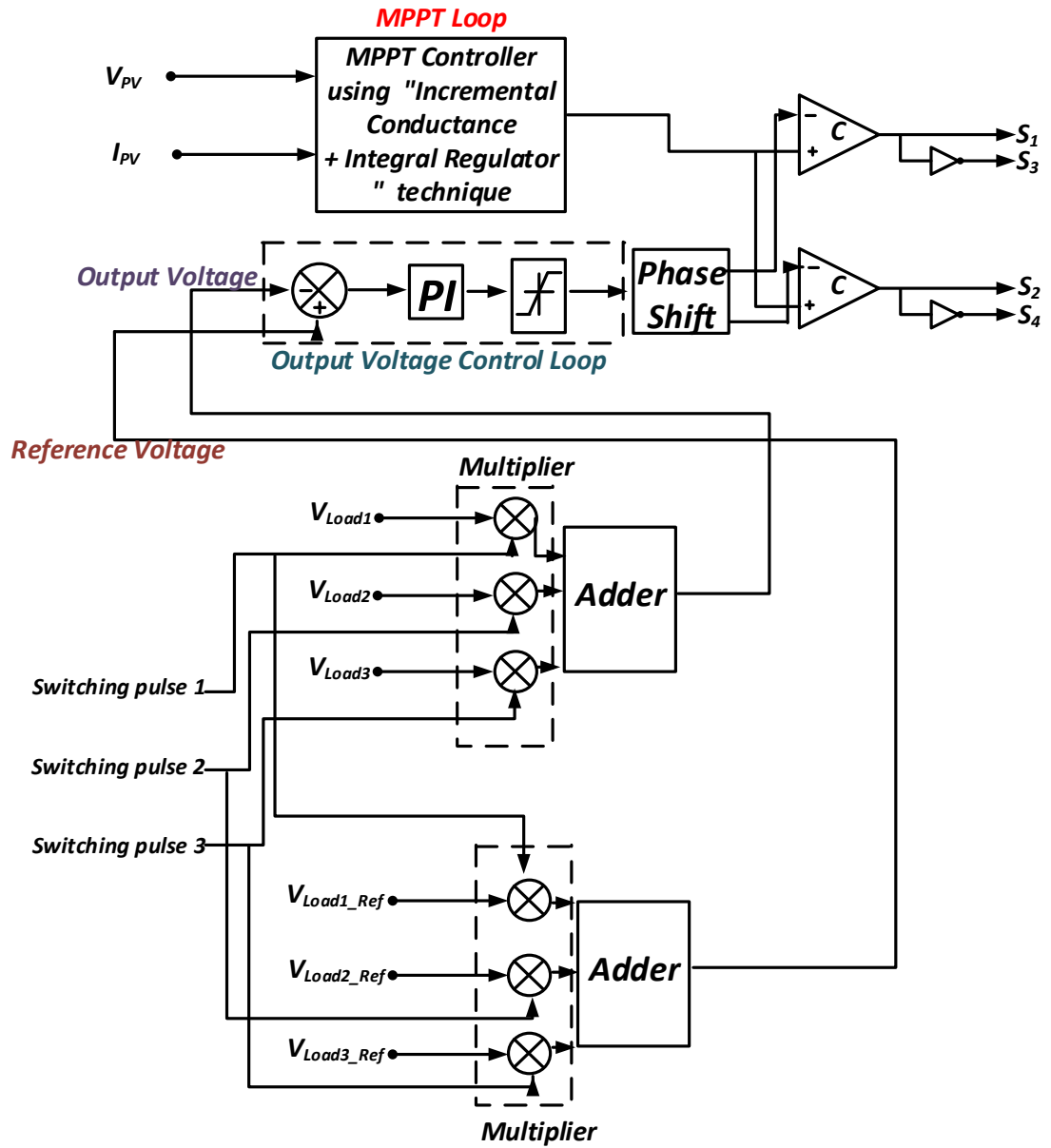


Figure 3.18: Schematic of control circuit

In mode 1,  $S_1$  and  $S_3$  complementarily conduct, and the on/off operation of  $S_2$  and  $S_4$  is complementary. When the output power of the PV array is lower than the load power, the battery should supply the difference. The primary side of ITPC is equivalent to a bidirectional Buck-Boost converter, while the secondary side is a Buck converter in discontinuous conduction mode. The output voltage can be controlled by phase shift on the primary side bridge arm, which can be approximated to adjust the duty cycle of Buck converter of secondary side to realize output voltage regulation. The control block diagram of the proposed control scheme is further illustrated in Figure 3.18.

The maximum power point tracking (MPPT) can be implemented by Incremental Conductance method. In the MPPT loop, the PV voltage is regulated to follow an optimal operating point of the PV array. Moreover, the PV voltage regulation loop is used to improve

the MPPT performance. But there is a problem in this method. If MPP lies on right side,  $dI/dV < -I/V$  and then the PV voltage must be decreased to reach the MPP [9]. If MPP lies on left side,  $dI/dV > -I/V$  and then the PV voltage must be increased to reach the MPP. But when it is near MPP then there is some oscillation. which is improved by using integral regulator. Duty cycle is corrected in final output in Integral Controlled Incremental Conductance method.

In the output voltage control loop, the phase angle of the modulation carrier is the control variable, which regulates the output voltage to follow the expected voltage. Output voltage control loop consists of proportional integral (PI) controller, which needs two variables: set point (sp) and process variable (pv) to reach the desired point. As the proposed converter has three different output levels, so during each period of the identical switches of the “battery circuit” and “triple output circuit”, “sp” and “pv” needs to be updated three times. And each time selection of “sp” and “pv” is done by the identical switches that establish synchronism between the “battery circuit” and “triple output circuit” of the standalone system. This novel single unit control scheme can protect voltage fluctuation for triple output levels.

Because of the block diode in the PV input, mode 1 can be switched to mode 2 by changing  $D \geq 0.5$  to  $D < 0.5$ . Likewise, the modes can be switched from 1 to 3 by controlling the phase shift angle between  $S1$  and  $S2$ . These transitions are smoothly achieved by this control scheme.

### 3.4.1 Incremental Conductance and integral control technique

The incremental conductance (IncCond) algorithm is derived by differentiating the PV array power with respect to voltage and setting the result equal to zero [117]. This is shown in the following equation:

$$\frac{dP}{dV} = \frac{d(VI)}{dV} = I + V \frac{dI}{dV} = 0 \text{ at the MPP} \quad (3.26)$$

$$-\frac{I}{V} = \frac{dI}{dV} \quad (3.27)$$

Note that the left-hand side of Eq. (3.4) represents the opposite of the PV array’s instantaneous conductance, while the right-hand side represents its incremental conductance.

Thus, at the MPP, these two quantities must be equal in magnitude, but opposite in sign. If the operating point is off of the MPP, a set of inequalities can be derived from Eq. (3.27) that indicates whether the operating voltage is above or below the MPP voltage. These relationships [118] are summarized in the following equations:

$$\frac{dI}{dV} = -\frac{I}{V} ; \left( \frac{dP}{dV} = 0 \right), \text{ at MPP} \quad (3.28)$$

$$\frac{dI}{dV} > -\frac{I}{V} ; \left( \frac{dP}{dV} > 0 \right), \text{ left of MPP} \quad (3.29)$$

$$\frac{dI}{dV} < -\frac{I}{V} ; \left( \frac{dP}{dV} < 0 \right), \text{ right of MPP} \quad (3.30)$$

Eqs. (3.29) and (3.30) are used to determine the direction in which a perturbation must occur to move the operating point toward the MPP, and the perturbation is repeated until Eq. (3.28) is satisfied. Once the MPP is reached, the MPPT continues to operate at this point until a change in current is measured. This change in current will correlate to a change in irradiance on the array.

As their radiance on the array increases, the MPP moves to the right with respect to the array voltage, as shown in Figure 3.19. To compensate for this movement of the MPP, the MPPT must increase the array's operating voltage. The opposite is true when a decrease in irradiance is detected (via a decrease in the measured current).

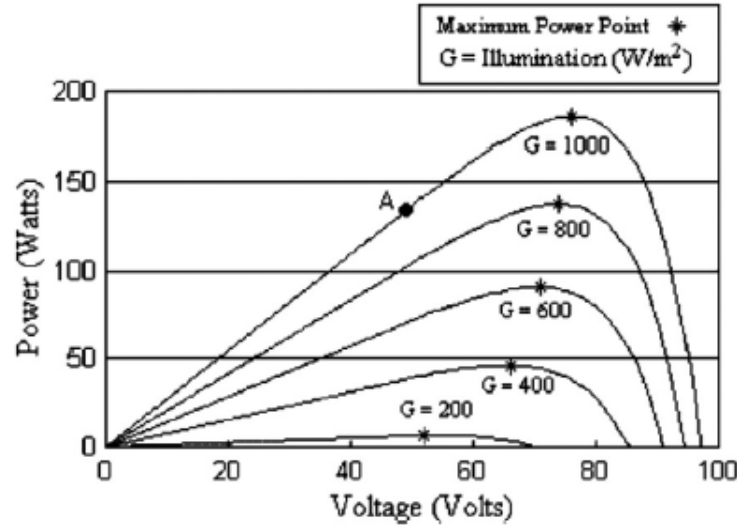


Figure 3.19: Photovoltaic array power-voltage relationship [119]

From the above mentioned it is clear that, the IncCond [119,120] method is based on the fact that the slope of the PV array power curve (Figure 3.19) is zero at the MPP, positive on the left of the MPP, and negative on the right.

Figure 3.20 shows a flow chart for the incremental conductance algorithm [117]. The present value and the previous value of the solar array voltage and current are used to calculate the values of  $dI$  and  $dV$ . If  $dV=0$  and  $dI=0$ , then the atmospheric conditions have

not changed and the MPPT is still operating at the MPP. If  $dV=0$  and  $dI>0$ , then the amount of sunlight has increased, raising the MPP voltage.

This requires the MPPT to increase the PV array operating voltage to track the MPP. Conversely, if  $dI<0$ , the amount of sunlight has decreased, lowering the MPP voltage and requiring the MPPT to decrease the PV array operating voltage. If the changes in voltage and current are not zero, the relationships in Eqs. (3.29) and (3.30) can be used to determine the direction in which the voltage must be changed in order to reach the MPP. If  $dI/dV>-I/V$ , then  $dP/dV>0$ , and the PV array operating point is to the left of the MPP on the P–V curve. Thus, the PV array voltage must be increased to reach the MPP. Similarly, if  $dI/dV<-I/V$ , then  $dP/dV<0$  and the PV array operating point lies to the right of the MPP on the P–V curve, meaning that the voltage must be reduced to reach the MPP. Here in lies a primary advantage of incremental conductance over the perturb and observe algorithm: incremental conductance can actually calculate the direction in which to perturb the array's operating point to reach the MPP, and can determine when it has actually reached the MPP. Thus, under rapidly changing conditions, it should not track in the wrong direction, as P&O can, and it should not oscillate about the MPP once it reaches it.

The increment size determines how fast the MPP is tracked. Fast tracking can be achieved with bigger increments but the system might not operate exactly at the MPP and oscillate about it instead; so there is a trade-off.

Kobayashi et al. [117] proposed a method that brings the operating point of the PV array close to the MPP in a first stage and then uses IncCond to exactly track the MPP in a second stage. Through proper control of the power converter, the initial operating point is set to match a load resistance proportional to the ratio of the open circuit voltage (VOC) to the short-circuit current (ISC) of the PV array. This two stage alternative also ensures that the real MPP is tracked in case of multiple local maxima.

Measurements of the instantaneous PV array voltage and current require two sensors. The IncCond method lends itself well to DSP and microcontroller control, which can easily keep track of previous values of voltage and current and make all the decisions as per Figure 3.20.

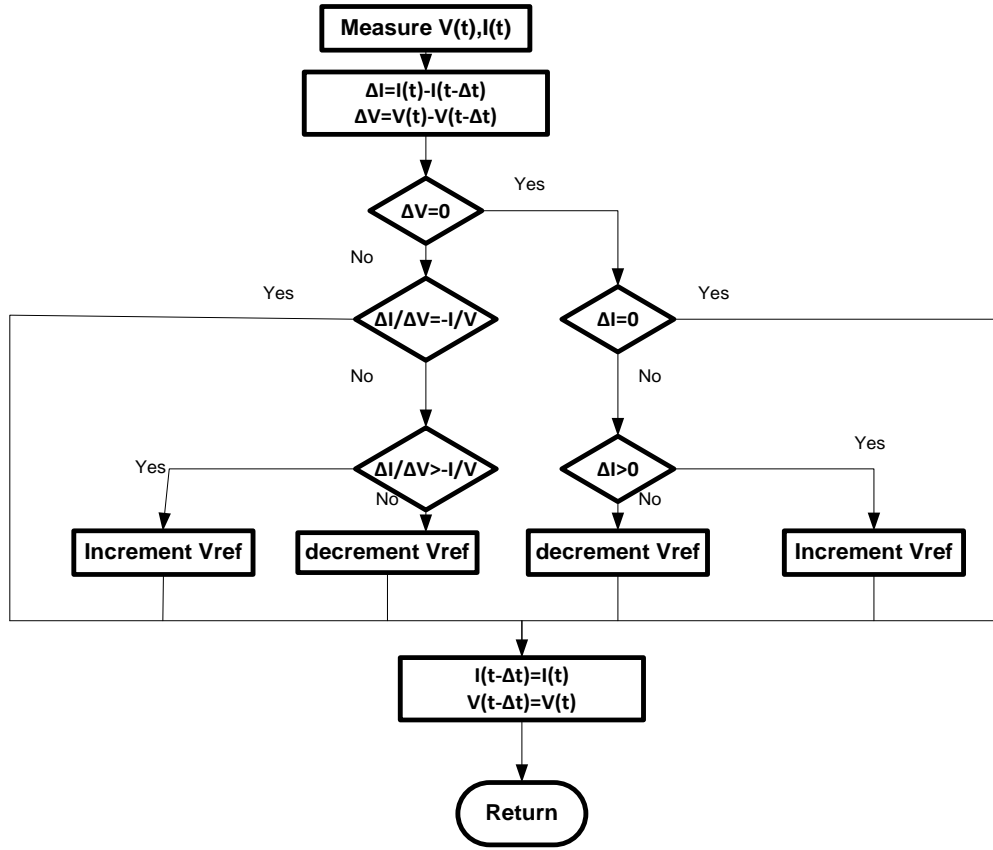


Figure 3.20: Incremental conductance algorithm flowchart [119]

### 3.4.2 Proportional integral controller

First analysis of the PID controller was made by Minorshy [121]. Due to its simplicity and acceptable results this most primitive controller is still used in the industry. The best known controller used in industry is the proportional-integral (PI) controller because of its simple structure and its robust performance in a wide range of operating conditions. This linear regulator is based on a very simple structure, whose functioning depends only on two parameters, namely the proportional gain ( $K_p$ ) and the integral gain ( $K_i$ ) [122]. Mathematically the functionality of a PI controller can be expressed as:

$$CO = K_p \Delta + K_i \int \Delta dt$$

Where,  $\Delta$  = set point(SP) – process variable(PV)

CO = controller output signal

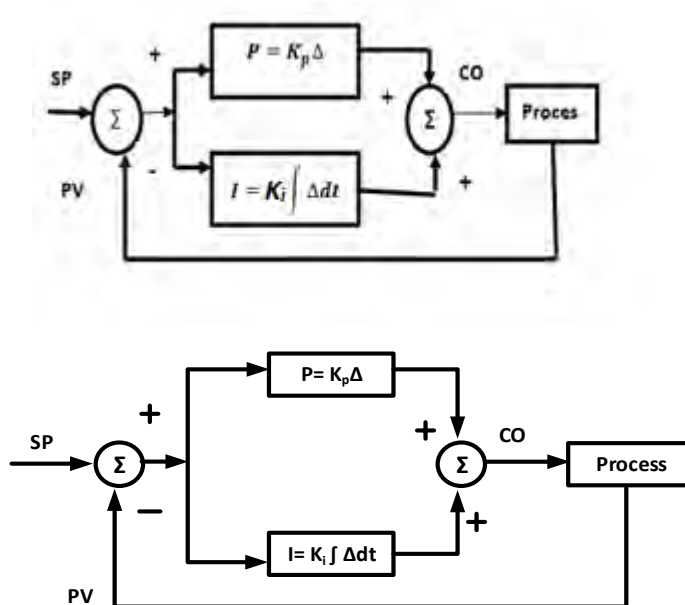


Figure 3.21: PI controller Structure

The integral term continually sums up error. Through constant summing, integral action accumulates influence based on how long and how far the measured PV has been from SP over time.

#### Effect of ( $K_p$ ):

- Increasing  $k_p$  will reduce the steady state error.
- After certain limit increasing  $k_p$  only causes overshoot.
- Increasing  $k_p$  reduces the rise time [123].

#### Effect of ( $K_i$ ):

- Integral control eliminates the steady state error.
- After certain limit, increasing  $k_i$  will only increase overshoot.
- Increasing  $k_i$  reduces the rise time a little.

The major inconvenience of this type of controllers is the necessity of the a priori knowledge of the various parameters of the system (i.e. induction motor). Any imperfections in the system model can deteriorate the controller performance. Moreover, PI controllers are sensitive to system parameter variations during operation and are required to be tuned externally in order to maintain satisfactory performance during operation where system parameters may vary under various operation conditions.

Several methods of tuning a PI controller have been invented; the most used are the poles assignment method and the Ziegler-Nichols method [124]. To surmount this inconvenience, it is possible to use a procedure of optimization to better design this type of controller. Genetic Algorithm methods [125] have been widely used in these control

applications. They are stochastic optimization methods based on the principles of natural biological evolution. The GA methods have been employed successfully to solve complex optimization problems. The use of GA methods in the determination of the different controller parameters is practical due to their fast convergence and reasonable accuracy. The parameters of the PI controller are determined by the minimization of an objective function.

## Chapter 4

### Comparison between Experimental and Simulated Work

In this chapter, the simulated waveforms of the circuit and practical work are focused. The simulation is done in MATLAB SIMULINK platform. Whereas practical work is done to compare the result.

#### 4.1 SIMULINK model of the circuit:

Here in Figure 4.1 the simulated circuit is shown. The circuit consists of three parts named the input circuit, the DC-DC converter circuit and the load circuit. In converter circuit the control circuit is also integrated. The parameters are used from MATLAB/SIMULINK blocks. The outputs are taken from the scope. The proposed system of single input triple output SHS system is implemented using the below mentioned circuit.

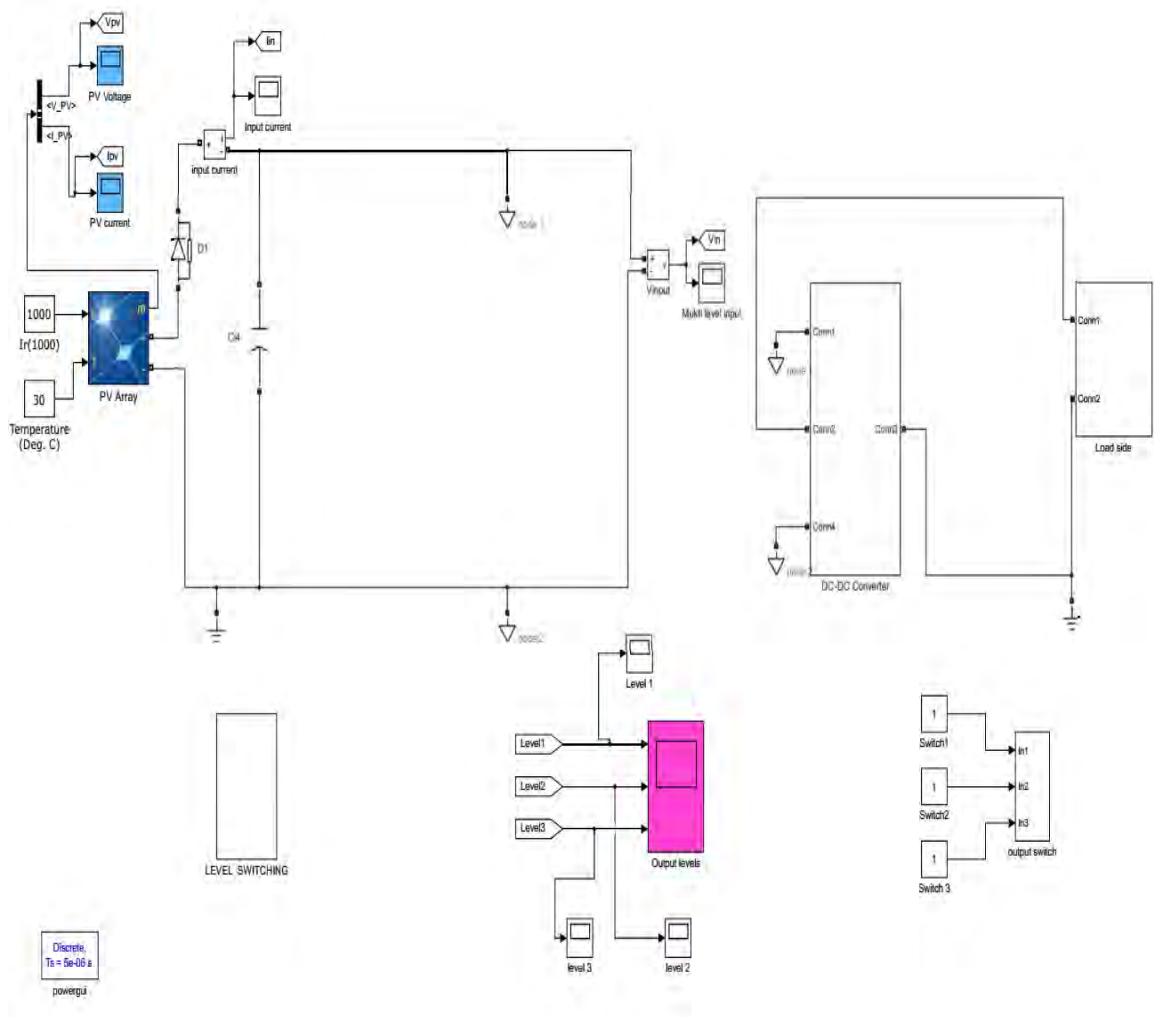
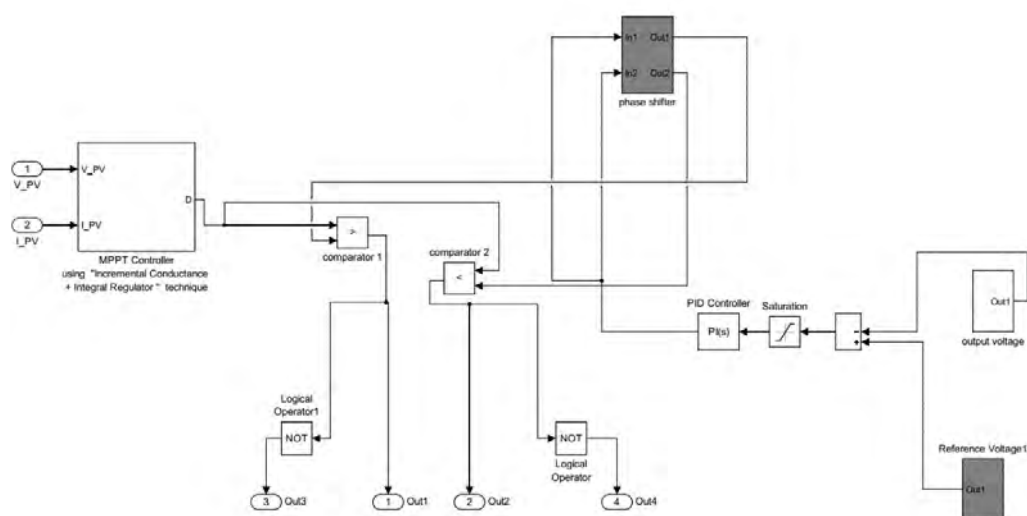


Figure 4.1: SIMULINK model of the entire circuit.

Figure 4.3 is the inner view of control circuit. Here for control mechanism MPP algorithm with integral regulator is used to control the gate pulses.



70

Figure 4.4 is the load circuit as we discussed in earlier, chapter 3. Here we can see the three SPDT switches are controlled using gate pulses. So that we can get the synchronous triple output from a single input of DC-DC converter.

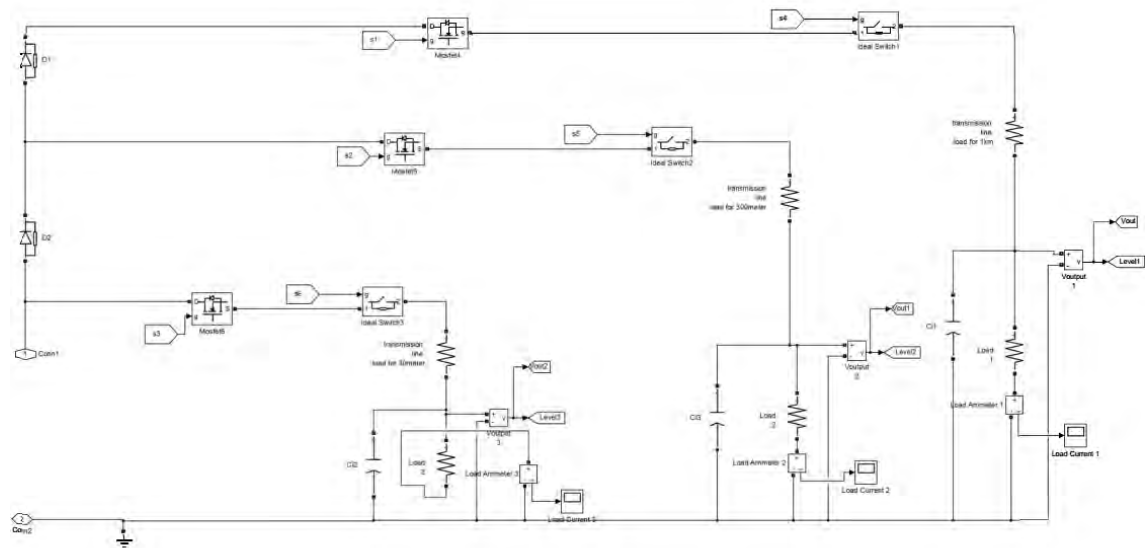


Figure 4.4: Simulink model of Load circuit

## 4.2 Simulated Waveforms

This output is from the solar panel which is almost 12.8 V. The simulated waveform is shown in Figure 4.5 with respect of time.

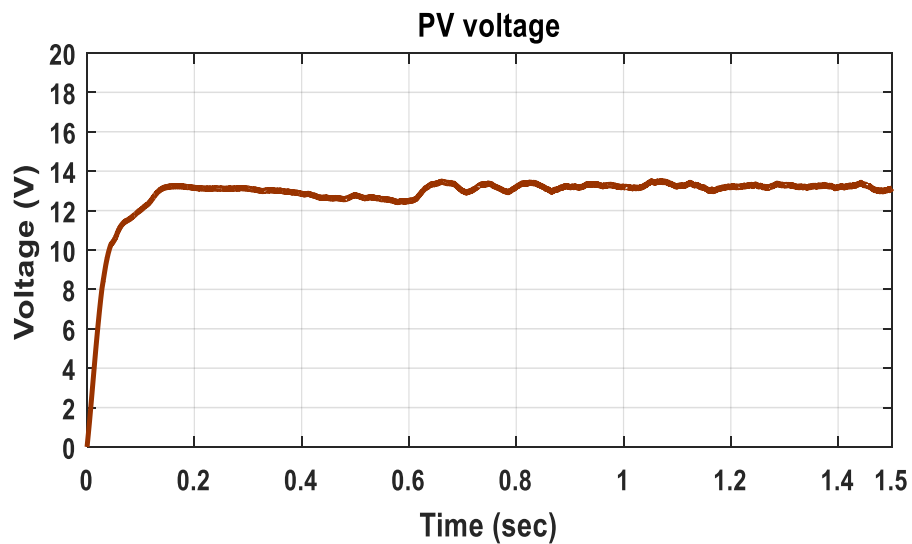


Figure 4.5: Voltage of solar panel

This is the input current. The current which one is fed to multilevel converter shown in Figure 4.6.

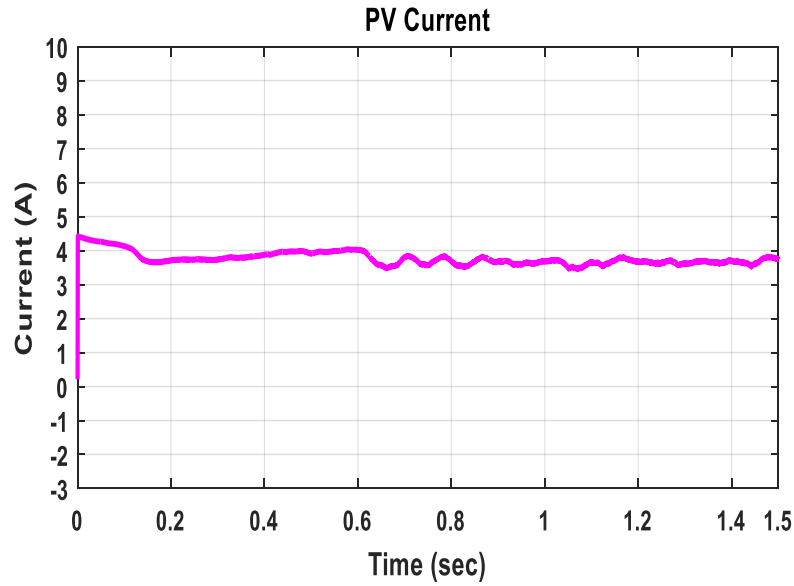


Figure 4.6: Current of solar panel

The gate pulses of converter are shown below in Figure 4.7:

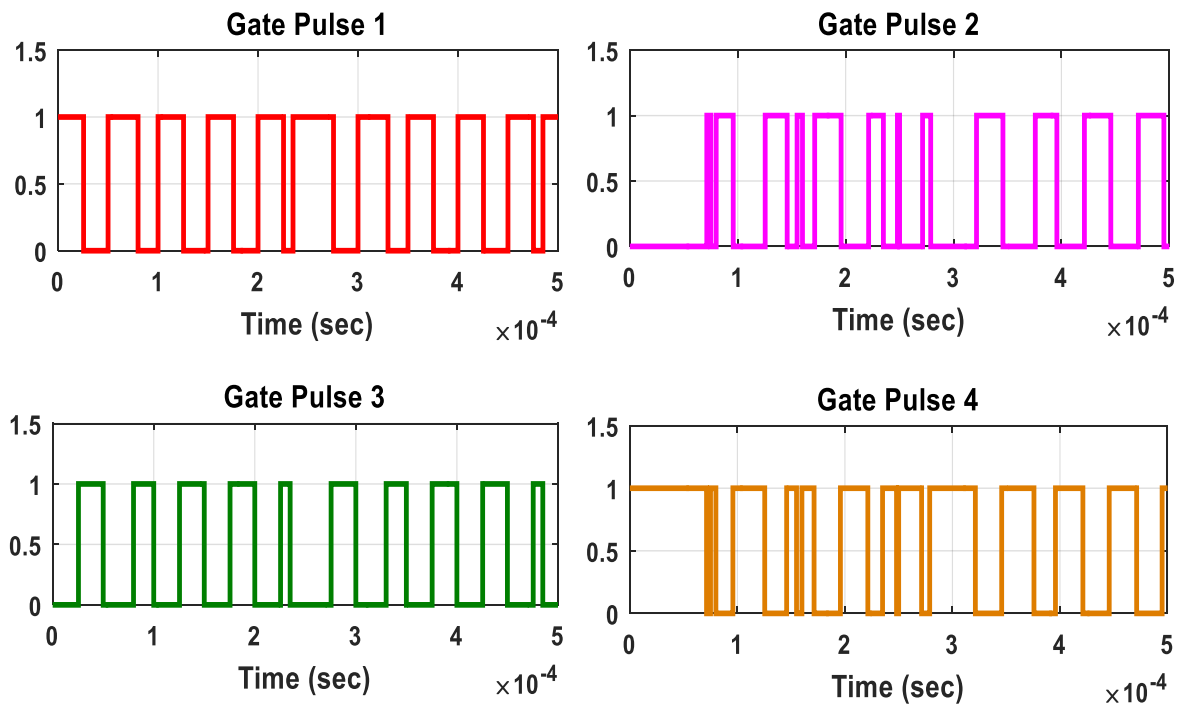


Figure 4.7: Gate pulses of the ITPC

These are the outputs of voltages of multilevel converter. From Figure 4.8 it is shown that the outputs are divided in three voltage levels.

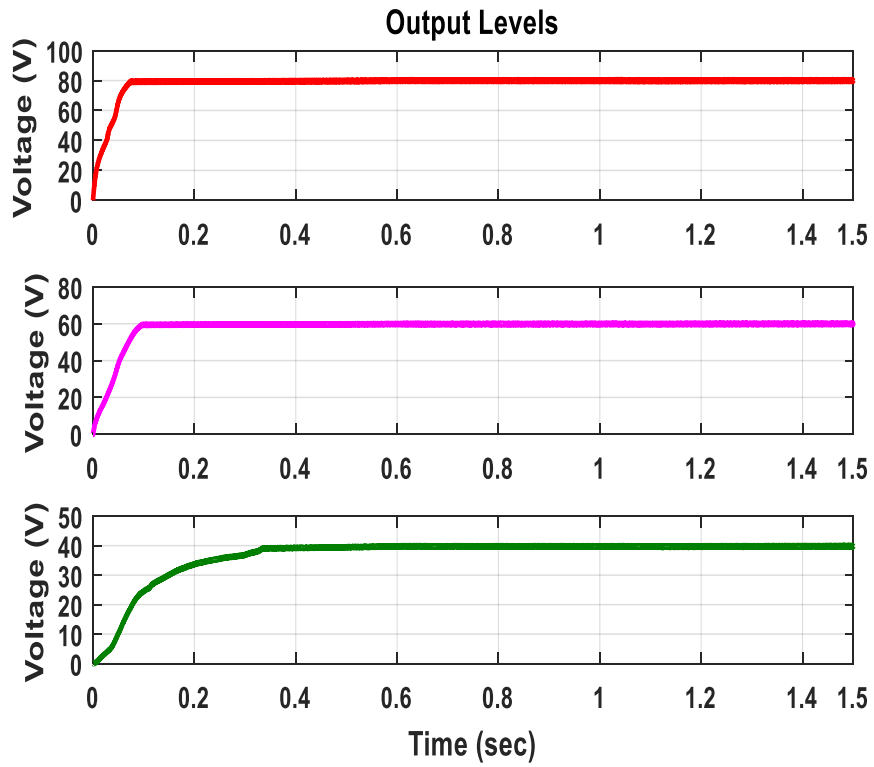


Figure 4.8: Multilevel voltage wave shapes

The output currents are shown below. Here in Figure 4.9 three levels of current as voltage of loads are shown.

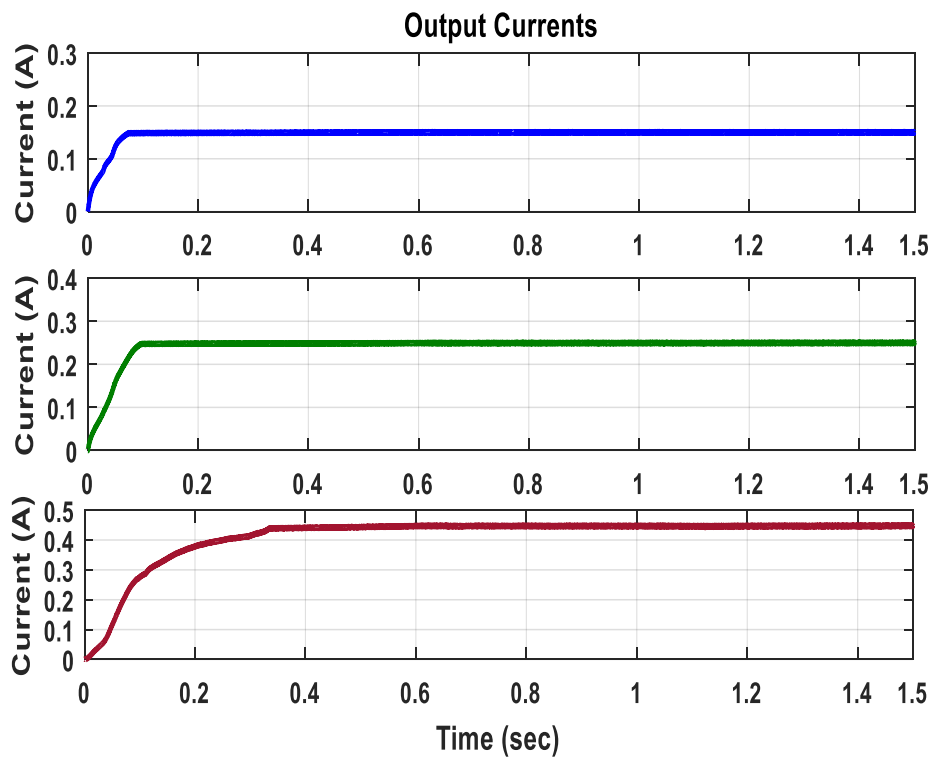


Figure 4.9: Multilevel current wave shapes

The gate pulses of battery circuit and load circuit are shown below. The three gate pulses of battery and load circuit, both will trigger in synchronous time are shown in Figure 4.10.

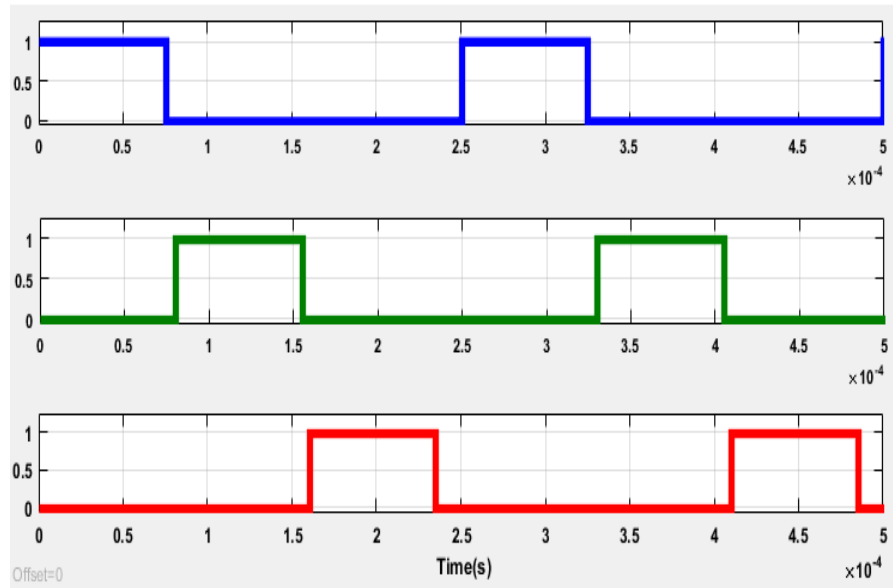


Figure 4.10: Gate pulses of dynamic ISSL scheme

#### 4.2.1 Electrical Properties:

In table 4.1 the simulated voltage, current and power of input and converter circuit is given. Here it is observed that the efficiency of the system is almost 98%.

Table 4.1: Electrical properties of input and output Flyback-Forward converter

Input			Converter Output		
Voltage (V)	Current (A)	Power (W)	Voltage (V)	Current (A)	Power (W)
13.3 V	3.7A	49.21 W	57.5 V	0.84A	48.3 W
			Efficiency: 98%		

In table 4.2 the three output voltage, current and power is shown.

Table 4.2: Electrical Properties of output levels

Output Levels								
Level 1			Level 2			Level 3		
Vo1 (V)	Io1 (A)	Po1 (W)	Vo2 (V)	Io2 (A)	Po2 (W)	Vo3 (V)	Io4 (A)	Po4 (W)
80	0.15	12	60	0.25	15	40	0.45	18

#### 4.2.2 Designed Parameters

Table 4.3 shows the designed parameter used to simulate the proposed system.

Table 4.3: Parameters of PV module

Electrical Parameters	Values
Maximum Power rating ( $P_M$ )	51.2 W
Rated Voltage ( $V_M$ )	12.8 V
Rated Current ( $I_M$ )	4 A
Open Circuit Voltage ( $V_{oc}$ )	16 V
Short circuit current ( $I_s$ )	4.4 A
Temp. coefficient of $I_s$ ( $k_i$ ) (%/deg.C)	.09
Temp. coefficient of $V_{oc}$ ( $k_v$ ) (%/deg.C)	-.36
Diode ideality factor (A)	2.591
Equivalent Series resistance ( $R_s$ )	0.31018
Equivalent Shunt resistance	70.7947

Table 4.4 is the DC-DC converters parameter. The transformer is used in flyback-forward converter for galvanic isolation.

Table 4.4: Parameters of Isolated Flyback-Forward converter

Electrical Parameters	Values
Transformer turns ratio	1:2
L	1e-6 H
C1	1e-6 F
C2	1e-6 F
Switching Frequency	20 KHz
Output Voltage Level 1,2,3	80,60,40 V

Table 4.5 is the listed values used to design the load circuit. Here capacitors are used to smooth the DC output and the resistances are used to define the loads.

Table 4.5: Parameters of Multiple output level circuit

Output Levels	Electrical Parameters	Values
Level 1	Capacitor (C)	100e-6 F
	Resistance (R)	533 $\Omega$
Level 2	Capacitor (C)	200e-6 F
	Resistance (R)	240 $\Omega$
Level 3	Capacitor (C)	600e-6 F
	Resistance (R)	89 $\Omega$

Table 4.6 defines the parameter used to design the battery circuit. Here capacitors are used to divide the voltage of the battery.

Table 4.6: Parameters of Battery circuit

Electrical Parameters	Values
Battery voltage	12 V
Capacitor C1	1e-4 s
Capacitor C2	1e-4 s
Capacitor C3	1e-4 s

Table 4.7 that shows the constants of proportional and integral controller used in the control circuit.

Table 4.7: Design control parameters

Proportional Integral to control output voltage	
Kp	0.98
Ki	0.1

### 4.2.3 Observation

In order to establish a dynamic ISSL scheme with control strategy including MPPT and output voltage regulation, simulation work is carried out in the MATLAB/SIMULINK environment. PV panel specifications are mentioned in Table 4.3 under 1000 W/m<sup>2</sup>

irradiance and 30°C temperature condition. Moreover, the simulation parameters of the isolated three port converter and the values of the inductors, capacitors and resistances of SITO converter are tabulated in Table 4.4, 4.5 and 4.6.

As shown in Figure 4.5 the PV voltage is regulated to 13.3V, which represents the MPP (maximum power point) for the simulated system. PV current more closely approximates DC, with an average value of about 3.7A is shown in Figure 4.6. However, resulting power generated by the PV panel can be approximated at 49.21 watt.

Figure 4.7 illustrates the gate pulses of the isolated three port flyback-forward converter incorporates with PPAS (PWM plus and phase angle shift) with ZVS. These pulses show clearly that the switching frequency is always fixed at 20 KHz (i.e., switching period = 50µs). As well as it is also observed that S1, S2 and S3, S4 have the same duty ratio with a phase shift.

The main contribution of research is to develop a single input triple output converter (SITO). Figure 4.8 displays triple voltage levels that can be used for multiple users of SHS. The three voltage levels of the SITO ITPC are 80V, 60V, 40V. Along with these, Figure 4.9 presents corresponding currents waveforms of 0.15A, 0.25A and 0.45A. As we know that if voltage is increased the current of the system is decreased to maintain constant power management. Here the level 1 shows HV system with minimal level of current and the remaining levels are vice versa. System is designed considering loads situated in different distance ranges. It is considered that “level 1” is a load of 12watt with 1km distance with transmission line resistance of 0.727 Ω. Along with this, “level 2” is designed as 15 watt with 300m distance and “level 3” is the nearest load of 18watt with 30m distance. It is also observed from triple output voltage levels, steady state arise earlier for the long distant high voltage level.

Fig 4.10 exhibits the gate pulses of the dynamic ISSL scheme, which is used for both “battery circuit” and “triple output level circuit” synchronously. These pulses have the same switching frequency of 4 KHz (i.e., switching period = 25ms) with 30% duty ratio. First pulse possesses no time delay, whereas second one is phase shifted version and delayed 5microsec from first one and the third one is delayed 5micro sec from second one and this pattern repeats continuously without any change.

Table 4.1 illustrates high efficient feature of the ITPC converter incorporated with proposed “battery circuit”, as it provides 98% efficiency. Therefore, Table 4.2 presents different electrical properties of multiple output levels. Furthermore, it is observed that

the dynamic SITO converter associated with unique ISSL provides an efficiency of 92% providing triple voltage levels at a time.

### 4.3 Experimental Setup

The experimental setup of the mentioned work is done without feedback control. Figure 4.11, 4.12, 4.13, 4.14, 4.15 and 4.16 are the figures of practical circuit, output and gate pulses that are implemented experimentally. The proposed topology is implemented by a prototype without feedback dual output system. The SIMULINK model is implemented practically would be helpful for future explanation. The different blocks are leveled in the diagrams. The practical circuit is designed for dual output single input. Two outputs are 16 volts and 6 volts are found from experimental circuit. If the duty cycle is varied, then the output is also changed. There are some conduction and switching losses due to MOSFETS.

#### 4.3.1 Waveforms

In Figure 4.11 the blocks are leveled separately for easier interpretation. Here the converter block is designed using ferrite core transformer, especially designed practically for flyback-forward converter. The system is designed for dual output from a synchronously operated to have multiple outputs at a time. The converter block mosfets are driven by ATmega 8P microcontroller. But the battery and load mosfets are driven by microcontroller and H-bridge amplifier using BD135. For isolation of gate pulses isolation transformers are used. In case of solar panel a DC source is used to have a prototype source.

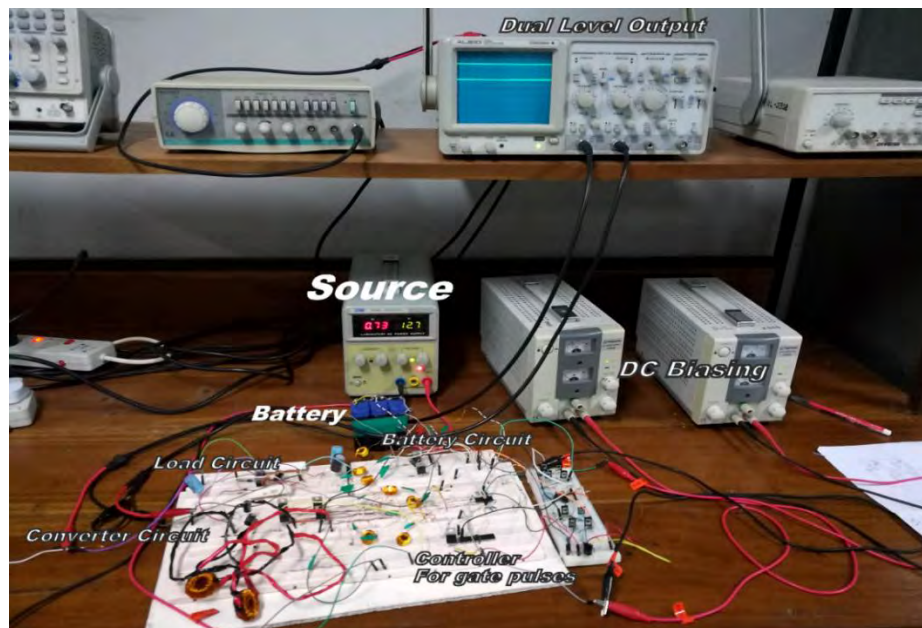


Figure 4.11: Overall Experimental Setup

In Figure 4.12 individual blocks are shown from top view for better appearance. The TL074 IC is used for converter transformers. As the transformers saturate in faster switching outputs from microcontroller. And also for giving a safer pulse to mosfets and controller from reverse current from isolation transformers.

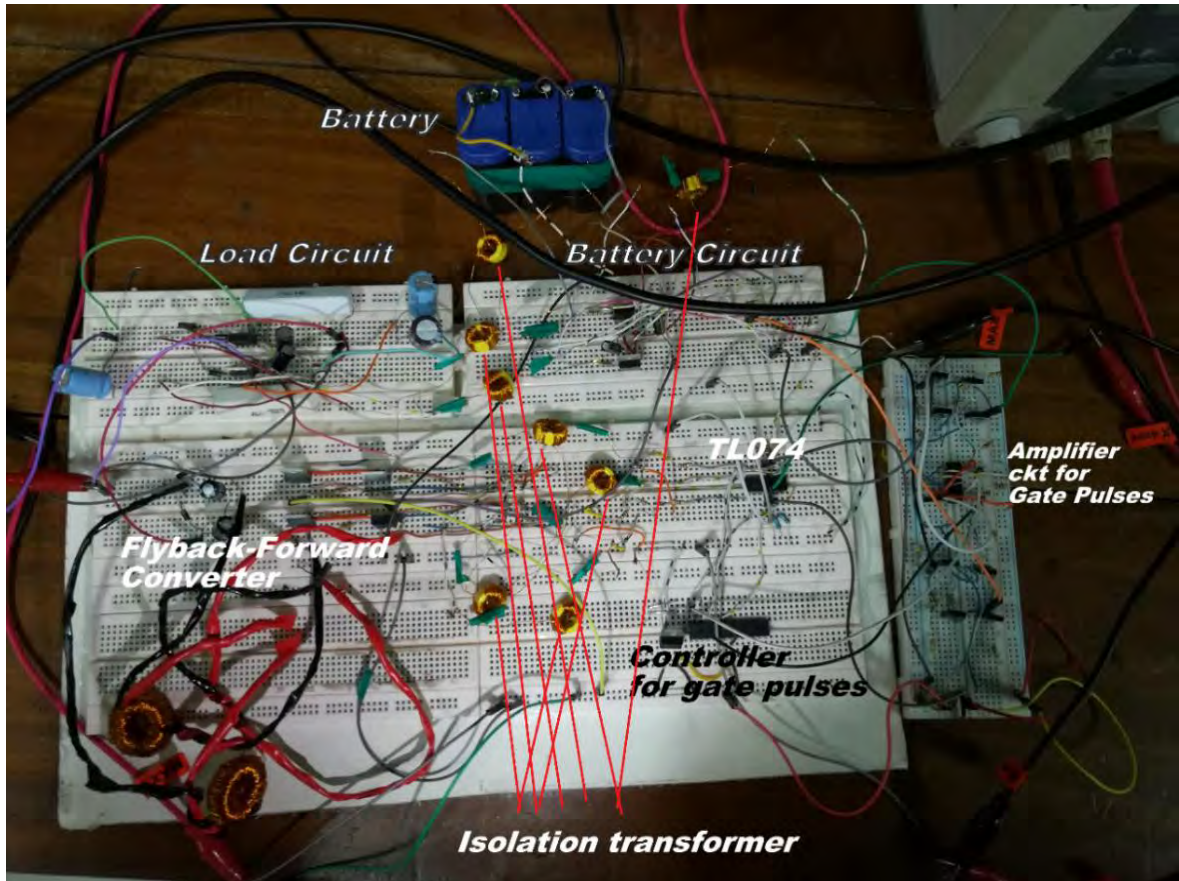


Figure 4.12: Top View of Individual Blocks

In Figure 4.13 the dual outputs are shown in closer view. Here the two outputs are shown from single output. One is 16 volts and the another one is 6 volts.

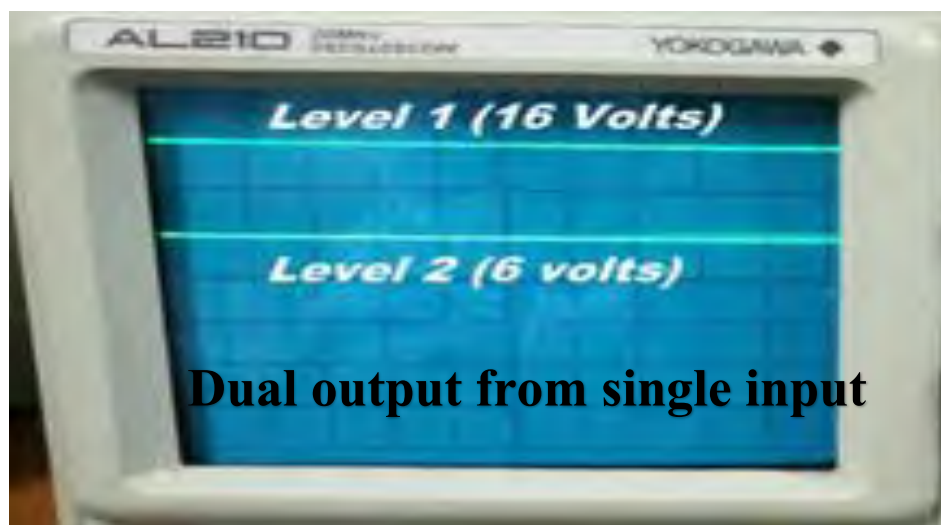


Figure 4.13: Two level Outputs from single input

In Figure 4.14 gate pulses of converter are shown. Here two pulses of mosfets S1 and S2 shown. The two pulse of same time period  $50\mu\text{s}$  and same pulse width  $12\mu\text{s}$  are used. The pulse S2 is delayed  $5\mu\text{s}$  from pulse S1. Both are generated from microcontroller ATmega 8P.



Figure 4.14: Gate Pulses for Isolated Flyback-Forward Converter

In Figure 4.15 the other two gate pulses of S3 and S4 are shown. Here the gate pulses are used those have same time period as the previous gate pulses. Infact the four gate pulses are interrelated on same time frame. Gate pulse S3 are delayed  $20\mu\text{s}$  from gate pulse S1 having a pulse width of 50% that means  $25\mu\text{s}$  whereas gate pulse S4 is delayed  $25\mu\text{s}$  from S1 having same pulse width of  $25\mu\text{s}$  as well.



Figure 4.15: Gate Pulses for Isolated Flyback-Forward Converter

In Figure 4.16 the gate pulses of battery and load circuit are displayed. Here the same gate pulses for output stage 1 is used. Which one is depicted as S5 and S7 for battery and load circuit respectively. The gate pulses have a time period of  $250\mu\text{s}$  and pulse width of  $120\mu\text{s}$ . And the gate pulses of output stage 2 are S6 and S8 used for battery and load circuit respectively. These are delayed over  $120\mu\text{s}$  from S5 and S7 and having a same time period as well.



Figure 4.16: Gate Pulses for Battery and Load circuit

In table 4.8 the parameter and the products are given which are used in experimental setup.

Table 4.8: Parameters of the prototype single input dual output converter

Parameter	Product/Value
D01-D02	1n4009
S1-S8	IRF540N
$N=n2:n1$	2:1
Battery Capacitor	$1\mu\text{F}/16\text{V}$
Load Capacitor	$100\mu/50\text{V}$ , $560\mu/50\text{V}$
Switching Frequency	20 kHz
Battery Voltage	12V
Output Voltage	16V, 6V
Isolation Transformer	Ferrite core 1:1
Amplifier circuit(Gate Pulse)	BD135
Load	$470\Omega/5\text{W}$ , $82\Omega/5\text{W}$

#### 4.3.2 Comparison Between Practical Data and Simulated Data

The comparison between simulated data and practical data is shown in Table 4.9. The efficiency for simulation and practical circuit are quite high.

Table 4.9: Comparison between practical data and simulated data

<i>Parameter</i>	<i>Input</i>		<i>Output</i>			
	<i>Simulated Data</i>	<i>Practical Data</i>	<i>1<sup>st</sup> Level</i>		<i>2<sup>nd</sup> level</i>	
			<i>Simulated Data</i>	<i>Practical Data</i>	<i>Simulated Data</i>	<i>Practical Data</i>
<b>Voltage (V)</b>	12 V	12 V	57 V	16 V	23 V	12 V
<b>Current (V)</b>	1.35 A	.23 A	.1425 A	.34 A	.2875 A	.146 A
<b>Power (W)</b>	16.2 W	2.76 W	8.1225 W	.544 W	6.6125 W	1.752 W
<b>Efficiency (%)</b>	<b>Simulated: 90.95%</b>					
	<b>Practical: 83.28%</b>					

Two level voltages are shown in experimental setup. The output voltage levels are found to be low for the practical circuit. This may be caused by the homemade inductors used in the circuit. The experimental setup shows a good efficiency also. It could be increased by giving the overall setup in PCB.

## Chapter 5

### Conclusion

A highly efficient dynamic SITO converter of multilevel topology is presented here. The system uses “Identically Switched Storage and Load (ISSL) with Shifted Pulse” topology. The proposed single input triple output (SITO) system is an isolated three port Flyback-Forward converter. The converter is fed by a PV cell with capacitor in parallel for the purpose of attenuating input current ripples. This ITPC topology achieves decoupled port control, provides flexible power flow and high power capability while making the system simple and cheap. The heart of the system is the “Battery Circuit”, from where single voltage level is divided into three distinct levels. It’s the vital part of the SITO converter for multiple feeding. Identically Switched Storage and Load (ISSL) with Shifted Pulse is proposed to serve the purpose of multiple users. Three identical gate pulses are used to synchronously turn on both battery and load circuit at a time. To improve the energy utilization and efficiency of low power photovoltaic (PV) system, Incremental conductance and integral regulator MPPT technique is incorporated with the control scheme. The salient features of the proposed multilevel topology is its modularity and scalability, which enable it to meet high to low level DC voltages. Simulation is performed on MATLAB SIMULINK. Hardware implementation is also executed to show the effective operation of the proposed topology. The proposed system shows the 98% efficiency in simulation. The experimental efficiency is also found to be high. The multiple output levels can be set according to the users need. The system can be customized depending on the requirement set by different organizations like IDCOL. The proposed system can be used in the solar home system program of IDCOL to reduce the wiring losses in the program.

#### 5.1 Future Scope

The following points may be incorporated with this research in future:

- Multiple renewable energy sources can be added for more reliable power supply.
- The experimental setup can be modified to satisfy the IDCOL requirements for SHS.
- A genetically tuned PI controller and fuzzy logic based MPPT systems can be used to improve the performance of control scheme.
- The converter efficiency can be further improved by adopting low-loss switching devices (e.g. GaN), better design of the coupled inductor, and better packaging design of the converter.

## References:

- [1] Renewables 2016, “Global status report”,2016. [Online], Available: [www.ren21.net/wpcontent/uploads/2016/06/GSR\\_2016\\_Full\\_Report.pdf](http://www.ren21.net/wpcontent/uploads/2016/06/GSR_2016_Full_Report.pdf) [Accessed: Mar.12, 2017]
- [2] “A record year for renewable energy”, 2016. [Online]. Available: [www.forbes.com/sites/rpapier/2016/06/03/a-record-year-for-renewable-energy/](http://www.forbes.com/sites/rpapier/2016/06/03/a-record-year-for-renewable-energy/) [Accessed: Feb. 15,2017]
- [3] “Renewable Energy - IIASA”, 2017. [Online]. Available: [www.iiasa.ac.at/web/home/research/...Energy.../GEA\\_Chapter11\\_renewables\\_hires.pdf](http://www.iiasa.ac.at/web/home/research/...Energy.../GEA_Chapter11_renewables_hires.pdf) [Accessed: Mar.17, 2017]
- [4] Muhammad, A., and Muneer, T., "Energy supply, its demand and security issues for developed and emerging economies." *Renewable and Sustainable Energy Reviews* 11.7 (2007): 1388-1413.
- [5] Betül, Ö., Görgün, E., and İncecik, S., "The scenario analysis on CO 2 emission mitigation potential in the Turkish electricity sector: 2006–2030." *Energy* 49 (2013): 395-403.
- [6] Katharina, G., Moritz, P., and Lindenberger, D., "A method for estimating security of electricity supply from intermittent sources: scenarios for Germany until 2030." *Energy Policy* 46 (2012): 193-202.
- [7] Fabricius, K., Langdon, C., Uthicke, S., Humphrey, C., Noonan, S., De’ath, G., Okazaki, R., Muehllehner, N., Glas, M., Lough, J., "Losers and winners in coral reefs acclimatized to elevated carbon dioxide concentrations." *Nature Climate Change* 1.3 (2011): 165-169.
- [8] Panwar, N. L., S. C. Kaushik, and Kothari, S., "Role of renewable energy sources in environmental protection: a review." *Renewable and Sustainable Energy Reviews* 15.3 (2011): 1513-1524.
- [9] Omar, E., Abu-Rub, H., and Blaabjerg, F., "Renewable energy resources: Current status, future prospects and their enabling technology." *Renewable and Sustainable Energy Reviews* 39 (2014): 748-764.
- [10] Khatib, H., "IEA World Energy Outlook 2011—A comment." *Energy policy* 48 (2012): 737-743.
- [11] Singhal, Kumar, A., Yadav, N., and Beniwal, N. S., "Global Solar Energy: A Review." *International Electrical Engineering Journal (IEEJ)* Vol 6 (2015): 1828-1833.
- [12] Yue, C.D. and Huang, G.R., “An evaluation of domestic solar energy potential in Taiwan incorporating land use analysis,” *Energy Policy*, vol. 39, no. 12, pp. 7988–8002, 2011.
- [13] Solangi, K., Islam, M., Saidur, R., Rahim, N., and Fayaz, H., “A review on global solar energy policy,”*Renewable and Sustainable Energy Reviews*, vol. 15, no. 4, pp. 2149–2163, 2011.
- [14] Tsoutsos, T., Frantzeskaki, N., and Gekas, V., “Environmental impacts from the solar energy technologies,” *Energy Policy*, vol. 33, no. 3, pp. 289–296, 2005
- [15] Parida, B., Iniyar, S., and Goic, R., “A review of solar photovoltaic technologies,” *Renewable and Sustainable Energy Reviews*, vol. 15, no. 3, pp. 1625–1636, 2011.

- [16] Abete, A., Scapino, F., Spertino, F., and Tommasini, R., “Ageing effect on the performance of a-Si photovoltaic modules in a grid connected system: experimental data and simulation results,” *Conference Record of the Twenty-Eighth IEEE Photovoltaic Specialists Conference - 2000* (Cat. No.00CH37036).
- [17] Bücher, K., “Site dependence of the energy collection of PV modules,” *Solar Energy Materials and Solar Cells*, vol. 47, no. 1-4, pp. 85–94, 1997.
- [18] Halder, P., “Potential and economic feasibility of solar home systems implementation in Bangladesh,” *Renewable and Sustainable Energy Reviews*, vol. 65, pp. 568–576, 2016.
- [19] Sobhan, S., Ahmad, T., Rahimi, M. J., Ullah, M. H., and Arif, S., “HOMER Based Feasibility Study of Off-Grid Biogas Power Generation Model Using Poultry Litter for Rural Bangladesh”, *American Journal of Engineering Research*, Volume-5, Issue-1, pp-21-33.
- [20] “Bangladesh Power Development Board”, 2017 [Online]. Available: [http://www.bpdb.gov.bd/bpdb/index.php?option=com\\_content&view=article&id=150&Itemid=16](http://www.bpdb.gov.bd/bpdb/index.php?option=com_content&view=article&id=150&Itemid=16) [Accessed: Mar. 16,2017]
- [21] Authorized, Disclosure. "Scaling up access to electricity: the case of Bangladesh", 2014, [Online], [Accessed: Jan. 12,2017]
- [22] The Daily Star. “Bangladesh’s gas reserve to last until 2031”, 2015 [Online] Available: <http://www.thedailystar.net/backpage/gas-reserve-last-until-2031-104479> [Accessed: June 29, 2015]
- [23] Islam, M. R., Islam, M. R., and Beg, M. R. A., “Renewable energy resources and technologies practice in Bangladesh,” *Renewable and Sustainable Energy Reviews*, vol. 12, no. 2, pp. 299–343, 2008.
- [24] “Power Cell”. Available: [http://www.powercell.gov.bd/index.php?page\\_id=267](http://www.powercell.gov.bd/index.php?page_id=267) [Accessed: Dec. 17,2016]
- [25] Li, W., and He, X., “Review of Nonisolated High-Step-Up DC/DC Converters in Photovoltaic Grid-Connected Applications,” *IEEE Transactions on Industrial Electronics*, vol. 58, no. 4, pp. 1239–1250, 2011.
- [26] Thounthong, P., “Model Based-Energy Control of a Solar Power Plant With a Supercapacitor for Grid-Independent Applications,” *IEEE Trans. Energy Conversion*, vol. 26, no. 4, pp. 1210-1218, 2011.
- [27] Elmitwally, A., Rashed, M., “Flexible Operation Strategy for an Isolated PV-Diesel Microgrid Without Energy Storage,” *IEEE Trans. Energy Conversion*, vol. 26, no. 1, pp. 235-244, 2011.
- [28] Valderrama-Blavi, H., Bosque, J. M., Guinjoan, F., Marroyo, L., and Martinez-Salamero, L., “Power Adaptor Device for Domestic DC Microgrids Based on Commercial MPPT Inverters,” *IEEE Trans. Ind. Electron.*, vol. 60, no. 3, pp. 1191-1203, Mar. 2013.
- [29] Wu, H., Sun, K., Chen, R., Hu, H., and Xing, Y., “Full-Bridge Three-Port Converters With Wide Input Voltage Range for Renewable Power Systems,” *IEEE Trans. Power Electron.*, vol. 27, no. 9, pp. 3965-3974, Sept. 2012.
- [30] Rashid, M. H., *Power electronics: Devices, circuits, and applications*, 4th ed. Harlow: Pearson Education, 2013.

- [31] Mohan N.T., Undeland M., Robbins W.P., *Power electronics: converters, applications and design*, 3rd ed. John Wiley & Sons: New York; 2004
- [32] Tao, H., Kotsopoulos, A., Duarte, J. L., and Hendrix, M. A. M., "Transformer-Coupled Multiport ZVS Bidirectional DC-DC Converter With Wide Input Range," *IEEE Trans. Power Electron.*, vol. 23, no. 2, pp. 771-781, Mar. 2008.
- [33] Li, W., Xiao, J., Zhao, Y., and He, X., "PWM Plus Phase Angle Shift (PPAS) Control Scheme for Combined Multiport DC/DC Converters," *IEEE Trans. Power Electron.*, vol. 27, no. 3, pp. 1479-1489, 2012.
- [34] Rodriguez-Diaz, E., Savaghebi, M., Vasquez, J. C., and Guerrero, J. M., "An overview of low voltage DC distribution systems for residential applications," *2015 IEEE 5th International Conference on Consumer Electronics - Berlin (ICCE-Berlin)*, 2015.
- [35] Middlebrook, R., "Transformerless DC-to-DC converters with large conversion ratios," *IEEE Transactions on Power Electronics*, vol. 3, no. 4, pp. 484-488, 1988.
- [36] Maksimovic, D., and Cuk, S., "Switching converters with wide DC conversion range," *IEEE Transactions on Power Electronics*, vol. 6, no. 1, pp. 151-157, 1991.
- [37] Axelrod, B., Berkovich, Y., and Ioinovici, A., "Switched-Capacitor/Switched-Inductor Structures for Getting Transformerless Hybrid DC-DC PWM Converters," *IEEE Transactions on Circuits and Systems I: Regular Papers*, vol. 55, no. 2, pp. 687-696, 2008.
- [38] Cengelci, E., Sulistijo, S. U., Woom, B. O., Enjeti, P., Teodorescu, R., and Blaabjerg, F., "A New Medium Voltage PWM Inverter Topology for Adjustable Speed Drives," in *Conf. Rec. IEEE-IAS Annu. Meeting*, St. Louis, MO, Oct. 1998, pp. 1416-1423.
- [39] Rodriguez, J. R., Bernet, S., Wu, B., Pontt, J., Kouro, S., "Multilevel voltage-source-converter topologies for industrial medium-voltage drives." *IEEE Transactions on Industrial Electronics* 54.6 (2007): 2930-2945.
- [40] Marchesoni, M., and Pierluigi T., "Diode-clamped multilevel converters: a practicable way to balance DC-link voltages." *IEEE Transactions on Industrial Electronics* 49.4 (2002): 752-765.
- [41] Grath, M., Peter, B., and Holmes, D. G., "Analytical modelling of voltage balance dynamics for a flying capacitor multilevel converter." *2007 IEEE Power Electronics Specialists Conference*. IEEE, 2007.
- [42] Pradipta, P., Ghosh, J., and Patra, A., "Control scheme for reduced cross-regulation in single-inductor multiple-output DC-DC converters." *IEEE Transactions on Industrial Electronics* 60.11 (2013): 5095-5104.
- [43] Nami, A., Zare, F., Ghosh, A., Blaabjerg, F., "Multi-output DC-DC converters based on diode-clamped converters configuration: topology and control strategy." *IET power electronics* 3.2 (2010): 197-208.
- [44] Chen, Liang, R. Y., Chen, T. J., Lin, J. F., Tseng, R. L., Ching, K., "Study and implementation of a current-fed full-bridge boost DC-DC converter with zero-current switching for high-voltage applications." *IEEE Transactions on Industry Applications* 44.4 (2008): 1218-1226.

- [45] Roberto, R., Charpentier, J. P., and Sharma, R., "High voltage direct current (HVDC) transmission systems technology review paper." *Energy week* 2000 (2000): 2.
- [46] Kang, F. S., Park, S. J., Cho, S. E., Kim, C. U., Ise, T., "Multilevel PWM inverters suitable for the use of stand-alone photovoltaic power systems", *IEEE Trans. Energy Conversion*, vol. 20, no. 4, pp. 906-915, Dec. 2005.
- [47] Liang, Nami, J., Dijkhuizen, F. and Demetriades, G. D., "Modular multilevel converters for HVDC applications: Review on converter cells and Functionalities", *IEEE Transactions on Power Electronics*, vol. 30, no. 1, pp. 18–36, Jan. 2015.
- [48] Rodriguez-Diaz, E., Savaghebi, M., Vasquez, J. C., and Guerrero, J. M., "An overview of low voltage DC distribution systems for residential applications", in *Consumer Electronics - Berlin (ICCE-Berlin)*, 2015 IEEE 5th International Conference on, 2015, pp. 318-322
- [49] Zhang, Y., Ravishankar, J., Fletcher, J., Li, R., and Han, M., "Review of modular multilevel converter based multi-terminal HVDC systems for offshore wind power transmission", *Renewable and Sustainable Energy Reviews*, vol. 61, pp. 572–586, Aug. 2016.
- [50] Rodriguez-Diaz, E., Chen, F., Vasquez, J. C., Guerrero, J. M., Burgos, R., and Boroyevich, D., "Voltage-Level Selection of Future Two-Level LVDC Distribution Grids: A Compromise Between Grid Compatibility, Safety, and Efficiency", *IEEE Electrification Mag.*, vol. 4, no. 2, pp. 20–28, Jun. 2016.
- [51] Pinomaa, A., Ahola, J., Kosonen, A., and Nuutinen, P., "HomePlug Green PHY for the LVDC PLC concept: applicability study", in *Proc. 19th Int. Symp. on Power-Line Commun. Its Appl., Austin, Texas, USA*, Mar. 2015, pp. 205–210.
- [52] Wai, R.J., and Jheng, K.H., "High-efficiency single-input multiple-output DC-DC converter", *IEEE Transactions on Power Electronics*, vol. 28, no. 2, pp. 886–898, Feb. 2013.
- [53] "Power Topics for Power Supply Users". [Online]. Available: <http://power-topics.blogspot.com/2007/10/isolated-non-isolated-DC-DC-converters.html>. [Accessed: Jan.15, 2017]
- [54] Irving, B. T., Panov, Y., & Jovanovic, M. M., "Small-signal model of variable-frequency flyback converter", In *Applied Power Electronics Conference and Exposition, 2003. APEC'03. Eighteenth Annual IEEE* (Vol. 2, pp. 977-982). IEEE.
- [55] Bose, B. K., "Power Electronics and Variable Frequency Drives: Technology and Applications", *IEEE Press*, Piscataway, NJ, 1997.
- [56] Czarkowski, D., Czarkowski, D., Pujara, L. R., & Kazimierczuk, M. K. (1995). Robust stability of state-feedback control of PWM DC-DC push-pull converter. *IEEE Transactions on Industrial Electronics*, 42(1), 108-111.
- [57] Arias, M., Diaz, M. F., Lamar, D. G., Balocco, D., Diallo, A. A., & Sebastián, J., "High-efficiency asymmetrical half-bridge converter without electrolytic capacitor for low-output-voltage AC–DC LED drivers", *IEEE Transactions on Power Electronics*, 28(5), 2539-2550.
- [58] Ninomiya, T., Higashi, T., & Harada, K., "Analysis of a ringing choke converter", *Electronics and Communications in Japan (Part II: Electronics)*, 70(5), 8-20, 1987.

- [59] Chen, L., Hu, H., Zhang, Q., Amirahmadi, A., and Batarseh, I., "A Boundary-Mode Forward-Flyback Converter With an Efficient Active LC Snubber Circuit", *IEEE Transactions on Power Electronics*, 29(6), 2944-2958, 2014.
- [60] Himmelstoss, F. A., and H. L. Votzi. "Combined Forward-Flyback-Converter with Only Two Diodes–Function and Modelling." *Communications–Scientific Letters of the University of Zilina* 13 (2011): 6-12.
- [61] Flicker, Y., and Himmelstoss, F. A., "Combined isolated forward-flyback-converter with only one diode as battery charger", *International Conference on Optimization of Electrical and Electronic Equipment (OPTIM)* (pp. 512-518). IEEE, 2014, May.
- [62] Hosenuzzaman, M., Rahim, N. A., Selvaraj, J., Hasanuzzaman, M., Malek, A. B. M. A., and Nahar, A., "Global prospects, progress, policies, and environmental impact of solar photovoltaic power generation", *Renewable and Sustainable Energy Reviews*, vol. 41, pp. 284–297, 2015.
- [63] Tyagi, V. V., Rahim, N. A., Rahim, N. A., Jeyraj, A., and Selvaraj, L., "Progress in solar PV technology: research and achievement", *Renewable and Sustainable Energy Reviews*, vol. 20, pp. 443-461, 2013.
- [64] Jäger-Waldau A., "PV status report 2014". Eur Union 2014;5:5–6.
- [65] Nayak, P. K., Garcia-Belmonte, G., Kahn, A., Bisquert, J., and Cahen, D., "Photovoltaic efficiency limits and material disorder", *Energy & Environmental Science*, vol. 5, no. 3, pp. 6022-6039, 2012
- [66] McCann, M. J., Catchpole, K. R., Weber, K. J., and Blakers, A. W., "A review of thin-film crystalline silicon for solar cell applications. Part 1: Native substrates", *Solar Energy Materials and Solar Cells*, vol. 68, no. 2, pp. 135-171, 2001.
- [67] El Chaar, L., and El Zein, N., "Review of photovoltaic technologies." *Renewable and Sustainable Energy Reviews*, vol. 15, no. 5 , pp. 2165-2175, 2011
- [68] Gorter, T., and Reinders, A. H. M. E., "A comparison of 15 polymers for application in photovoltaic modules in PV-powered boats", *Applied energy*, vol. 92, pp. 286-297, 2012.
- [69] Masson, G., Latour, M., Rekingier, M., Theologitis, I. T., and Papoutsis, M., "Global market outlook for photovoltaics 2013-2017", *European Photovoltaic Industry Association*, pp.12-32, 2013.
- [70] Manna, T. K., and Mahajan, S. M., "Nanotechnology in the development of photovoltaic cells", *International Conference on Clean Electrical Power*. IEEE, 2007, pp. 379-386.
- [71] Deb, S. K., "Recent developments in high efficiency photovoltaic cells", *Renewable energy*, vol.15.1, pp. 467-472, 1998.
- [72] Raugei, M., Bargigli, S., and Ulgiati, S., "Life cycle assessment and energy pay-back time of advanced photovoltaic modules: CdTe and CIS compared to poly-Si ", *Energy*, vol. 32, no. 8 , pp. 1310-1318, 2007.
- [73] Jungbluth, N., "Life cycle assessment of crystalline photovoltaics in the Swiss ecoinvent database", *Progress in Photovoltaics: Research and Applications*, vol.13, no.5, pp. 429-446, 2005.
- [74] Carlson, D. E., and Wronski, C. R., "Amorphous silicon solar cell", *Applied Physics Letters*, vol. 28, no.11, pp.671-673, 1976.

- [75] Markvart T., "Solar electricity", 2nd ed. Chichester, UK: John Wiley & Sons, 2001.
- [76] Hashimoto, I., "Present status of research and development of PV technology in Japan", *Photovoltaic Energy Conversion, 2003. Proceedings of 3rd World Conference on.* IEEE, Vol. 3, 2003, pp. 2522-2526.
- [77] Yang, J., Banerjee, A., and Guha, S., "Amorphous silicon based photovoltaics—from earth to the "final frontier" ", *Solar energy materials and solar cells*, vol.78, no.1, pp. 597-612, 2003.
- [78] Franklin, E., Everett, V., Blakers, A., and Weber, K., "Sliver solar cells: High-efficiency, low-cost PV technology", *Advances in OptoElectronics*, 2007, pp.1-9.
- [79] Yamaguchi, M., "Present status and prospects of photovoltaic technologies in Japan", *Renewable and sustainable energy reviews*, vol.5, no.2, pp.113-135, 2001.
- [80] Repins, I., Contreras, M. A., Egaas, B., DeHart, C., Scharf, J., Perkins, C. L., To, B., Noufi, R., "19.9%-efficient ZnO/CdS/CuInGaSe<sub>2</sub> solar cell with 81.2% fill factor", *Progress in Photovoltaics: Research and applications*, vol.16, no.3, pp.235-239, 2008.
- [81] Powalla, M., "The R&D potential of CIS thin-film solar modules", *Proc. Euro. Photovolt. Solar Energy Conf.*, vol. 21, 2006, pp. 1789-1795.
- [82] Looser, R., Vivar, M., and Everett, V., "Spectral characterisation and long-term performance analysis of various commercial Heat Transfer Fluids (HTF) as Direct-Absorption Filters for CPV-T beam-splitting applications", *Applied Energy*, vol.113, pp. 1496-1511, 2014.
- [83] Cotal, H., and Sherif, R., "Temperature dependence of the IV parameters from triple junction GaInP/InGaAs/Ge concentrator solar cells", *4th World Conference on Photovoltaic Energy Conference IEEE*, Vol. 1, 2006, pp. 845-848
- [84] Zahedi, A., "Review of modelling details in relation to low-concentration solar concentrating photovoltaic", *Renewable and Sustainable Energy Reviews*, vol.15, no.3, pp. 1609-1614, 2011.
- [85] Gilot, J., Wienk, M. M., and Janssen, R. A., "Measuring the external quantum efficiency of two-terminal polymer tandem solar cells", *Advanced Functional Materials*, vol.20, no.22, pp.3904-3911, 2010.
- [86] Lizin, S., Van Passel, S., De Schepper, E., Maes, W., Lutsen, L., Manca, J., and Vanderzande, D., "Life cycle analyses of organic photovoltaics: a review", *Energy & Environmental Science*, vol.6, no.11, pp. 3136-3149, 2013.
- [87] Pei, Z., Devi, B. P., and Thiyagu, S., "Study on the Al-P3HT: PCBM interfaces in electrical stressed polymer solar cell by X-ray photoelectron spectroscopy", *Solar Energy Materials and Solar Cells*, vol.123, pp. 1-6, 2014.
- [88] Capasso, A., Salamandra, L., Chou, A., Di Carlo, A., and Motta, N., "Multi-wall carbon nanotube coating of fluorine-doped tin oxide as an electrode surface modifier for polymer solar cells", *Solar Energy Materials and Solar Cells*, vol.122, pp.297-302, 2014.
- [89] Zhang, Z., He, Z., Liang, C., Lind, A. H., Diyaf, A., Peng, Y., and Wilson, J. I., "A preliminary development in hybrid a-silicon/polymer solar cells", *Renewable Energy*, vol.63, pp.145-152, 2014.

- [90] O'regan, B., and Grfitzeli, M., "A low-cost, high-efficiency solar cell based on dye-sensitized", *Nature*, vol.353, no. 6346 , pp. 737-740, 1991.
- [91] Nazeeruddin, M. K., Baranoff, E., and Grätzel, M., "Dye-sensitized solar cells: a brief overview", *Solar energy*, vol. 85, no.6, pp.1172-1178, 2011.
- [92] Ahmad, I., McCarthy, J. E., Bari, M., and Gun'ko, Y. K., "Carbon nanomaterial based counter electrodes for dye sensitized solar cells", *Solar Energy* , vol.102 , pp.152-161, 2014.
- [93] Jin, H., Qin, L., Hao, C., Wang, L., and Jiao, F., "The study and exploration of a new generation of photovoltaic energy storage system", *Energy Procedia*, vol.12, pp. 986-993, 2011.
- [94] Chen, S., and Chen, X., "KVV solar power generation system application and operation", *Power Electronics*, vol.10, no.30, pp. 42-44, 2009.
- [95] Carrero, C., Amador, J. and Arnaltes, S., "A Single Procedure for Helping PV Designers to Select Silicon PV Modules and Evaluate the Loss Resistances", *Renewable Energy*, vol. 32, pp.2579-2589, 2007
- [96] Liu, S., and Dougal, R., "Dynamic Multiphysics Model for Solar Array", *IEEE Transactions on Energy Conversion*, vol.17, pp.285-294, 2002
- [97] Ahmad, T., Sobhan, S., & Nayan, M. F., "Comparative Analysis between Single Diode and Double Diode Model of PV Cell: Concentrate Different Parameters Effect on Its Efficiency", *Journal of Power and Energy Engineering*, vol. 4, no.3, pp.31-46, 2016.
- [98] Xiao, W., Dunford, W.G. and Capel, A., "A Novel Modeling Method for Photovoltaic Cells", 2004 *IEEE 35<sup>th</sup> Annual Power Electronics Specialists Conference, PESC 04*, vol. 3, pp.1950-1956, 2004.
- [99] Alboteanu, L., Manolea, G. and Ravigan, F., "Methods of Modeling for Photovoltaic Cells", *Annals of the University of Craiova, Electrical Engineering Series*, no. 32, 2008.
- [100] Eltawil, M. A., and Zhao, Z., "MPPT techniques for photovoltaic applications," *Renewable and Sustainable Energy Re-views*, vol. 25, pp. 793–813, 2013.
- [101] Brito, M. A. G. D., Sampaio, L. P., Luigi, G., Melo, G. A. E., and Canesin, C. A., "Comparative analysis of MPPT techniques for PV applications," *2011 International Conference on Clean Electrical Power (ICCEP)*, 2011.
- [102] Teulings, W., Marpinard, J., Capel, A., and O'sullivan, D., "A new maximum power point tracking system," *Proceedings of IEEE Power Electronics Specialist Conference - PESC '93*.
- [103] Tan, C. W., Green, T. C., and Hernandez-Aramburo, C. A., "A current-mode controlled maximum power point tracking converter for building integrated photovoltaics," *2007 European Conference on Power Electronics and Applications*, 2007.
- [104] Buresch, M., "Photovoltaic energy systems: design and installation", New York: McGraw-Hill, 1983.
- [105] Hohm, D. P., and Ropp, M. E., "Comparative study of maximum power point tracking algorithms," *Prog. Photovolt: Res. Appl. Progress in Photovoltaics: Research and Applications*, vol. 11, no. 1, pp. 47–62, 2002.
- [106] Hart, G., Branz, H., and Cox, C., "Experimental tests of open-loop maximum-power-point tracking techniques for photovoltaic arrays," *Solar Cells*, vol. 13, no. 2, pp. 185–195, 1984.

- [107] Pandey, A. K., Tyagi, V. V., Jeyraj, A., Selvaraj, L., Rahim, N. A., and Tyagi, S. K., "Recent advances in solar photovoltaic systems for emerging trends and advanced applications", *Renewable and Sustainable Energy Reviews*, 53, 859-884, 2016.
- [108] "Agency WeoIE. World Energy Outlook. Tokyo: International Energy Agency"; 2013. [Online]. Available: <https://www.iea.org/newsroom/news/2013/november/world-energy-outlook-2013.html>. [Accessed: Dec. 25, 2016]
- [109] Pode R., "Solution to enhance the acceptability of solar-powered LED lighting technology", *Renew Sustain Energy Rev* 2010;14:1096–103.
- [110] Sastry O, Kamala Devi V, Pant P, Prasad G, Kumar R, Bandyopadhyay B., "Development of white LED based PV lighting systems", *Sol Energy Mater Sol Cells* 2010;94:1430–3.
- [111] Komatsu S., Kaneko S., Ghosh P. P., "Are micro-benefits negligible? The implications of the rapid expansion of solar home systems (SHS) in rural Bangladesh for sustainable development", *Energy Policy* 2011;39:4022–31.
- [112] Krishnaswami, H., and Mohan, N., "Three-Port Series-Resonant DC-DC Converter to Interface Renewable Energy Sources With Bidirectional Load and Energy Storage Ports", *IEEE Trans. Power Electron.*, vol. 24, no. 10, pp. 2289-2297, Oct. 2009.
- [113] Hu, Y., Xiao, W., Cao, W., Ji, B., and Morrow, D. J., "Three-Port DC-DC Converter for Stand-Alone Photovoltaic Systems", *IEEE Transactions on Power Electronics*, vol. 30, no.6, pp. 3068-3076, 2015.
- [114] Hu, Y., Deng, Y., Lu, X., Tao, Y., and He, X., "A three-port high step-up DC-DC converter for PV system", In *ECCE Asia Downunder (ECCE Asia)*, 2013 *IEEE*, pp. 285-290, June, 2013.
- [115] Attaianese, C., Nardi, V., and Tomasso, G., "A novel SVM strategy for VSI dead-time-effect reduction", *IEEE Trans. Ind. Appl.*, vol. 41, no. 6, pp. 1667–1674, Nov./Dec. 2005.
- [116] Abu-Qahouq, J. A., Mao, H., Al-Atrash, H. J., and Batarseh, I., "Maximum efficiency point tracking (MEPT) method and digital dead time control implementation", *IEEE Trans. Power Electron.*, vol. 21, no. 5, pp. 1273–1281, Sep. 2006
- [117] Kobayashi, K., Takano, I., and Sawada, Y., "A study of a two stage maximum power point tracking control of a photovoltaic system under partially shaded insolation conditions", *Solar energy materials and solar cells*, vol. 90, no.18, pp. 2975-2988, 2006.
- [118] Hussein, K. H., Muta, I., Hoshino, T., and Osakada, M., "Maximum photovoltaic power tracking: an algorithm for rapidly changing atmospheric conditions", *IEE Proceedings-Generation, Transmission and Distribution*, vol.142, no.1, pp. 59-64, 1995.
- [119] Wu, W., Pongratananukul, N., Qiu, W., Rustom, K., Kasparis, T., and Batarseh, I., "DSP-based multiple peak power tracking for expandable power system", In *Eighteenth Annu. IEEE Appl. Power Electron. Conf. Expo*, February 2003, pp. 525-530.

- [120] Waszynek, O., "Dynamic behavior of a class of photovoltaic power systems", *IEEE transactions on power apparatus and systems*, vol.9, pp. 3031-3037, 1983.
- [121] Minorshy, N., "Directional stability of automatically steered bodies", *Journal of the American Society for Naval Engineers*, vol. 34, no. 2, pp. 280-309, 1922.
- [122] Selvaraj, J., and Rahim, N. A., "Multilevel Inverter for grid-connected PV system employing digital PI controller," *IEEE Transactions on Industrial Electronics*, vol. 56, no. 1, pp. 149–158, Jan. 2009.
- [123] Awasthi, S.K., Sehgal S., and Kumar, H., "Comparative Analysis of Different Modes of a PID controller using a Hydraulic Level Control Trainer," *Futuristic Trends in Engineering, Science, Humanities, and Technology FTESHT*, 2016, pp.50-54.
- [124] TEMEL, S., YAĞLI, S., GÖREN, S., "P, PD, PI, PID CONTROLLERS," Middle East Technical University.
- [125] Man, K. F., Tang, K. S., and Kwong, S., "Genetic algorithms: concepts and designs", *Springer Science & Business Media*, 2012.
- [126] Hasanuzzaman, M., Rahim, N., Saidur, R., and Kazi, S., "Energy savings and emissions reductions for rewinding and replacement of industrial motor," *Energy*, vol. 36, no. 1, pp. 233–240, 2011.
- [127] Hasanuzzaman, M., Rahim, N., Hosenuzzaman, M., Saidur, R., Mahbubul, I., and Rashid, M., "Energy savings in the combustion based process heating in industrial sector," *Renewable and Sustainable Energy Reviews*, vol. 16, no. 7, pp. 4527–4536, 2012.
- [128] Neto, M. B., Carvalho, P., Carioca, J., and Canafistula, F., "Biogas/photovoltaic hybrid power system for decentralized energy supply of rural areas," *Energy Policy*, vol. 38, no. 8, pp. 4497–4506, 2010.
- [129] "IPCC, Climate Change 2007: The Physical Science Basis. Geneva Intergovernmental Panel on Climate Change"; 2007. [Online], Available [https://www.ipcc.ch/publications\\_and\\_data/publications\\_ipcc\\_fourth\\_assessment\\_report\\_wg1\\_report\\_the\\_physical\\_science\\_basis.html](https://www.ipcc.ch/publications_and_data/publications_ipcc_fourth_assessment_report_wg1_report_the_physical_science_basis.html). [Accessed: Dec 26, 2016]
- [130] Halder, P. K., "Potential and economic feasibility of solar home systems implementation in Bangladesh," *Renewable and Sustainable Energy Reviews*, vol. 65, pp. 568–576, 2016.
- [131] Abete, A., Scapino, F., Spertino, F., and Tommasini, R., "Ageing effect on the performance of a-Si photovoltaic modules in a grid connected system: experimental data and simulation results," *Conference Record of the Twenty-Eighth IEEE Photovoltaic Specialists Conference - 2000 (Cat. No.00CH37036)*.
- [132] Bücher, K., "Site dependence of the energy collection of PV modules," *Solar Energy Materials and Solar Cells*, vol. 47, no. 1-4, pp. 85–94, 1997.
- [133] Wang, Z., and Li, H., "An Integrated Three-Port Bidirectional DC-DC Converter for PV Application on a DC Distribution System," *IEEE Trans. Power Electron.*, vol. 28, no. 10, pp. 4612-4624, Oct. 2013.
- [134] Cai, W., Liu, B., Duan, S., Jiang, L., "Power flow control and optimization of a three-port converter for photovoltaic-storage hybrid system," *Energy Conversion Congress and Exposition (ECCE)*, pp. 4121-4128, 2012.

- [135] Chen, Y. M., Yu, X., Huang, A. Q., “A new nonisolated three-port DC-DC converter with high step-up/down ratio,” *IEEE Energy Conversion Congress and Exposition (ECCE)*, pp. 1520-1526, 2012.
- [136] Tao, H., Kotsopoulos, A., Duarte, J. L., and Hendrix, M. A. M., “Transformer-Coupled Multiport ZVS Bidirectional DC-DC Converter With Wide Input Range,” *IEEE Trans. Power Electron.*, vol. 23, no. 2, pp. 771-781, Mar. 2008.